Buckling Analysis of Tri-axial Woven Fabric Composite Structures

Duosheng Xu

A Thesis

in

The Department

of

Mechanical and Industrial Engineering

Presented in Partial Fulfillment of the Requirements

For the Degree of Doctor of Philosophy at

Concordia University

Montreal, Quebec, Canada

August 2004

Your file Votre référence
ISBN: 0-612-96963-0
Our file Notre référence
ISBN: 0-612-96963-0

ABSTRACT

Buckling Analysis of Tri-axial Woven Fabric Composite Structures

Duosheng Xu, Ph.D.

Concordia University, 2004

The buckling of a structure may have an adverse effect on the structural performance and may cause instability of the structure or even failure of a structure, especially in structures with thin elements. Single layered tri-axial woven fabric composite structures belong to this type of thin structures. The load at which buckling will occur has to be determined. It is the purpose of the present dissertation to perform this task. The study of the dissertation covers the following aspects:

- A curved beam model for non-linear finite element analysis is presented. Based on the continuum mechanics principles, the finite element updated Langrangian incremental formulation for non-linear analysis is derived. Example problems are solved and comparison of the present results with those from literature is made. The effectiveness of the formulation and the validity of the corresponding computer code are demonstrated.

- The buckling analyses of several simple tri-axial composite structures, such as straight composite beam and curved composite beam subjected to different boundary conditions, simply-supported composite structure with two intersected curved tows and simply-supported tri-axial woven composite structure with three intersected curved tows, that are a part of tri-axial woven fabric composite tow structures are performed. In order to further confirm the accuracy of the numerical solutions, approximate analytical solutions corresponding to these tow structures are derived. The numerical results obtained are in very good agreement with the analytical solutions for the straight beam, curved beam and curved beam structures. The effect of the resin on the curved tri-axial woven composite tow structures is also investigated.

- The buckling behavior of more complicated tri-axial woven fabric composite structures is studied. These more complicated structures include basic tri-axial structure, modified basic tri-axial structure and enlarged basic tri-axial structure where additional weavings are added to make the sample longer and wider. The basic tri-axial structure is subjected to uni-directional or bi-directional loading. The sensitivity of the buckling behavior of the basic tri-axial structure to the change in the boundary conditions and to the imperfection due to initial configuration is investigated. The sensitivity analysis of buckling behavior to the in-plane aspect ratio of the structure is also conducted. Their numerical results and corresponding physical explanations are given. In order to gain some insight into the buckling behavior of more complicated tri-axial woven fabric composite

structures, the buckling analysis of the modified and enlarged basic tri-axial composite structures subjected to uni-directional loading is also conducted. Numerical results reveal that these modified and enlarged basic tri-axial composite structures have almost the same buckling behavior as the basic tri-axial structure. In order to provide confirmation to the numerical solutions and to provide simpler ways to obtain the results, approximate analytical solution corresponding to the basic structure subjected to uni-directional loading and bi-directional loading has been derived by using multi-layered plate theory and equivalent energy method. The numerical result obtained for the basic tri-axial structure is compared with the analytical solution for corresponding tri-axial structures. The comparison shows good agreement between the two solutions. The upper bound of the value of the buckling load for the tri-axial woven fabric composite structure is obtained from analytical solution. The investigation of the effect of the resin on the basic tri-axial woven composite structure shows that the Young's modulus of the resin has little effect on the buckling behavior of the basic tri-axial structure due to the interaction of the woven tows constituting the structure.

- The value of the buckling load is normalized. Extension to the buckling of real life large tri-axial structures is discussed. Buckling load of a real life large tri-axial structure can be obtained approximately by subtracting from the value of the approximate analytical solution by 8%. Thus determined value of buckling load for a real life larger sized tri-axial structure is on the safe side.

Acknowledgements

I would like to thank all those faculty members who have contributed to my education. In particular, I wish to thank sincerely the thesis supervisors, Dr. Suong V. Hoa and Dr. Rajamohan Ganesan for their support and guidance during this study. I am also grateful to my supervisors for their careful reading and corrections of this thesis.

I thank the graduate students of the Department of Mechanical and Industrial Engineering for their friendship.

Finally, I would like to express a deep appreciation to my wife, Xiaoning Dai, and my daughter, Yi Xu, for their patience, encouragement and supports. I also thank my parents and father-in-law for their support and encouragement.

Table of Contents

List of Figures xi

List of Tables xvi

List of symbols xvii

Chapter 1 Introduction 1

1.1 Tri-axial composite structure 1

1.2 Decomposition of the tri-axial structures into simple models 3

1.3 Stability analysis of a single curved composite beam 7

1.4 Literature survey 8

1.5 Objectives of the thesis 14

1.6 Organization of the thesis 16

Chapter 2 Curved beam and resin structure 19

2.1 Principle of virtual displacements 19

2.2 Formulation for tow elements 21

2.2.1 Description of element geometry 21

2.2.2 Displacement approximation of element 22

2.2.3 Strain-displacement relationship 24

2.2.4 Stress-strain relationship 25

2.3 Formulation for resin layer element 26

2.3.1 Basic assumptions 26

2.3.2 Element geometry and displacement description 29

2.3.3 Strain-displacement and stress-strain relationships 31

2.4 Equilibrium equation 33

2.5 Determination of buckling load 33

2.6 Conclusion 35

Chapter 3 Approximate analytical solutions for buckling loads of curved beam structures 36

3.1 Simply-supported full sinusoidal beam 36

3.2 Two intersected half sinusoidal beam structure 44

3.3 Three intersected full sinusoidal beam structure 49

3.4 Conclusion 52

Chapter 4 Finite element buckling analysis of curved beam structures 53

4.1 Buckling behavior of single isotropic arch beam with clamped ends 54

4.2 Simply-supported straight beam made of individual composite tow 56

4.3 Straight cantilever beam made of tri-axial composite 58

4.4 Simply-supported curved beam made of individual composite tow 60

4.5 Cantilever curved composite beam 63

4.6 Simply-supported two intersected curved composite tow structure 64

4.7 Simply-supported three intersected curved tri-axial composite structure 70

4.8 Conclusion 73

Chapter 5 Buckling analysis of more complicated tri-axial structures 74

5.1 Simply-supported basic structure subjected to uni-directional loading along x_1 direction 75

5.2 Simply supported basic structure subject to loading along x_2 direction 83

5.3 Simply-supported modified basic tri-axial structure subjected to uni-directional loading along x_1 direction 84
5.4 Sensitivity analysis due to the change in boundary conditions 87
5.5 Buckling analysis of the basic structure with imperfection due to initial configuration 89
5.6 Simply-supported enlarged basic structure subjected to uni-directional loading along x_1 direction 92
5.7 Simply-supported basic tri-axial structure subjected to bi-directional loading 97
5.8 Conclusion 101
Chapter 6 Approximate solutions for simply-supported basic tri-axial composite structure 103
6.1 Basic tri-axial structure subjected to uni-directional loading 103
6.1.1 Equivalent conditions for a simply-supported composite beam and simply-supported single layered composite plate 105
6.1.1.1 Equilibrium equation for a simply-supported individual composite beam 106
6.1.1.2 Equilibrium equation for a simply-supported rectangular single layered composite plate 106
6.1.1.3 Equivalent conditions for simply-supported composite beam and simply-supported single layered rectangular composite plate 107
6.1.2 Equivalent conditions for a simply-supported off-axis composite beam and simply-supported off-axis single layered composite plate 108

6.1.2.1 Equilibrium equations for simply-supported individual off-axis composite beam 109
6.1.2.2 Equilibrium equation for simply-supported off-axis single layered composite plate 115
6.1.2.3 Equivalent conditions for the simply-supported off-axis composite beam and the simply-supported off-axis single layered composite plate 117
6.1.3 Discussion of the equivalent conditions for the composite beam and single layered composite plate 118
6.1.4 Determination of the geometric parameters of the equivalent single layered plates 119
6.1.5 Equivalent multi-layered composite plate and its equilibrium equation and buckling analysis 121
6.2 Basic tri-axial structure subjected to bi-directional loading 128
6.3 Conclusion 142
Chapter 7 Conclusions 143
Chapter 8 Contributions of the research and recommendations for the future work 145
8.1 Contributions of the research 145
8.2 Recommendations for the future work 146
References 148

List of Figures

Fig. 1. 1: A photograph of tri-axial woven fabric composite structure 2

Fig. 1. 2: Tri-axial woven fabric composite structure 3

Fig. 1. 3: Basic tri-axial composite structure with six woven intersected curved tows 4

Fig. 1. 4: Tri-axial woven tow structure with three intersected curved tows 6

Fig. 1. 5: Composite tow structure with two intersected curved tows 6

Fig. 1. 6: Simplest curved composite tow structure 6

Fig. 2. 1: Motion of body in Cartesian co-ordinate system 20

Fig. 2. 2: Three-dimensional curved beam element 22

Fig. 2. 3: Tows and resin 26

Fig. 2. 4: Two-node resin element 27

Fig. 2. 5: Deformation of cross-section of tows and resin 28

Fig. 2. 6: Mapping from $o_x x_{R1} x_{R2} x_{R3}$ to $o_\eta \eta_{R1} \eta_{R2} \eta_{R3}$ 29

Fig. 3. 1: Sinusoidal beam 37

Fig. 3. 2: Tri-axial tow structure with two intersected curved tows 44

Fig. 3. 3: Curve of non-dimensional buckling load versus stiffness ratio $E_L A / E_L I$ for two intersected curved beam structure 48

Fig. 3. 4: Woven tri-axial tow structure with three intersected curved tows 49

Fig. 4. 1: Arch beam with clamped ends 54

Fig. 4. 2: Load versus maximum deflection curve for the arch—Curve I 55

Fig. 4. 3: Load versus maximum deflection curve for the arch—Curve II 56

Fig. 4. 4: Simply-supported straight tri-axial composite beam 57

Fig. 4. 5: Load versus deflection curve for simply-supported straight tow. 57

Fig. 4. 6: Straight cantilever composite beam made of individual tow 58

Fig. 4. 7: Load versus deflection curve for clamped straight tow..... 59

Fig. 4. 8: Simply-supported curved composite beam 60

Fig. 4. 9: Configuration of the fiber tow and resin. 61

Fig. 4. 10: Load versus deflection curve for simply-supported curved tow 61

Fig. 4. 11: Deformed and undeformed shapes of simply-supported curved composite tow 62

Fig. 4. 12: Load versus maximum deflection curve for cantilever curved tow 63

Fig. 4. 13: Deformed and undeformed shapes of cantilever curved beam 64

Fig. 4. 14: Load versus maximum deflection curve of simply-supported two intersected tow structure..... 66

Fig. 4. 15: Buckling load for two-tow structure versus Young's modulus of the resin.... 67

Fig. 4. 16: Deformation patterns of two-tow structure 68

Fig. 4. 17: Curve of non-dimensional buckling load versus stiffness ratio E_LA/ E_LI for two intersected curved beam structure..... 69

Fig. 4. 18: Load versus maximum deflection curve of simply-supported three intersected tow structure..... 72

Fig. 4. 19: Buckling load for three-tow structure versus Young's modulus of the resin.. 72

Fig. 5. 1: Basic composite structure with six woven intersected curved tows..... 75

Fig. 5. 2: Basic structure with six intersected tows subjected to uni-directional loading. 76

Fig. 5. 3: Central line of a full sine wave of an individual tow of the basic structure and its element meshing..... 77

Fig. 5. 4: Load versus maximum deflection curve corresponding to the structure shown in Fig. 5.2; u_{3max} is the maximum deflection of the structure referred to the unloaded configuration 80

Fig. 5. 5: Total non-dimensional load per unit width of the basic tri-axial structure, $P_T/E_L I(\pi/L)^2 W$, versus non-dimensional maximum deflection curve 81

Fig. 5. 6: Buckling load for basic structure versus Young's modulus of the resin 82

Fig. 5. 7: Basic structure with six intersected tows subjected to uni-directional loading in x_2 direction 83

Fig. 5. 8: Load versus maximum deflection curve of the structure as shown in Fig. 5.7 . 84

Fig. 5. 9: Tri-axial woven composite structure with eight intersected curved tows 85

Fig. 5. 10: Tri-axial woven composite structure with ten intersected curved tows 85

Fig. 5. 11: Load versus maximum deflection curve for tri-axial woven structures shown in figures 5.2, 5.9 and 5.10 86

Fig. 5. 12: Basic structure with clamped and simply-supported boundary conditions under uni-directional loading 88

Fig. 5. 13: Load versus maximum deflection curve for basic composite structure with clamped and simply-supported boundary conditions 89

Fig. 5. 14: Load versus maximum deflection curves of the basic tri-axial structure with different initial deflections 91

Fig. 5. 15: Simply-supported enlarged basic composite structure 92

Fig. 5. 16: Load versus maximum deflection curve of the enlarged basic tri-axial structure under uni-directional loading 93

Fig. 5. 17: Total non-dimensional load per unit width of the tri-axial structure, $P_T/E_LI(\pi/L)^2W$, versus non-dimensional maximum deflection curve 95

Fig. 5. 18: Buckling load versus the number of tows in tri-axial structure..... 96

Fig. 5. 19: Total buckling load per unit width versus the number of tows in tri-axial structure..... 96

Fig. 5. 20: Basic tri-axial structure with six intersected tows subjected to bi-directional loading..... 97

Fig. 5. 21: Curve of buckling load versus the loads in x_2 direction for Case 1 98

Fig. 5. 22: Bi-directional loading with the same increment of the loads both in x_1 and x_2 directions for Case 2 99

Fig. 6. 1: Typical tri-axial woven fabric composite tow structure..... 104

Fig. 6. 2: (a) Simply-supported beam; (b) Simply-supported rectangular plate 106

Fig. 6. 3: (a) Simply-supported off-axis composite beam; 109

Fig. 6.3: (b) Simply-supported off-axis single layered composite plate..... 109

Fig. 6. 4: (a) Simply-supported off-axis beam; (b) Beam element; M is the bending moment of the cross- section and V is the shear force of the cross-section..... 110

Fig. 6. 4: (c): Beam element in x_1x_3 plane; (d): Beam element in x_1x_2 plane..... 110

Fig. 6. 5: Differential slice of a beam before and after bending under the action of moment M_2 only..... 112

Fig. 6. 6: Moment and stress relation over a cross-section..... 113

Fig. 6. 7: Equivalent plates to the corresponding beams and strip 120

Fig. 6. 8: Simply-supported equivalent rectangular composite plate..... 123

Fig. 6. 9: Comparison of buckling load between numerical solution and analytical solution 127

Fig. 6. 10: Bi-directionally loaded simply-supported rectangular plate 130

Fig. 6. 11: Local coordinate system of tow BB' in Fig. 5.20 133

Fig. 6. 12: Comparison of the finite element solution and approximate solution 140

List of Tables

Table 4. 1: Material properties of tri-axial composite tow and resin 53

Table 4. 2: List of non-dimensional buckling loads of NFES and AAS 69

Table 5. 1 List of FES of basic tri-axial structure subjected to bi-directional loading 99

Table 6. 1: List of the non-dimensional buckling loads for the simply-supported tri-axial woven fabric composite structures 127

Table 6. 2: Material properties of the tri-axial woven fabric composite structure 129

Table 6. 3: Comparison of finite element solution and approximate solution 139

List of symbols

Notation

The following convention for tensor and vector subscripts and superscripts is employed:

- A left superscript denotes the time of the configuration in which the quantity occurs.
- A left subscript denotes the time of the configuration, in which the co-ordinate is measured with respect to which is differentiated, if the quantity considered is a derivative; otherwise the left subscript denotes the time of the configuration in which the quantity is measured.
- Right lower case subscripts denote the components of a tensor or vector. Differentiation is denoted by a subscript following a comma, with the subscript indicating the co-ordinate with respect to which is differentiated.
- Right upper case subscript R corresponds to the resin.

a_k, b_k	Height and width of cross-sectional dimensions of the beam at nodal point k
a_p, b_p	Height and width of cross-sectional dimensions of the laminated plate
$\bar{a}$	Thickness of single layered equivalent plate
A	Cross-sectional area of a beam
$\bar{b}$	Width of single layered equivalent plate
B_{ij}	Elements of matrix in stress–strain and–curvature relation
c_i	Coefficient of deflection equation

${}_0^tC_{ijrs}$	Component of constitutive tensor at time t referred to configuration at time 0
${}_tC_{ijrs}$	Component of tangent constitutive tensor at time t referred to configuration at time t
d	Coefficient of displacement equation in x_1 direction
ds, ds_0	Deformed and undeformed length of a beam element
D_{ij}	Elements of Matrix in stress–strain and–curvature relation
${}_te_{ij}$	Component of linear part of strain increment of configuration at time t
E_L, E_T	Longitudinal and transverse Young's moduli of composite tow
E_{p1}, E_{p2}	Young's modulus of the tri-axial woven fabric structure along x_1 and x_2 directions
E_R	Young's modulus of the resin
E_{x_i}	Young's modulus along x_i direction
G_{LT}, G_{TT}	Longitudinal-transverse and transverse-transverse shear moduli
G_R	Shear modulus of the resin
h_i	Finite element interpolation function associated with nodal point k
I	Moment of inertia of the beam cross-section
l_{ij}	Elements of matrix T_c
L	Length of the beam
M_2, M_3	Bending moments in x_2 and x_3 directions
P, P'	Axial load and transverse load
P_{cr}	Critical load

P_p	Load applied to equivalent laminated plate
$\overline{P}$	Load applied to a single layered equivalent plate
Q_i	Concentrated load
Q_{ij}	Coefficients of stress-strain relation in fiber coordinate system
$Q_{x_i x_j}$	Coefficients of stress-strain relation in global coordinate system
r, s, q	Natural element co-ordinates
${}_0^t S_{ij}$	Component of second Piola-Kirchhoff stress tensor in configuration at time t referred to configuration at time 0
${}_t^{t+\Delta t} S_{ij}$	Component of second Piola-Kirchhoff stress tensor in configuration at time $t+\Delta t$ referred to configuration at time t
${}_t S_{ij}$	Component of second Piola-Kirchhoff stress increment at time t
$t, t+\Delta t$	Time
T_M	Matrix of the mapping from $O_x x_{R1} x_{R2} x_{R3}$ to $O_\eta x_{\eta 1} x_{\eta 2} x_{\eta 3}$
T_ε	Transformation matrix of strains from global coordinate system to local coordinate system
T_L	Transformation matrix of strains from $O_\eta x_{\eta 1} x_{\eta 2} x_{\eta 3}$ to $O_x x_{R1} x_{R2} x_{R3}$
$u_{b1/2}$	Displacement components along x_1 direction due to bending moment M_2
u_{bi}	Components of displacements of beam
${}^t u_i$, ${}^{t+\Delta t} u_i$	Component of displacement vector from initial position at time 0 to configuration at time t, and $t+\Delta t$
u_i	Increment in displacement component, $u_i = {}^{t-\Delta t} u_i - {}^t u_i$

${}^{t}u_i^k$	Displacement component of nodal point k in configuration at time t
u_i^k	Increment in ${}^{t}u_i^k$
${}_{t}u_{i,j}$, ${}_{t+\Delta t}u_{i,j}$	Derivative of displacement increment with respect to co-ordinate ${}^{t}x_j$ and ${}^{t+\Delta t}x_j$
$\bar{u}_{pi}$	Displacement components of a single layered plate along x_i direction
u_{pi}	Displacement components of an equivalent laminated plate
U_b	Strain energy of the tri-axial woven fabric structure
U_p	Strain energy of the equivalent plate
U_t	Total strain energy of the beam structure
${}^{t}V$, ${}^{t+\Delta t}V$	Volume of body in configuration at time t and $t+\Delta t$
V_2, V_3	Shear forces in x_2 and x_3 directions
V_p	Volume of equivalent plate
${}^{t}\mathbf{V}_q^k$ ${}^{t}\mathbf{V}_s^k$ ${}^{t}\mathbf{V}_r^k$	Directional unit vectors of the beam cross-section at a node k at time t
$\mathbf{V}_q^k$ $\mathbf{V}_s^k$ $\mathbf{V}_r^k$	Increments of directional unit vectors of the beam cross-section at a node k
${}^{t+\Delta t}W$	External virtual work expression corresponding to configuration at time $t+\Delta t$
${}^{t}x$, ${}^{t+\Delta t}x$	Cartesian co-ordinate in configuration at time t and $t+\Delta t$
${}^{t}x_i^k$, ${}^{t+\Delta t}x_i^k$	Cartesian co-ordinate of nodal point k in configuration at time t and $t+\Delta t$
${}^{0}_{t}x_{i,j}$, ${}^{t}_{0}x_{i,j}$	Derivative of co-ordinate in configuration at time 0 and t with respect to co-ordinates ${}^{0}x_j$ and ${}^{t}x_j$

${}_0^t\mathbf{X}$	Deformation gradient of the configuration at time t referred to configuration at time 0
Z	Initial rise parameter of a curved beam
δ	Variation
ΔL	Length of hexagon in tri-axial structure
ε_0	Strain of the reference plane of the beam
$\varepsilon_{1/2}$	Strain in x_1 direction due to bending moment M_2
${}_0^t\varepsilon_{ij}$	Component of Green-Lagrange strain tensor in configuration at time t, referred to configuration at time 0
${}_t^{t+\Delta t}\varepsilon_{ij}$	Component of Green-Lagrange strain tensor in configuration at time $t+\Delta t$, referred to configuration at time t
${}_t\varepsilon_{ij}$	Component of strain increment Green-Lagrange tensor referred to configuration at time t
ε_{pij}	Lagrangian strain components of the equivalent plate
$\sigma_{1/2}$	Stress corresponding to strain $\varepsilon_{1/2}$
σ_{pij}	Stress components of the equivalent plate
${}_t\eta_{ij}$	Component of non-linear part of strain increment of configuration at time t.
${}^0\rho, {}^t\rho$	Specific mass of body in configuration at time 0, and t
${}^t\tau_{ij}$	Component of Cauchy stress tensor in configuration at time t Matrices
${}^t\boldsymbol{\tau}$	Cauchy stress matrix and vector of in configuration at time t
ξ	Parameter of beam equation

v_{LT}, v_{LT}	Poisson's ratio of composite tow
v_{p1}, v_{p2}	Poisson's ratio of tri-axial woven fabric structure
θ	Fiber or tow orientation
$\theta_1^k, \theta_2^k, \theta_3^k$	Increments of the rotations of the local coordinate system about global coordinate system at node k
θ_{b2}, θ_{b3}	Cross-sectional rotations
κ	Change in curvature of a beam

Chapter 1

Introduction

1.1 Tri-axial composite structure

Due to their attractive properties such as light weight, high strength, high stiffness, low density, etc., composite materials have been increasingly used in many engineering fields such as aerospace, automobile, sports equipment, and marine structures. It is also well known that textile fabric composites have been attractive for industrial applications as a reinforcement of composite materials. For example, the composite materials reinforced with woven and braided fabric preforms have been considered for potential structural applications in the aircraft and automotive industries. Fabric-reinforced textile composites potentially have better out-of-plane stiffness, strength, and toughness properties than laminates composed of plies. Among these textile fabrics, tri-axial woven fabrics have many attractive properties. It has been stated [1] that the tri-axial woven fabrics have more isotropic responses to both tensile and shear deformations compared with the conventional biaxial fabrics. In addition, the tri-axial woven fabrics are stiffer and easier to handle. Consequently, tri-axial woven fabrics can also be individually used in some composite structures such as satellite dishes.

In this application, the tri-axial woven fabric composite used for a satellite dish is a single-ply material made from carbon fibers and epoxy. It is composed of three carbon fiber tows woven at 0^0, 60^0 and 120^0 orientations and impregnated with resin. The resin is

also used between the interlaced parts of the tows to bond the tows together. A portion of a photograph of this tri-axial woven fabric composite structure is shown in Fig. 1.1. It is a flat structure. In the application of the satellite dishes, it is curved and is subjected to transverse pressure. However, for convenience, a flat tri-axial structure will be studied in the present dissertation since the in-plane loading applied a flat structure may be transformed to transverse loading applied to a structure with curvature.

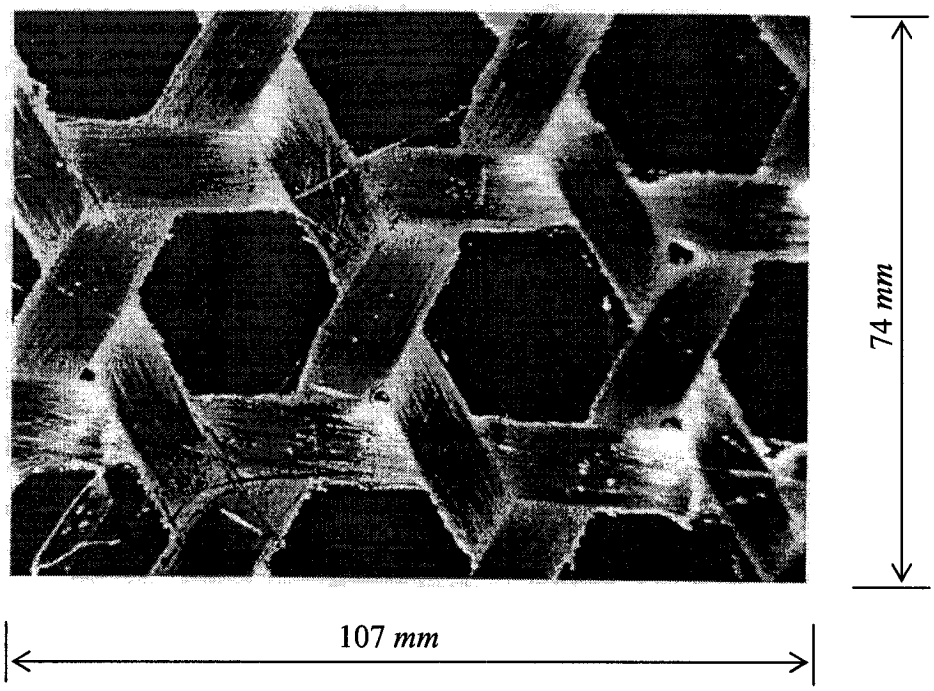

Fig. 1. 1: A photograph of tri-axial woven fabric composite structure. Scale: 1:13.45

A typical larger sized tri-axial structure is shown in Fig. 1.2. It can be seen in these figures that holes occupy more than 50% of the surface area of the structure. These holes reduce the mass of the material and at the same time allow the escape of impacting air, which in turn reduces the load to be supported.

For design purposes, it is of interest to understand the mechanical behavior of the tri-axial composite structure. Works on the characterization of the mechanical properties

of the materials such as the determination of elastic modulus, deflection due to bending and thermal expansion coefficient have been carried out by Qi Zhao and S.V. Hoa [2-6]. Due to the complex nature of the structure, it is of great interest to understand its stability

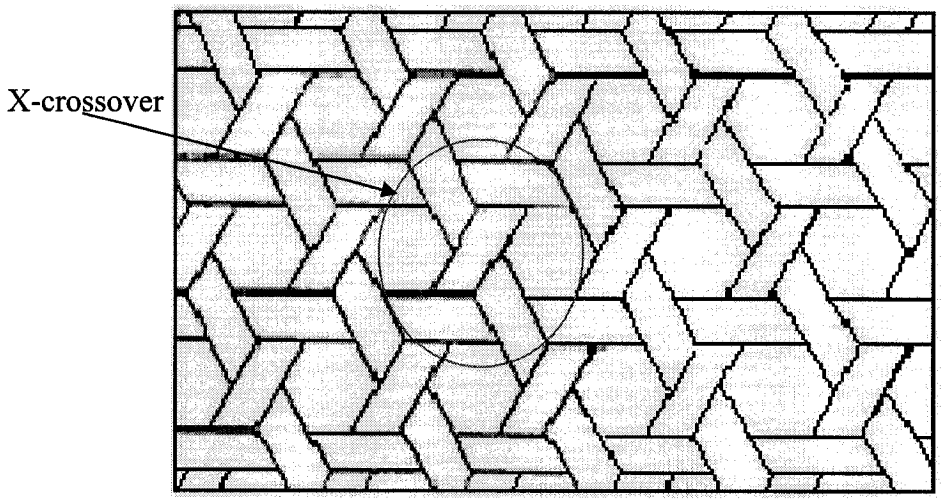

Fig. 1. 2: Tri-axial woven fabric composite structure

when subjected to compressive loads because the satellite dish will be subjected to in-plane compressive loads during its service. When the loading becomes larger or reaches its critical value, the satellite dish may undergo failure due to instability or buckling. This is the objective of the present study, namely the buckling behavior of the tri-axial composite structure subjected to in-plane compressive loading.

1.2 Decomposition of the tri-axial structures into simple models

The tri-axial woven fabric composite structure consists of three yarns interlacing one over the other along the three directions. It is an array of cells of hexagonal shape or

a series of X-crossovers connected to each other. The X-crossover is so named since it has the shape of the capital "X" and is composed of four interlaced tows woven with two tows at 0^0 orientations and two tows one each in directions of 60^0 and 120^0 as shown in Fig. 1.2. The hexagonal shape of the structure is the basic tri-axial structure constituting the whole tri-axial woven fabric composite structure. The basic tri-axial structure as shown in Fig. 1.3 is composed of six woven intersected tri-axial curved composite tows which are bonded at their interlaced parts by resin. The more complicated and larger sized tri-axial composite structure with more interlaced tows can actually be obtained by either adding more X-crossovers to the basic structure horizontally to obtain a rectangular shape of configuration, or by adding equal number of X-crossovers to the basic tri-axial structure both vertically and horizontally to obtain a quasi-square configuration (here quasi means almost but not exactly the square in-plane shape).

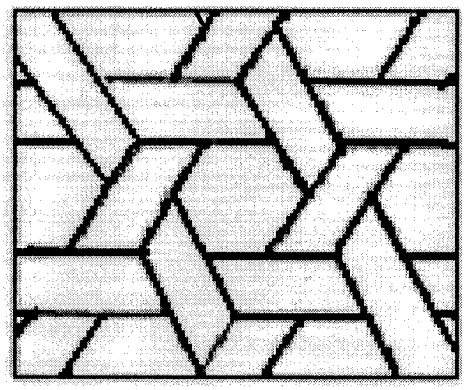

Fig. 1. 3: Basic tri-axial composite structure with six woven intersected curved tows

The thus obtained tri-axial woven fabric composite structure is very complicated. It is very difficult to perform its buckling analysis analytically. Therefore, some numerical methods have to be used to investigate its buckling behavior. However, due to

the limited memory of the personal computer, the numerical analysis of the buckling behavior for a large sized tri-axial composite structure is impossible. In order to study the buckling behavior of tri-axial woven structure subjected to in-plane loading condition, it is appropriate to examine the behavior of a representative basic tri-axial structure of the whole structure. Based on the results obtained from a basic tri-axial structure, the buckling behavior of the modified basic tri-axial structure that is obtained by adding one or two X-crossovers to the basic tri-axial structure horizontally or enlarged basic tri-axial structure that is obtained by adding four X-crossovers both horizontally and vertically, two each in both directions can be analyzed next. The understanding of the behavior of these tri-axial structures may then be extended to understand the behavior of the larger structure.

In order to arrive at the analysis of the basic tri-axial structure, it is necessary to analyze first simpler structures to build up the experience and the knowledge base. Also it would be easier to check the results at different steps. The basic structure is composed of a simpler structure: the so called unit cell. A representative unit of the tri-axial woven fabric composite structure can be the one shown in Figure 1.4. It consists of three curved tows interlaced over each other along the corresponding directions. The resin representing the adhesive layer is put between the interlaced parts of the two tows. It can be seen easily from this figure that a further simpler form of this tri-axial structure is the two intersected curved tow structure. Therefore, the subsequent analysis of the tri-axial structure will be the structure with two curved tri-axial tows connected with each other by resin. This structure is shown in Fig. 1.5. There is only one connection between two tows and this connection is positioned at mid-lengths of the tows for the sake of symmetry.

This situation is not a representative of the unit cell in Figure 1.4, but it serves to give some insight into the interaction between two tows. Further division of the two tow structure shown in Fig. 1.5 should be an individual curved tri-axial tow structure. Fig. 1.6 can be one of the representatives of the individual curved tri-axial tow structure. In order to simulate the curvature of the tow and its wave like form in the actual structure, a type of sinusoidal curve is depicted in Fig. 1.6 to approximate the central line of the individual curved tri-axial tow. This is the simplest form of the curved tri-axial tow structure.

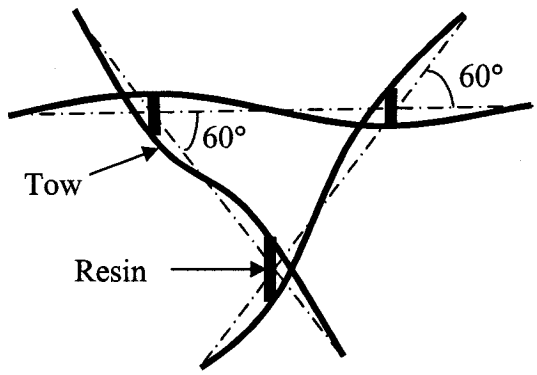

Fig. 1. 4: Tri-axial woven tow structure with three intersected curved tows

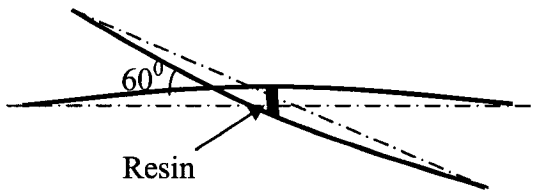

Fig. 1. 5: Composite tow structure with two intersected curved tows

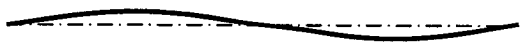

Fig. 1. 6: Simplest curved composite tow structure

For the individual curved tri-axial tow structure, the dimensions of the cross-section of the tow are only 0.2×0.84 *mm*, but its length is much larger than these two dimensions. The ratio of the dimension of the cross-section of a tow to its length is very small. At this point, we can consider the individual tow to behave like a beam. Besides, because the thickness of the tow is also very small compared to other two dimensions and the real cross-section is very flat, this beam can be considered as thin beam. Therefore, the individual curved tri-axial tow can be considered as a thin curved beam, while the tri-axial woven fabric composite tow structures can be modeled as their corresponding curved beam structures.

As for the resin at the cross over of the tows used as an adhesive layer, it can be represented by a bar. The further assumptions and corresponding explanation will be made in the corresponding chapters.

Above all, it can be concluded that the tri-axial woven fabric composite tow structures can be modeled as their corresponding curved beam structures with resin bars at the cross over of the beams.

1.3 Stability analysis of a single curved composite beam

For a curved beam structure, when it is loaded by compression, it may undergo large deformation, including large displacements and large rotations. In order to simulate its deformation effectively, the curved beam has to be modeled with six degrees-of-freedom. In addition, the kinematic relations between displacements and rotations of the

structure and loads applied will no longer be linear. Thus, a non-linear analysis has to be performed.

Non-linear analyses can be classified into three types: materially-nonlinear analysis, geometrically-nonlinear analysis and combination of both. As a start, we will only perform the geometrically-non-linear buckling analysis.

For the curved beam model, the cross-section shape of the tow is assumed to be rectangular. This is slightly different from the actual cross-section of the tow which is elliptic in reality. However, the real cross-section is fairly flat and for buckling analysis, the approximation of rectangular cross section may be acceptable. This simplifies the analysis greatly. The torsional rigidity of the tow is not taken into consideration. This implies negligible effects of stress components corresponding to deformation of the cross-section in its own plane. In modeling, we also assume that plane sections originally normal to the centerline axis remain plane and undistorted under deformation but not necessarily normal to this axis. This kinematic assumption does not allow for warping effects in torsion.

1.4 Literature survey

Tri-axial woven fabric technology has been around for many years. Considerable effort has been made to investigate the material properties of the tri-axial woven fabric composite material and to perform its structural stress analysis. For example, many researchers [1,2,4,5,7-18] have developed models for the prediction of the mechanical properties of tri-axial materials. Some of them [3,17] have conducted experiments to determine the material constants. Others [2,6,19] have developed models to perform

stress analysis and failure prediction. None of them has conducted buckling analysis of tri-axial woven fabric composite tow structures. Since in some applications of tri-axial woven structures, for example, the satellite dish mentioned before, the structure may undergo large deformation under the action of compression loads and may fail due to buckling of the structure, it is very important to conduct this kind of analysis. The "curved beam model" for the tri-axial woven fabric composite structure has been discussed in Section 1.2. For the present literature survey, we will mainly focus on the buckling analysis of the curved beam and curved beam structures.

Thin beams of different configurations and cross-sectional shapes constitute a technically important class of structural components in engineering. Because of their structural efficiency and as an independent structural component or stiffeners of plates and shells, thin-walled beams of different cross-sectional shapes are widely used in different engineering applications. An important subject in designing these structures is the accurate prediction of their buckling strength, which has drawn considerable attention over the years. Many established theories [20,21] and finite element models [22-25] have been proposed for the buckling analysis of a straight thin beam, and usually the effect of non-uniform or warping-torsional behavior was considered [21,24,25] to tackle the thin beam more effectively. In the case of the straight thin beam, the generalized stress-strain relations for compression, flexure and warping are all uncoupled. Such uncoupling effect leads to great simplicity in the buckling behavior of the straight thin beams which may only buckle by flexure, by torsion or by a combination of both.

However, in the instability analysis of an initially curved beam, the generalized stress-strain relations for compression, flexure and warping are all coupled. The use of

curvilinear coordinates results in difficulties in dealing with high-order terms in the non-linear strains and numerical techniques (for example, numerical volume integral) of the virtual work equation, since the curvature should be taken into account correctly. In general, the effect of curvature on the final numerical results is very significant. Hence, the analysis of the curved beam or curved beam structure is more difficult than that of a straight beam or straight beam structure.

Since the first applications of computers to non-linear analysis of the structures, various non-linear beam elements have been presented [26-32]. The stiffness coefficients were derived by Morris [33] for a curved beam using the equilibrium conditions with the warping effect neglected. The effect of warping was included by El-Amin and Brotton [34] in their curved beam element for the bending and torsional behaviors. Using the exact displacement field for the linear problems, Chaudhuri and Shore [35] and Yoo [36] derived individually a finite element for curved beams of a thin-walled section. The curved beam element derived by El-Amin and Kasem [37] employed a higher-order polynomial function for the angle of twist. Considering the coupling between the in-plane and out-of-plane loads and deformation, Lebeck and Knowlton [38] developed a finite element for a circular ring with nonsymmetrical sections.

In the 1980s, a few researchers devoted their effort to the analytical studies of the curved beam. For example, Yoo [39] studied the flexural-torsional stability of curved beam; Yoo and Pfeiffer [40] carried out the elastic stability of curved beams; Yang and Kuo [41] conducted the static stability for curved thin walled beam. However, the results given by these researchers were found to be in conflict with those obtained from the classical solutions given by Timoshenko [20] and Vlasov [21]. Some later papers

explained the reasons of these large discrepancies [42-46]. It was pointed out [42, 45] that the errors existed in the analytical equations [39, 40], which were caused by directly substituting curvature terms of the curved beam into the strain and potential energies of the straight beam. The wrong results obtained by Yang and Kuo [41] were owing to the neglect of the contribution from the radial forces [43, 46]. In fact, most of these errors can be attributed to the omission of one or more large rotation and high-order curvature terms in the derivation of the non-linear strain-displacement relations. Saleeb and Gendy [47] in 1991 presented the second-order non-linear strain expressions for the finite rotations. However, there were some errors in their second-order terms of non-linear strain expressions for which may lead to the completely wrong critical buckling load in some cases [48]. A year later in 1992, Saleeb, Chang and Gendy [49] developed a simple, two-noded finite element model for the three-dimensional buckling analysis of beam assemblages. After that, Saleeb and Gendy [50] in 1994 developed a model for the fully non-linear analysis of thin-walled framed structures by using the simple, two-node, C^0-model developed in [49]. The corresponding governing equations were obtained based on a consistent linearization of an incremental mixed variational principle of modified Hellinger/Reissner type with independent assumptions for displacement and strain fields. All coupled significant modes of deformations, i.e., stretching, bending, shear, torsion and warping, were accounted for in the generalized-beam theory.

Based on the above models and discussions [39-47], Hu, et. al [48] derived the correct second-order terms in the non-linear strain expressions for finite rotations and showed the effects of these second-order terms on the critical buckling load. The researchers also developed two kinds of displacement-based iso-parametric curved beam

elements without restriction to shallow or deep circular beam problems and applicable to a wide range of thicknesses. These iso-parametric curved beam elements could be used for buckling analysis including shear and warping effects and for the investigation of the influence of the membrane/shear/warping locking phenomenon on the spatial buckling analysis of curved beams.

To eliminate the so-called membrane/shear/warping locking in the straight and curved beam analysis, some other extensive research has also been conducted [51-57]. Chen and Blanford [51] presented an iso-parametric straight beam element including the warping deformation with selective reduced integration evaluation. Dvorkin, Celentano, Cuitino and Gioai [52] suggested a C^1-type straight beam element based on Vlasov's solutions for non-uniform torsion problem. Hence, the interpolation functions were similar to those proposed by Yang et al. [46]. Moreover, two kinds of linear and quadratic iso-parametric curved beam elements were proposed [53, 54] on the basis of Timoshenko's beam theory in which warping deformation is neglected. A so-called strain element was proposed by Ashwell et al. [55, 56], which can eliminate the locking. The displacement functions of this element were derived from the strain-displacement relations based on Euler-Bernoulli beam theory which does not include shear effect and is not applicable to the beams with high depth. Choi and Lim [57] extended this kind of element by considering the transverse shear deformation based on Timoshenko's beam theory without consideration of warping deformation.

In the development of a geometrically non-linear finite three-dimensional beam element, an updated Lagrangian and a total Lagrangian formulations were presented by Bathe et al. [58, 59]. They were based on the Lagrangian incremental equilibrium

equations from continuum mechanics theory and were used in elastic, elastic-plastic, static and dynamic analysis. Since then, many researchers used and extended these methods for buckling analysis of curved beam element. Here are some of the examples: Ferguson and Clark [60] introduced a family of 2- and 3-dimensional superparametric curved beam elements as a special form of general 2- and 3-dimensional isoparametric continuum elements and studied the buckling problems of the curved beam using Lagrangian approach. Frey and Cescotto [61] used non-linear nodal rotations to formulate incremental total Lagrangian description. Surana and Sorem [62] developed a geometrically non-linear formulation using the total Lagrangian approach based on the basic curved beam geometry and configuration given by Ferguson and Clark [60]. This formulation allows large load steps and permits large rotations between successive load increments with good convergence. More examples of the publications of the Lagrangian approach are included in previous references.

In the implementation of the Lagrangian approach or formulations, appropriate displacement interpolation functions are the key point. It can eliminate membrane/shear/ warping locking by introducing appropriate terms in the interpolation functions. It can be applied to all kinds of non-linear problems, including geometrically non-linear, materially non-linear or the combination of both geometrically and materially non-linear problem. Better interpolation functions can produce more accurate results. For the interpolation functions of the curved beam elements, Bathe [63] presented 3- and 4-node isoparametric element interpolation functions and confirmed that these functions are very effective and efficient for the curved beam elements. Bathe and Bolourchi [64] also proved that updated Lagrangian and total Lagrangian formulations were mathematically the same.

The only difference is that in the total Lagrangian formulation all static and kinematic variables are referred to the initial configuration at time 0, while in the updated Lagrangian formulation all static and kinematic variables are referred to the configuration at time t, i.e., the last known configuration. The two formulations generated the same final element stiffness matrices and nodal point force vectors if the same number of beam elements was employed to model a structure. However, for the beam element, either straight beam element or curved beam element, the updated lagrangian formulation was computationally more effective than the total Lagrangian formulation.

1.5 Objectives of the thesis

The tri-axial woven fabric composite structures may undergo large deformation, including large displacements and large rotations, when subjected to the compression of in-plane loading. Large deformations may cause buckling behavior of the tri-axial composite structures. Since the buckling of a structure may have an adverse effect on the structural performance and may cause instability of the structure or even failure of a structure, the load at which buckling will occur has to be determined. As a start and considering the limitation of PC computer memory and CPU speed, only geometrically non-linear finite analysis will be performed and the buckling behavior of the basic tri-axial structure will be analyzed in the present dissertation.

Hence, the general objectives of the dissertation research are: To develop an effective mechanical and mathematical model of the single layered tri-axial woven fabric composite structure for large displacements and large rotations so that it can be used to perform the geometrically non-linear buckling analysis of the structure; To perform the

corresponding numerical buckling analysis of a series of less complicated and small in-plane sized tri-axial tow structures from which a generalized conclusion can be made. The specific objectives of the study are described as follows:

1. Develop a mechanical model – beam model – to idealize the tows in the tri-axial composite tow structure. This includes the development of a mathematical model – incremental updated Lagrangian formulation – using non-linear continuum mechanics theory. This model can be employed to simulate the large deformation (large displacements and large rotations) procedures of the tri-axial woven fabric structure numerically, and to perform the buckling analysis of the tri-axial structure and to determine its corresponding buckling load.
2. Conduct numerically the buckling analysis of the following structures: composite straight beam, curved beam that is a part of woven fabric tri-axial composite tow structures subjected to different boundary conditions and some simple intersected composite tow structures such as composite structure with two intersected curved tows and unit cell with three intersected curved composite tows in order to gain some insight into the buckling behavior of more complicated tri-axial woven fabric composite structures.
3. Derive the approximate analytical solutions corresponding to each curved composite tow structure using bifurcation theory in order to further confirm the accuracy of the numerical solutions.
4. Perform numerically the buckling analysis of the basic tri-axial woven fabric composite structure subjected to uni-directional loading, including the sensitivity analysis of the buckling load of the basic tri-axial structure to the change in the

boundary conditions and to the imperfection due to initial configuration as well as to the in-plane aspect ratio of the structure.

5. Derive the approximate analytical solutions corresponding to basic tri-axial composite structure subjected to uni-directional loading using multi-layered plate theory in order to provide confirmation to the numerical solutions and to provide simpler ways to obtain the results.
6. Carry out numerically the buckling analysis of the basic tri-axial woven fabric composite structure subjected to bi-directional loading. At the same time, conduct the derivation of the approximate analytical solutions corresponding to basic tri-axial composite structure subjected to bi-directional loading using the principle of energy equivalence in order to make the confirmation to the numerical solutions and to provide simpler ways to obtain the results.
7. Determine buckling behavior of real life larger tri-axial composite structure by extrapolating the results obtained for smaller sized tri-axial composite structure.

1.6 Organization of the thesis

In Chapter one, the tri-axial woven fabric composite structure is decomposed into substructures. This is to carry out the effective numerical buckling analysis for the structure. The objectives of the dissertation are given in the last part of the Chapter.

In Chapter two, the governing equations for the incremental non-linear analysis of the curved beam element and resin element are derived based on the principle of virtual displacements in continuum mechanics theory and updated Lagrangian formulation. The

corresponding techniques used to determine the value of the buckling load are also given in this Chapter.

In Chapter three, approximate analytical solutions for the buckling loads of some simple curved beam structures, including simply-supported individual curved composite beam, simply-supported composite tow structure with two intersected curved beams and simply-supported composite tow structure with three intersected beams, are derived in order to provide confirmation to the numerical non-linear finite element solution to the buckling loads for these structures and more importantly to prove the accuracy of the computer software especially developed for the present project.

In Chapter four, buckling analysis for these simple curved beam structures is conducted using the incremental non-linear finite element analysis model developed in Chapter two. The confirmation to the numerical solution is made by comparing both numerical and analytical solutions of these structures. These analyses provide some insight into the buckling behavior of more complicated tri-axial woven fabric composite structures.

In Chapter five, the buckling analysis of the basic tri-axial structure subjected to uni-directional and bi-directional loading is carried out numerically. A parametric study of the basic tri-axial structure is also performed to study the influence of the change in parameters of aspect ratio of the tri-axial structure and the change in boundary conditions on the buckling load and sensitivity of the buckling behavior to the imperfections due to initial configuration of the structure.

In Chapter six, an approximate analytical solution for the buckling load of uni-directionally loaded and bi-directionally loaded basic tri-axial structure is developed

using multi-layered plate theory and the equivalent energy method. Confirmation to the numerical results obtained in Chapter five is made. Approximate analytical solution can be used as a simpler way to obtain the buckling load analytically. For application purpose, extrapolation of the results obtained for smaller tri-axial composite structures is made to determine buckling behavior of real life larger tri-axial composite structures.

In Chapter seven, major conclusions of the research are made.

In Chapter eight, the highlights of the research and recommendations for the future work are presented.

Chapter 2

Curved beam and resin structure

In this Chapter, the equilibrium equation for a combined curved beam and resin layer will be presented based on the principle of virtual displacements in continuum mechanics theory. The governing equations for the incremental non-linear analysis of the curved beam element and resin element will be derived by using updated Lagrangian formulation. These equations will be used in the following chapters to perform the buckling analysis of the different curved beam structures.

2.1 Principle of virtual displacements [63]

The basis of the displacement-based finite element solution is the principle of virtual displacements. Consider the motion of a general body in a fixed Cartesian co-ordinate system as shown in Fig. 2.1, and assume that the body can experience large displacements and large strains. The aim is to evaluate the equilibrium positions of the body at the discrete time points $0, \Delta t, 2\Delta t, 3\Delta t, \cdots$, where Δt is an increment in time. To develop the solution strategy, assume that the solutions measured in the co-ordinate system corresponding to all time steps from time 0 to time t, inclusive, have been obtained. Then the solution process for the next required equilibrium position corresponding to time $t + \Delta t$ is typical and is applied repetitively until the complete

solution path has been solved for. Hence, in the analysis we follow all the particles of the body in their motion, from original to the final configuration of the body.

Consider the equilibrium of the body in Fig. 2.1 again at time $t + \Delta t$. The principle of virtual displacements requires that

$$\int_{t+\Delta t V} {}^{t+\Delta t}_{t}S_{ij}\ \delta\ {}^{t+\Delta t}_{t}\varepsilon_{ij}\ d\ {}^{t+\Delta t}V = \delta\, {}^{t+\Delta t}W \tag{2-1}$$

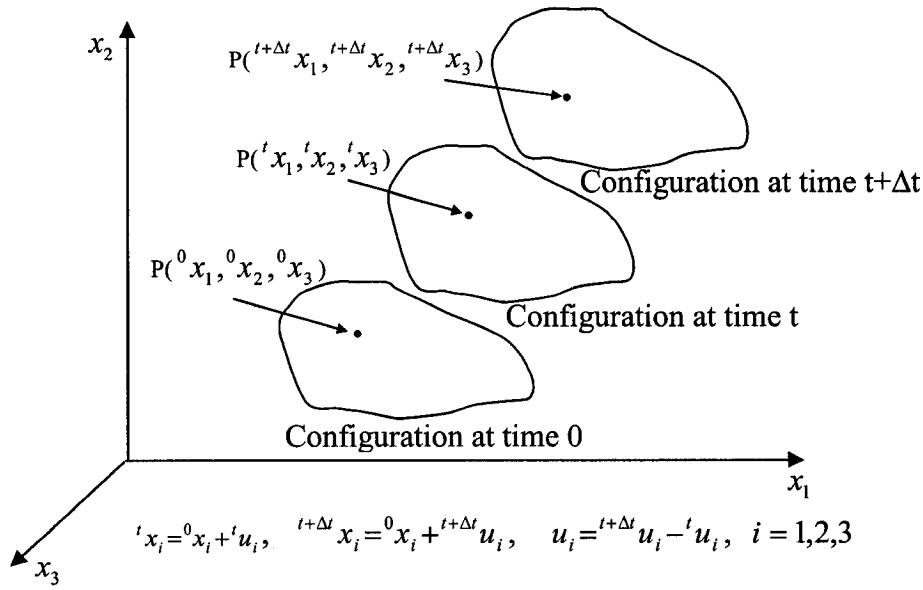

Fig. 2. 1: Motion of body in Cartesian co-ordinate system

where ${}^{t+\Delta t}_{t}S_{ij}$ are Cartesian components of Second Piola-Kirchhoff stress tensor and ${}^{t+\Delta t}_{t}\varepsilon_{ij}$ are Cartesian components of the Green-Lagrange strain tensor corresponding to the deformatiom from the configuration at time t to the configuration at time $t + \Delta t$ and referring to the configuration at time t. ${}^{t+\Delta t}W$ is the total external virtual work. The left hand side of equation (2-1) includes the contributions from both resin and tows of the

structures. Finite element models for both of them will be presented in the following two sections, respectively. Equation (2-1) can not be solved directly since the configuration at time $t+\Delta t$ is unknown.

2.2 Formulation for tow elements

The elements constituting the tri-axial woven fabric composite structure are curved beams. In this section, formulation for a general three-dimensional curved beam element for finite element analysis will be presented.

2.2.1 Description of element geometry

Consider a general three-dimensional curved beam of rectangular cross section as shown in Fig. 2.2. Co-ordinates x_1, x_2, x_3 form the global co-ordinate system, η_1, η_2, η_3 represent the local co-ordinate system attached to the beam (so called body attached co-ordinate system), and r,s,q is the natural co-ordinate system. The section dimensions can be specified by a_k and b_k and a set of vectors ${}^t\mathbf{V}_q^k$, ${}^t\mathbf{V}_s^k$ and ${}^t\mathbf{V}_r^k$ at a node k at time t (where the left superscript t could also be 0 or $t+\Delta t$, referring to time 0 or time $t+\Delta t$, respectively. The same notation will be employed in the following sections). The directions of ${}^t\mathbf{V}_q^k$, ${}^t\mathbf{V}_s^k$ can be conveniently selected to be the q, s directions at time t. In this case the Cartesian co-ordinates (x_1, x_2, x_3) of a point P(r,s,q) within the element for a m-noded element at time t can be written as

$$ {}^t x_i = \sum_{k=1}^{m} h_k \, {}^t x_i^k + \frac{q}{2} \sum_{k=1}^{m} a_k \, h_k \, {}^t V_{qi}^k + \frac{s}{2} \sum_{k=1}^{m} b_k \, h_k \, {}^t V_{si}^k \qquad i=1,2,3 \qquad (2\text{-}2) $$

where h_k (k=1,2,3,4) is the 4-node beam element interpolation functions [63].

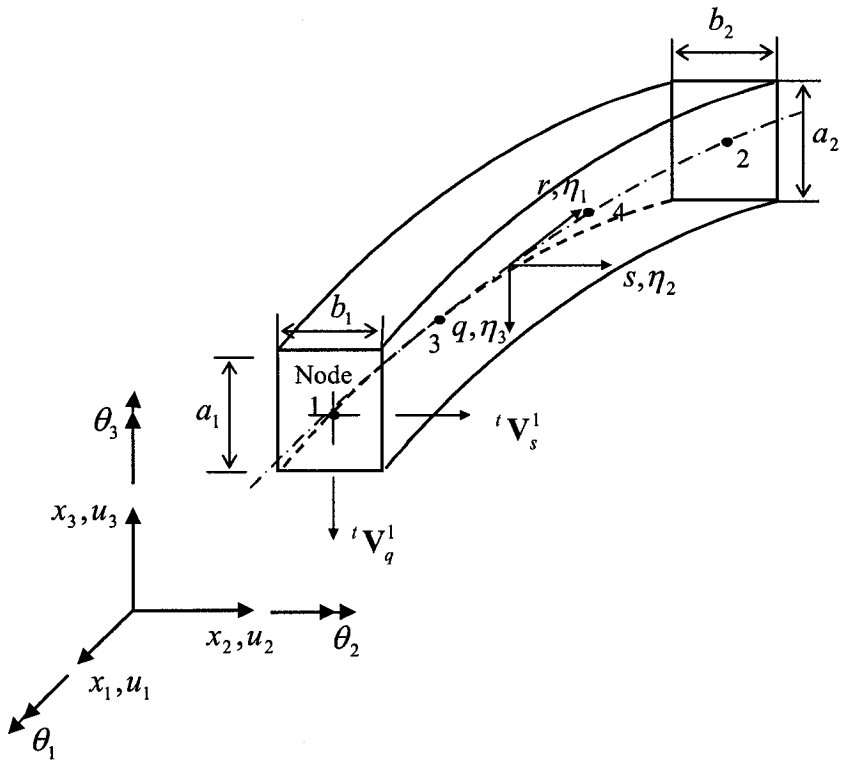

Fig. 2. 2: Three-dimensional curved beam element

2.2.2 Displacement approximation of element

The displacement field follows from the assumptions that the cross-section normals remain straight during deformation. In the iso-parametric element solution, the displacements approximation and their increment at a point P(r,s,q) within the element for a m-noded element at time t are interpolated in terms of the nodal translations ${}^tu_i^k$, i = 1,2,3 along the global co-ordinate axes and the rotations ${}^t\theta_i^k$, i = 1,2,3 about global co-ordinate axes using

$${}^tu_i={}^tx_i-{}^0x_i=\sum_{k=1}^{m}h_k\,{}^tu_i^k+\frac{q}{2}\sum_{k=1}^{m}a_kh_k({}^tV_{qi}^k-{}^0V_{qi}^k)+\frac{s}{2}\sum_{k=1}^{m}b_kh_k({}^tV_{si}^k-{}^0V_{si}^k) \qquad (2\text{-}3)$$

$$u_i = {}^{t+\Delta t}u_i - {}^{t}u_i = \sum_{k=1}^{m} h_k u_i^k + \frac{q}{2}\sum_{k=1}^{m} a_k h_k V_{qi}^k + \frac{s}{2}\sum_{k=1}^{m} b_k h_k V_{si}^k \tag{2-4}$$

where

$$V_{qi}^k = {}^{t+\Delta t}V_{qi}^k - {}^{t}V_{qi}^k \tag{2-5}$$

$$V_{si}^k = {}^{t+\Delta t}V_{si}^k - {}^{t}V_{si}^k \tag{2-6}$$

are the increments of unit directional vectors at node k and can be obtained by using the following second-order approximations

$$\mathbf{V}_q^k = \boldsymbol{\theta}_k \times {}^{t}\mathbf{V}_q^k + \frac{1}{2}\boldsymbol{\theta}_k \times (\boldsymbol{\theta}_k \times {}^{t}\mathbf{V}_q^k) \tag{2-7}$$

$$\mathbf{V}_s^k = \boldsymbol{\theta}_k \times {}^{t}\mathbf{V}_s^k + \frac{1}{2}\boldsymbol{\theta}_k \times (\boldsymbol{\theta}_k \times {}^{t}\mathbf{V}_s^k) \tag{2-8}$$

By substituting equations (2-5), (2-6), (2-7) and (2-8) into equation (2-4), incremental displacements can be expressed as

$$\begin{aligned} u_i = {}^{t+\Delta t}u_i - {}^{t}u_i = {} & \sum_{k=1}^{m} h_k u_i^k + \frac{q}{2}\sum_{k=1}^{m} a_k h_k (\theta_{i+1}^k {}^{t}V_{q(i+2)}^k - \theta_{i+2}^k {}^{t}V_{q(i+1)}^k) + \\ & \frac{s}{2}\sum_{k=1}^{m} b_k h_k (\theta_{i+1}^k {}^{t}V_{s(i+2)}^k - \theta_{i+2}^k {}^{t}V_{s(i+1)}^k) - \\ & \frac{q}{4}\sum_{k=1}^{m} a_k h_k (((\theta_{i+1}^k)^2 + (\theta_{i+2}^k)^2) {}^{t}V_{qi}^k - \theta_i^k \theta_{i+1}^k {}^{t}V_{q(i+1)}^k - \theta_i^k \theta_{i+2}^k {}^{t}V_{q(i+2)}^k) - \\ & \frac{s}{4}\sum_{k=1}^{m} b_k h_k (((\theta_{i+1}^k)^2 + (\theta_{i+2}^k)^2) {}^{t}V_{si}^k - \theta_i^k \theta_{i+1}^k {}^{t}V_{s(i+1)}^k - \theta_i^k \theta_{i+2}^k {}^{t}V_{s(i+2)}^k) \\ = {} & u_{Li} + u_{Ni} \end{aligned} \tag{2-9}$$

where $i = 1,2,3$, and $i+1$ takes the value of 1 when $i = 3$ and $i-1$ takes the value of 3 when $i = 1$; u_{Li}, u_{Ni} are linear terms and non-linear terms specified by single underlining and double underlining in equation (2-9), respectively.

2.2.3 Strain-displacement relationship

Green-Lagrangian strain tensor in the configuration at time t referred to the initial configuration is defined as

$$ {}^{t}_{0}\boldsymbol{\varepsilon} = \frac{1}{2}({}^{t}_{0}\mathbf{X}^{T}\ {}^{t}_{0}\mathbf{X} - \mathbf{I}) \tag{2-10} $$

where deformation gradient at time t is

$$ {}^{t}_{0}\mathbf{X} = \begin{bmatrix} {}^{t}_{0}x_{1,1} & {}^{t}_{0}x_{1,2} & {}^{t}_{0}x_{1,3} \\ {}^{t}_{0}x_{2,1} & {}^{t}_{0}x_{2,2} & {}^{t}_{0}x_{2,3} \\ {}^{t}_{0}x_{3,1} & {}^{t}_{0}x_{3,2} & {}^{t}_{0}x_{3,3} \end{bmatrix} \tag{2-11} $$

in which comma subscript denotes the differentiation with respect to ${}^{0}x_{i}$.

Considering the strain increments ${}^{t+\Delta t}_{t}\varepsilon_{ij}$, the following relations hold

$$ {}^{t+\Delta t}_{t}\varepsilon_{ij} = {}_{t}\varepsilon_{ij} \tag{2-12} $$

$$ {}_{t}\varepsilon_{ij} = {}_{t}e_{ij} + {}_{t}\eta_{ij} \tag{2-13} $$

in which the linear parts of strain increments are

$$ {}_{t}e_{ij} = \frac{1}{2}({}_{t}u_{i,j} + {}_{t}u_{j,i}) \tag{2-14} $$

the non-linear parts of strain increments are

$$ {}_{t}\eta_{ij} = \frac{1}{2}\ {}_{t}u_{k,i}\ {}_{t}u_{k,j} \tag{2-15} $$

where the comma subscript denotes the differentiation with respect to ${}^{t}x_{i}$.

2.2.4 Stress-strain relationship

Stresses and strains employed in Updated Lagrangian formulation are Second Piola-Kirchhoff stresses, Cauchy stresses and Green-Lagrange strains.

The relation between the second Piola-Kirchhoff stress tensor in the configuration at time t and measured in the configuration at time 0 and Green-Lagrange strain tensor at time t referred to the initial configuration can be expressed as

$$ {}_0^tS_{ij} = {}_0^tC_{ijrs}\ {}_0^t\varepsilon_{rs} \tag{2-16} $$

where ${}_0^tC_{ijrs}$ is the constitutive tensor.

The relation between the second Piola-Kirchhoff stresses and Cauchy stresses is as follows

$$ {}^t\tau_{mn} = \frac{{}^t\rho}{{}^0\rho}\ {}_0^tx_{m,i}\ {}_0^tS_{ij}\ {}_0^tx_{n,j} \tag{2-17} $$

where ${}^t\rho$ and ${}^0\rho$ are mass densities of the element in the configuration at time t and time 0, respectively. The relation between them is as follows

$$ \frac{{}^t\rho}{{}^0\rho} = \frac{1}{\det({}_0^t\mathbf{X})} \tag{2-18} $$

The incremental stress decomposition is

$$ {}_t^{t+\Delta t}S_{ij} = {}^t\tau_{ij} + {}_tS_{ij} \tag{2-19} $$

where ${}^t\tau_{ij}$ is Cartesian components of the Cauchy stress tensor and ${}_tS_{ij}$ is Cartesian components of Second Piola-Kirchhoff stress increment tensor referred to the configuration at time t.

2.3 Formulation for resin layer element

The resin layer is placed between the two interlaced tows and is used to bond the tows together. The bonded tows constitute an integral body. In this section, basic assumptions for resin layer element will be made and the corresponding formulation for finite element analysis will be presented.

2.3.1 Basic assumptions

The thickness of the resin layer is about one-third of the thickness of the tow and has the value of 0.067 *mm*. The horizontal cross-section of the resin layer is a parallelogram as shown in Fig. 2.3. Each side is along one of the interlaced tows, but is

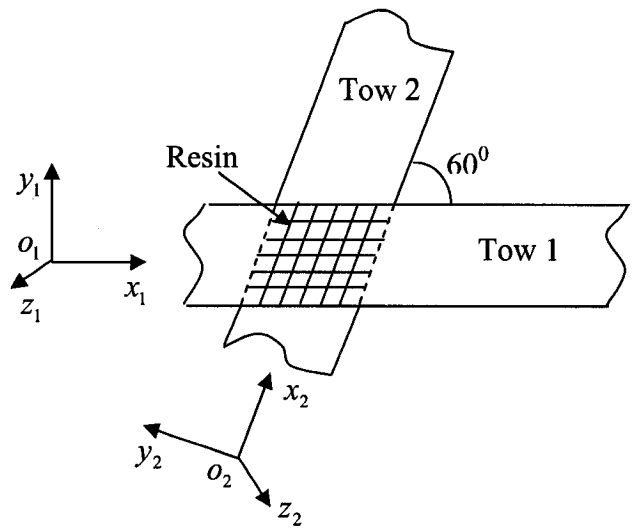

Fig. 2. 3: Tows and resin

intersected with another tow at an angle of 60^0. The dimensions of both sides are 0.87×0.87 *mm*. For the strains of the resin layer, only out-of-plane normal strain and in-plane shear strain are assumed to be non-zero. Details are as follows.

First, the strains of resin layer, $\varepsilon_{\eta_{R2}\eta_{R2}}$ and $\varepsilon_{\eta_{R3}\eta_{R3}}$, in local resin co-ordinate system shown in Fig. 2.4 can be neglected. Actually, no strains of the resin layer at the interfaces between resin and tow 1 along y_1 direction and between resin and tow 2 along y_2 direction, corresponding to $\varepsilon_{y_1y_1}$ and $\varepsilon_{y_2y_2}$ in local beam co-ordinate systems $O_1x_1y_1z_1$ and $O_2x_2y_2z_2$ in Fig. 2.3, will be allowed since the strains of the interlaced tows in these two directions are neglected due to their higher order nature as stated in the previous section.

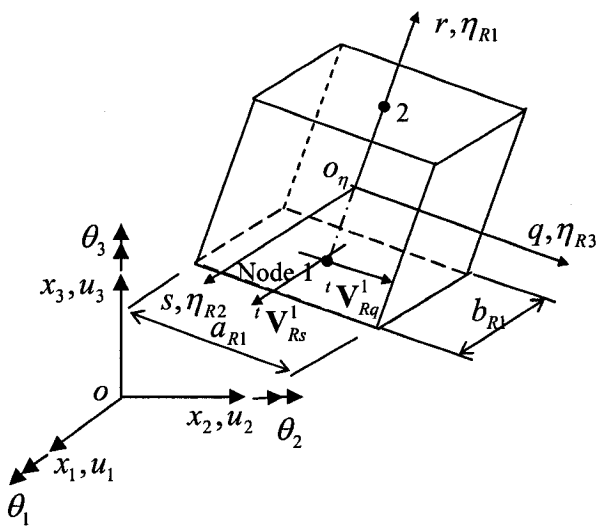

Fig. 2. 4: Two-node resin element

The top tow tends to stretch the resin layer if it deforms downward; while the bottom tow tries to compress the resin layer, and vice versa. Because the thickness of the resin layer is very small compared with the horizontal dimensions of the resin layer, deformation due to compression of bottom part of the resin may cancel a part of the deformation due to tension of the top part of the resin shown in Fig. 2.5. Therefore, the strains of the resin in horizontal plane, corresponding to $\varepsilon_{\eta_{R2}\eta_{R2}}$ and $\varepsilon_{\eta_{R3}\eta_{R3}}$ in local resin co-ordinate system shown in Fig. 2.4, should be of small order of magnitude and will be neglected in the

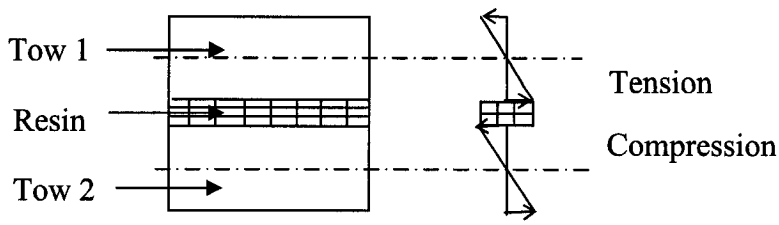

Fig. 2. 5: Deformation of cross-section of tows and resin

present case.

Second, the shear strains, $\varepsilon_{\eta_{R1}\eta_{R2}}$ and $\varepsilon_{\eta_{R1}\eta_{R3}}$, are negligible. This is because the shear deformations of the tows in their local co-ordinate planes $O_1y_1z_1$ and $O_2y_2z_2$ corresponding to tow 1 and tow 2, respectively, are neglected. These planes approximately are corresponding to the two local vertical co-ordinate planes, $O_\eta\eta_{R1}\eta_{R2}$ and $O_\eta\eta_{R1}\eta_{R3}$, of the resin. Therefore, the shear strains, $\varepsilon_{\eta_{R1}\eta_{R2}}$ and $\varepsilon_{\eta_{R1}\eta_{R3}}$, may be of small order of magnitude and can be neglected.

Third, uniform shear strain, $\varepsilon_{\eta_{R2}\eta_{R3}}$, (or no warping due to torsion) will be assumed due to small thickness of the resin. The equation used to express the relation between the shear stress and shear strain is $S_{\eta_{R2}\eta_{R3}} = G_R\varepsilon_{\eta_{R2}\eta_{R3}}$.

Finally, the linear stress-strain relation of the resin, $S_{\eta_{R1}\eta_{R1}} = E_R\varepsilon_{\eta_{R1}\eta_{R1}}$, in local co-ordinate system of the resin is assumed. The displacements of the two intersecting points between the center lines of the two interlaced tows and the resin may be different. It will cause deformation, either stretching or compressing the resin along its thickness. Due to small thickness and large cross-sectional dimensions of the resin, correspondingly, the linear stress-strain relation of the resin will be employed in the present analysis.

2.3.2 Element geometry and displacement description

In order to employ the geometric interpolation functions used in the case of a rectangular cross-sectional beam, the following mapping, which maps the parallelogram on the plane of $x_{R2}x_{R3}$ in the local co-ordinate system $x_{R1}x_{R2}x_{R3}$ into a rectangular on the plane of $\eta_{R2}\eta_{R3}$ in co-ordinate system $\eta_{R1}\eta_{R2}\eta_{R3}$ (body attached, so called mapped local co-ordinate system) as shown in Fig. 2.6 (x_{R1} and η_{R1} are not shown in Fig. 2.6), is used. After the strains are found in global co-ordinate system, they will be transformed into the mapped local system and local system consecutively at Gauss integration points.

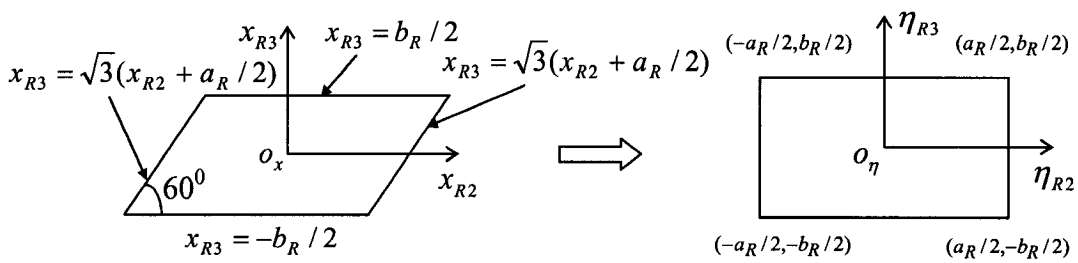

Fig. 2. 6: Mapping from $o_x x_{R1}x_{R2}x_{R3}$ to $o_\eta \eta_{R1}\eta_{R2}\eta_{R3}$

$$\begin{Bmatrix} \eta_{R1} \\ \eta_{R2} \\ \eta_{R3} \end{Bmatrix} = \begin{bmatrix} 1 & 0 & 0 \\ 0 & 1 & -\frac{1}{\sqrt{3}} \\ 0 & 0 & 1 \end{bmatrix} \begin{Bmatrix} x_{R1} \\ x_{R2} \\ x_{R3} \end{Bmatrix} \quad \text{or} \quad \boldsymbol{\eta}_R = \mathbf{T}_M \mathbf{x}_R \tag{2-20}$$

Consider a general three-dimensional two-node bar of rectangular cross section as shown in Fig. 2.4. Co-ordinates $\eta_{R1}, \eta_{R2}, \eta_{R3}$ represent the mapped local co-ordinate system attached to the bar. The cross-sectional dimensions can be specified by a_{Rk} and

b_{Rk}, which are the dimensions of the parallelogram, and a set of vectors ${}^{t}\mathbf{V}_{Rq}^{k}$, ${}^{t}\mathbf{V}_{Rs}^{k}$ and ${}^{t}\mathbf{V}_{Rr}^{k}$ at a node k at time t. The Cartesian co-ordinates (x_1, x_2, x_3) of a point P(r,s,q) within the element for a m-noded element at time t can be written as

$$ {}^{t}x_i = \sum_{k=1}^{m} h_k \, {}^{t}x_i^k + \frac{q}{2}\sum_{k=1}^{m} a_{Rk} h_k \, {}^{t}V_{Rqi}^{k} + \frac{s}{2}\sum_{k=1}^{m} b_{Rk} h_k \, {}^{t}V_{Rsi}^{k} \qquad i=1,2,3 \tag{2-21} $$

where the nodal co-ordinates ${}^{t}x_i^k$ are also the co-ordinates of the nodes corresponding to the related tows. This is because the above mapping did not change the scaling in x_{R1} direction and the co-ordinates of each center of the cross-section.

In the iso-parametric element solution, the displacements approximation and their increment at a point P(r,s,q) within the element for a m-noded element at time t are interpolated in terms of the nodal translations ${}^{t}u_i^k$, $i = 1,2,3$ along the global co-ordinate axes and the rotations ${}^{t}\theta_i^k$, $i = 1,2,3$ about global co-ordinate axes using

$$ {}^{t}u_i = {}^{t}x_i - {}^{0}x_i = \sum_{k=1}^{m} h_k \, {}^{t}u_i^k + \frac{q}{2}\sum_{k=1}^{m} a_{Rk} h_k ({}^{t}V_{Rmi}^{k} - {}^{0}V_{Rmi}^{k}) + \frac{s}{2}\sum_{k=1}^{m} b_{Rk} h_k ({}^{t}V_{Rsi}^{k} - {}^{0}V_{Rsi}^{k}) \tag{2-22} $$

$$ u_i = {}^{t+\Delta t}u_i - {}^{t}u_i = \sum_{k=1}^{m} h_k u_i^k + \frac{q}{2}\sum_{k=1}^{m} a_{Rk} h_k V_{Rqi}^{k} + \frac{s}{2}\sum_{k=1}^{m} b_{Rk} h_k V_{Rsi}^{k} \tag{2-23} $$

where

$$ V_{Rqi}^{k} = {}^{t+\Delta t}V_{Rqi}^{k} - {}^{t}V_{Rqi}^{k} \tag{2-24} $$

$$ V_{Rsi}^{k} = {}^{t+\Delta t}V_{Rsi}^{k} - {}^{t}V_{Rsi}^{k} \tag{2-25} $$

are the increments of unit directional vectors at node k and can be obtained by using the following first-order approximations

$$ \mathbf{V}_{Rq}^{k} = \boldsymbol{\theta}_k \times {}^{t}\mathbf{V}_{Rq}^{k} \tag{2-26} $$

$$\mathbf{V}_{Rs}^{k} = \boldsymbol{\theta}_{k} \times {}^{t}\mathbf{V}_{Rs}^{k} \tag{2-27}$$

By substituting equations (2-24)-(2-27) into equation (2-23), incremental displacements can be expressed as

$$u_i = {}^{t+\Delta t}u_i - {}^{t}u_i = \sum_{k=1}^{m} h_k u_i^k + \frac{q}{2}\sum_{k=1}^{m} a_{Rk} h_k ({}^{t}\theta_{i+1}^{k}\, {}^{t}V_{Rq(i+2)}^{k} - {}^{t}\theta_{i+2}^{k}\, {}^{t}V_{Rq(i+1)}^{k}) + \frac{s}{2}\sum_{k=1}^{m} b_{Rk} h_k ({}^{t}\theta_{i+1}^{k}\, {}^{t}V_{Rs(i+2)}^{k} - {}^{t}\theta_{i+2}^{k}\, {}^{t}V_{Rs(i+1)}^{k}) \tag{2-28}$$

where $i = 1,2,3$ and $i+1$ takes the value of 1 when $i = 3$ and $i-1$ takes the value of 3 when $i = 1$.

2.3.3 Strain-displacement and stress-strain relationships

The incremental decomposition of Piola-Kirchhoff stress of the resin is

$${}^{t+\Delta t}_{t}S_{Rij} = {}^{t}\tau_{Rij} + {}_{t}S_{Rij} \tag{2-29}$$

where ${}^{t}\tau_{Rij}$ is Cauchy stress of the resin at time *t*.

Considering that only the linear strain terms are included, the Green-Lagrange strain of the resin can be expressed as

$${}^{t+\Delta t}_{t}\varepsilon_{Rij} = {}_{t}\varepsilon_{Rij} = {}_{t}e_{Rij} \tag{2-30}$$

Stress-strain relation in incremental form is given by

$${}_{t}S_{Rij} = {}_{t}C_{Rijrs}\ {}_{t}e_{Rrs} \tag{2-31}$$

The incremental strain-displacement relation in the tensor form in global co-ordinate system is given by

$$ {}_t e_{ij} = \frac{1}{2}({}_t u_{i,j} + {}_t u_{j,i}) \tag{2-32} $$

Since only the strain along the thickness in x_{R1} direction and shear strain in $x_{R2}x_{R3}$ plane are considered, the strain vector in local co-ordinate system can be written as

$$ {}_t\hat{\bar{\mathbf{e}}}_R = \begin{Bmatrix} {}_t\bar{e}_{R11} \\ 2\,{}_t\bar{e}_{R23} \end{Bmatrix} \tag{2-33} $$

where the over-bar of the quantities corresponds to their local values.

Transformation matrix of strains from the global co-ordinate system into the mapped local co-ordinate system is given by

$$ \mathbf{T}_\varepsilon = \begin{bmatrix} l_{11}^2 & l_{12}^2 & l_{13}^2 & l_{11}l_{12} & l_{12}l_{13} & l_{11}l_{13} \\ l_{21}^2 & l_{22}^2 & l_{23}^2 & l_{21}l_{22} & l_{22}l_{23} & l_{21}l_{23} \\ l_{31}^2 & l_{32}^2 & l_{33}^2 & l_{31}l_{32} & l_{32}l_{33} & l_{31}l_{33} \\ 2l_{11}l_{12} & 2l_{12}l_{22} & 2l_{13}l_{23} & l_{12}l_{21}+l_{11}l_{22} & l_{13}l_{22}+l_{12}l_{23} & l_{13}l_{21}+l_{11}l_{23} \\ 2l_{21}l_{31} & 2l_{22}l_{32} & 2l_{23}l_{33} & l_{22}l_{31}+l_{21}l_{32} & l_{23}l_{32}+l_{22}l_{33} & l_{23}l_{31}+l_{21}l_{33} \\ 2l_{11}l_{31} & 2l_{12}l_{32} & 2l_{13}l_{33} & l_{12}l_{31}+l_{11}l_{32} & l_{13}l_{32}+l_{12}l_{33} & l_{13}l_{31}+l_{11}l_{33} \end{bmatrix} \tag{2-34} $$

where l_{ij} are the direction cosines of the global co-ordinate axes in mapped local co-ordinate system at Gauss integration points.

Transformation matrix of strains from the mapped local co-ordinate system into the local co-ordinate system is given by

$$ \mathbf{T}_L = \begin{bmatrix} 1 & 0 & 0 & 0 & 0 & 0 \\ 0 & -\frac{2}{\sqrt{3}} & 0 & 0 & 1 & 0 \end{bmatrix} \tag{2-35} $$

The incremental Piola-Kirchhoff stress strain relation in local co-ordinate system at time t is as follows

$$\begin{Bmatrix} {}_tS_{R11} \\ {}_tS_{R23} \end{Bmatrix} = \begin{bmatrix} E_R & 0 \\ 0 & G_R \end{bmatrix} \begin{Bmatrix} {}_te_{R11} \\ 2_te_{R23} \end{Bmatrix} \tag{2-36}$$

where the E_R and G_R are Young's modulus and shear modulus of elasticity of the resin.

2.4 Equilibrium equation

Substituting the stress-strain relation of both tow and resin, that is, equations (2-12, 13, 19, 29, 30) into equation (2-1), and considering that all variables in equation (2-1) are referred to the configuration at time t, i.e. the updated configuration of the body, one obtains the equilibrium equation of body in global co-ordinate system at time $t+\Delta t$ as follows

$$\int_{{}^tV_T} {}_tS_{ij}\delta\, {}_t\varepsilon_{ij}\, d^tV_T + \int_{{}^tV_T} {}^t\tau_{ij}\,\delta\eta_{ij}\, d^tV_T + \int_{{}^tV_R} {}_tS_{Rij}\,\delta\, {}_te_{Rij}\, d\,{}^tV_R =$$

$$\delta^{t+\Delta t}W - \int_{{}^tV_T} {}^t\tau_{ij}\,\delta\, {}_te_{ij}\, d^tV_T - \int_{{}^tV_R} {}^t\tau_{Rij}\,\delta\, {}_te_{Rij}\, d^tV_R \tag{2-37}$$

where the subscript T of V denotes the volume of the tow and R of V the volume of the resin. Substituting the stress-strain and strain-displacement relations and the displacement interpolation into equation (2-37), one can obtain the formulation of iso-parametric finite elements. This procedure has been presented by Bathe [63]. In order to confirm the numerical results of equation (2-37), approximate analytical solutions will be given first.

2.5 Determination of buckling load

Since the buckling of a structure may have an adverse effect on the structural performance and may cause instability of the structure, the load at which buckling will

occur should be determined. The techniques or the methods for determining the value of the buckling load have been described by many researchers, such as Bathe [63], Hu [48], Cook [65], and etc. Basically the most frequently used method the so called "eigenvalue method" [63] is to find the value of the buckling load through solving a system of eigenvalue problem equations for a linearized buckling analysis system. This method is found to be not very effective in the present case due to the uncertainty of the nonlinear geometric stiffness matrix at different applied loads. Therefore, it is necessary to find another approximate method to obtain this value.

In buckling behavior a small load increment results in relatively large deflection of the structure. This can be seen in any load versus maximum deflection curve, for example, Fig. 4.3 in Section 4.1, when buckling happens, the curve tends to be flat, that is, the magnitude of the slope of this curve tends to approach a very small number. If a critical value of the slope of the curve is to be set in advance, it can be said that buckling has happened when the magnitude of the slope of this curve is less than the predetermined critical value. The value of the load corresponding to this point is the value of the buckling load. In practical calculation, the value of the buckling load can be obtained approximately by checking the magnitude of the slope of the straight line between any two consecutive points in the load versus maximum deflection curve. If the magnitude of the slope is less than the predetermined critical value, the value of the load at the left side of the two points is defined as the value of the buckling load. The critical value of the slope in the present case is set to be equal to 5. Note that in the normalized load versus non-dimensional maximum deflection curve, the value of the normalized load

is much larger than the value of the non-dimensional maximum deflection. In this sense, five (5) is a very small number.

2.6 Conclusion

Non-linear finite element formulation for the buckling analysis of a curved composite beam and resin structure has been developed using the principle of virtual displacement in continuum mechanics theory and an updated Lagrangian approach. An approximate method for determination of the value of the buckling load is presented. This formulation and approximate method can be employed to conduct the buckling analysis of the tri-axial woven fabric composite structures in the following chapters.

Chapter 3

Approximate analytical solutions for buckling loads of curved beam structures

In order to provide a confirmation to the numerical finite element solution and verification of the developed computer software, approximate analytical solutions of buckling load for some simple curved composite beam structures, such as simply-supported full sinusoidal composite beam, composite tow structure with two intersected curved tows and tri-axial tow structure with three intersected curved tows will be derived in this Chapter. It will provide confirmation to the numerical results obtained from Chapter 4.

3.1 Simply-supported full sinusoidal beam

Suppose that the curved composite beam takes the form of a full sinusoidal beam that is simply-supported at both ends under loads as shown in Fig. 3.1.

Assume that the plane sections remain plane after bending; the effect of transverse shear is negligible; the loads and the bending moments act in a plane passing through a principal axis of inertia of the cross-section; the initial rise of the beam is not large as

compared to the cross-sectional dimensions; deflections are small as compared to the cross-sectional dimensions; the material points on the undeformed midline (mid-plane)

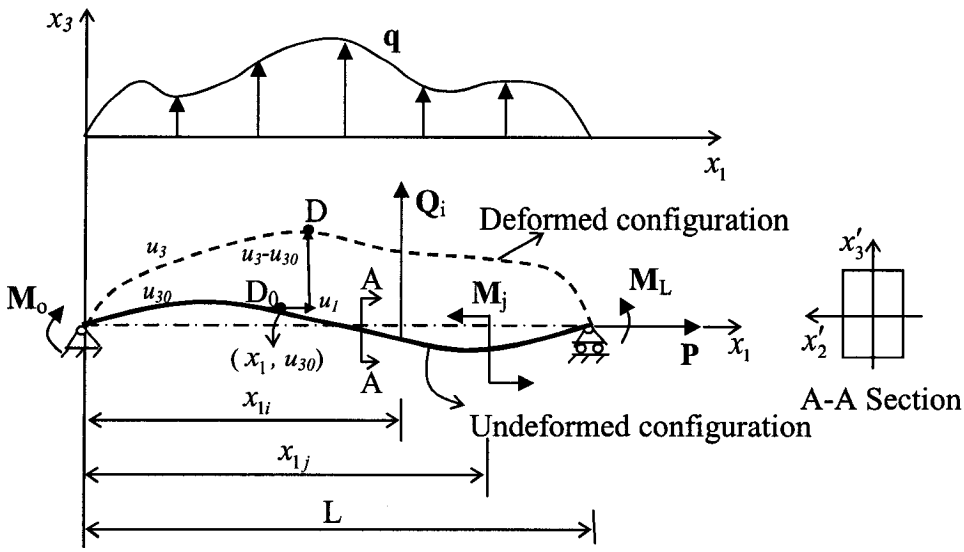

Fig. 3. 1: Sinusoidal beam

are characterized by $u_{30}(x_1)$ shown in Fig. 3.1. Let $u_1(x_1)$ and $u_3(x_1)$ denote the location of material points on the deformed midline. On the basis of these assumptions, the strain at any material point is given by

$$\varepsilon = \varepsilon_0 + x_3'\kappa \tag{3-1}$$

where ε_0 and κ denote the reference-plane (mid-plane) extensional strain and change in curvature, respectively.

Let D_0 and D denote the undeformed and deformed positions of a material point of the reference line. The co-ordinates of D_0 and D are (x_1, u_{30}) and $(x_1 + u_1, u_3)$, respectively. For small strains, the reference plane extensional strain, ε_0, is given by

$$\varepsilon_0 = \frac{ds - ds_0}{ds_0} \tag{3-2}$$

where ds_0 and ds are the undeformed and deformed lengths of elements on the reference line.

$$\text{Since} \begin{cases} (ds)^2 = (dx_1 + du_1)^2 + (du_3)^2 \\ (ds_0)^2 = (dx_1)^2 + (du_{30})^2 \end{cases} \tag{3-3}$$

and are approximated to the second order by using Taylor series expansion, one obtains

$$\begin{cases} ds = dx_1(1 + \frac{du_1}{dx_1} + \frac{1}{2}(\frac{du_1}{dx_1})^2 + \frac{1}{2}(\frac{du_3}{dx_1})^2) \\ \frac{1}{ds_0} = \frac{1}{dx_1}(1 - \frac{1}{2}(\frac{du_{30}}{dx_1})^2) \end{cases} \tag{3-4}$$

Substituting equation (3-4) into equation (3-2) and considering that $(\frac{du_1}{dx_1})^2 << (\frac{du_3}{dx_1})^2$, the reference-plane extensional strain, ε_0, can be further written in the following form

$$\varepsilon_0 = \frac{du_1}{dx_1} + \frac{1}{2}(\frac{du_3}{dx_1})^2 - \frac{1}{2}(\frac{du_{30}}{dx_1})^2 - \frac{1}{2}(\frac{du_{30}}{dx_1})^2(\frac{du_1}{dx_1} + \frac{1}{2}(\frac{du_3}{dx_1})^2) \tag{3-5}$$

The general expression for the change in the curvature of a curved beam, κ, is given by

$$\kappa = -\left[\frac{\frac{d^2u_3}{dx_1^2}}{(1 + (\frac{du_3}{dx_1})^2)^{\frac{3}{2}}} - \frac{\frac{d^2u_{30}}{dx_1^2}}{(1 + (\frac{du_{30}}{dx_1})^2)^{\frac{3}{2}}} \right] \tag{3-6}$$

For small initial curvature, the expression for the change in curvature, κ, after Taylor series expansion of equation (3-6) to the second order of the slope of the deflection, can be written as

$$\kappa = -(\frac{d^2u_3}{dx_1^2} - \frac{d^2u_{30}}{dx_1^2}) + \frac{3}{2}\left[\frac{d^2u_3}{dx_1^2}(\frac{du_3}{dx_1})^2 - \frac{d^2u_{30}}{dx_1^2}(\frac{du_{30}}{dx_1})^2 \right] \tag{3-7}$$

and

$$\kappa^2 = (\frac{d^2u_3}{dx_1^2} - \frac{d^2u_{30}}{dx_1^2})^2 - 3(\frac{d^2u_3}{dx_1^2} - \frac{d^2u_{30}}{dx_1^2})\left[\frac{d^2u_3}{dx_1^2}(\frac{du_3}{dx_1})^2 - \frac{d^2u_{30}}{dx_1^2}(\frac{du_{30}}{dx_1})^2\right] \tag{3-8}$$

Strain energy of the beam is given by

$$U = \frac{1}{2}\int_V \sigma\varepsilon\, dV = \frac{1}{2}\int_V E_L\varepsilon^2\, dV \tag{3-9}$$

where the stress-strain relation, $\sigma = E_L\varepsilon$, is employed.

Assume that u_1, u_3 are functions of x_1, then

$$\int_A x_3' dA = 0 \tag{3-10}$$

Substitution of equations (3-1) and (3-10) into equation (3-9) leads to

$$U = \frac{1}{2}\int_0^{S_0^*}(E_L A\varepsilon_0{}^2 + E_L I\kappa^2)ds^* \tag{3-11}$$

where I is the moment of inertia of the cross-section, S_0^* is the length of the reference line of the beam and the finite element length ds^* of the beam can be approximated as being accurate to the second order

$$ds^* = \sqrt{(dx_1)^2 + (du_3)^2} \approx dx_1(1 + \frac{1}{2}(\frac{du_3}{dx_1})^2) \tag{3-12}$$

Substituting from equation (3-12), equation (3-11) can be written as

$$U = \frac{1}{2}\int_0^L (E_L A\varepsilon_0^2 + E_L I\kappa^2)(1 + \frac{1}{2}(\frac{du_3}{dx_1})^2)dx_1 \tag{3-13}$$

Work done by external forces is given by

$$W = \int_0^L (q(u_3 - u_{30}) + \sum_i Q_i\delta(x_1 - x_{1i})(u_3 - u_{30}) + \sum_j M_j\eta(x_1 - x_{1j})(\frac{du_3}{dx_1} - \frac{du_{30}}{dx_1}))dx_1 \tag{3-14}$$

$$- M(\frac{du_3}{dx_1} - \frac{du_{30}}{dx_1})\Big|_0^L + Pu_1\Big|_0^L$$

where $\delta(x_1 - x_{1i})$ is the Dirac δ-function and $\eta(x_1 - x_{1j})$ is the Doublet function.

The total potential of the beam is given by

$$U_T = U - W$$

Substitution of equations (3-5), (3-8) and (3-14) yields

$$\begin{aligned} U_T = \frac{1}{2}\int_0^L [E_L A(\frac{du_1}{dx_1} + \frac{1}{2}(\frac{du_3}{dx_1})^2 - \frac{1}{2}(\frac{du_{30}}{dx_1})^2 - \frac{1}{2}(\frac{du_{30}}{dx_1})^2(\frac{du_1}{dx_1} + \frac{1}{2}(\frac{du_3}{dx_1})^2))^2 + \\ E_L I((\frac{d^2u_3}{dx_1^2} - \frac{d^2u_{30}}{dx_1^2})^2 - 3(\frac{d^2u_3}{dx_1^2} - \frac{d^2u_{30}}{dx_1^2})(\frac{d^2u_3}{dx_1^2}(\frac{du_3}{dx_1})^2 - \frac{d^2u_{30}}{dx_1^2}(\frac{du_{30}}{dx_1})^2))] \\ (1 + \frac{1}{2}(\frac{du_3}{dx_1})^2)dx_1 - \int_0^L [q(u_3 - u_{30}) + \sum_i Q_i \delta(x_1 - x_{1i})(u_3 - u_{30}) + \\ \sum_j M_j \eta(x_1 - x_{1j})(\frac{du_3}{dx_1} - \frac{du_{30}}{dx_1})]dx_1 + M(\frac{du_3}{dx_1} - \frac{du_{30}}{dx_1})\Big|_0^L - Pu_1\Big|_0^L \end{aligned} \tag{3-15}$$

This is the general form of the total potential of a beam. In the present case, if only the compressive axial load is considered, the total potential takes the following form

$$\begin{aligned} U_T = \frac{1}{2}\int_0^L [E_L A(\frac{du_1}{dx_1} + \frac{1}{2}(\frac{du_3}{dx_1})^2 - \frac{1}{2}(\frac{du_{30}}{dx_1})^2 - \frac{1}{2}(\frac{du_{30}}{dx_1})^2(\frac{du_1}{dx_1} + \frac{1}{2}(\frac{du_3}{dx_1})^2))^2 + \\ E_L I((\frac{d^2u_3}{dx_1^2} - \frac{d^2u_{30}}{dx_1^2})^2 - 3(\frac{d^2u_3}{dx_1^2} - \frac{d^2u_{30}}{dx_1^2})(\frac{d^2u_3}{dx_1^2}(\frac{du_3}{dx_1})^2 - \frac{d^2u_{30}}{dx_1^2}(\frac{du_{30}}{dx_1})^2))] \\ (1 + \frac{1}{2}(\frac{du_3}{dx_1})^2)dx_1 - Pu_1\Big|_0^L \end{aligned} \tag{3-16}$$

Boundary conditions for a simply-supported beam are

$$u_3(0) = u_3(L) = 0; \quad u_3''(0) = u_3''(L) = 0; \quad u_1(0) = 0 \text{ (roller support)} \tag{3-17}$$

Assume that the initial configuration of the beam is

$$u_{30} = Z\sin(\frac{2\pi}{L}x_1) \qquad 0 \le x_1 \le L \tag{3-18}$$

where the Z is the initial rise parameter.

The deflection of the beam may be represented by an infinite sine series, each term of which satisfies the boundary conditions (3-17),

$$u_3 = u_{30} + \sum_{n=1}^{\infty} c_n \sin(\frac{n\pi}{L}x_1) \qquad 0 \le x_1 \le L \tag{3-19}$$

where $c_n, n = 1,2,\cdots$ are the undetermined coefficients of the deflection of the beam.

The axial displacement of the material points may be represented by u_1, which satisfies the boundary conditions (3-17),

$$u_1 = d(1-\cos(\frac{\pi}{2L}x_1)) \qquad 0 \le x_1 \le L \tag{3-20}$$

where d is the undetermined coefficient of axial displacement of the beam.

Substituting equations (3-18) through (3-20) into the expression for the total potential, equation (3-16), and performing the corresponding integration and neglecting the higher order terms of undetermined coefficients yields

$$\begin{aligned} U_T = {} & Pd + \frac{E_L A}{2L}d^2(1-\frac{61}{63}\pi^2(\frac{Z}{L})^2) + \frac{1}{4}E_L A(\frac{\pi}{L})^2 d(c_1{}^2 + \sum_{n=2}^{\infty} c_n{}^2 n^2) + \\ & \frac{1}{32}E_L AL(\frac{\pi}{L})^4(c_1{}^4 + 2c_1{}^2\sum_{n=2}^{\infty} c_n{}^2 n^2 + \sum_{n=2}^{\infty} c_n{}^4 n^4) + \frac{1}{4}E_L IL(\frac{\pi}{L})^4(c_1{}^2 + \sum_{n=2}^{\infty} c_n{}^2 n^4) - \\ & \frac{5}{32}E_L IL(\frac{\pi}{L})^6(c_1{}^4 + 2c_1{}^2\sum_{n=2}^{\infty} c_n{}^2 n^2(1+n^2) + \sum_{n=2}^{\infty} c_n{}^4 n^6 + 8Z^2(c_1{}^2 + \sum_{n=2}^{\infty} c_n{}^2 n^4)) \end{aligned} \tag{3-21}$$

We are interested in finding buckling load at which instability is possible. We find it by first writing the equilibrium equations and then studying the character of these static

equilibrium equations. To find the static equilibrium positions, we use the principle of the stationary value of the total potential, or

$$\begin{cases} \dfrac{\partial U_T}{\partial c_n} = 0, \quad n = 1,2,3,\cdots \\ \\ \dfrac{\partial U_T}{\partial d} = 0 \end{cases} \tag{3-22}$$

This leads to

$$\frac{1}{2}E_L A(\frac{\pi}{L})^2 dc_1 + \frac{1}{8}E_L AL(\frac{\pi}{L})^4 (c_1^3 + c_1\sum_{n=2}^{\infty} c_n^2 n^2) + \frac{1}{2}E_L IL(\frac{\pi}{L})^4 c_1$$

$$-\frac{5}{8}E_L IL(\frac{\pi}{L})^6 (c_1^3 + c_1\sum_{n=2}^{\infty} c_n^2 n^2(1+n^2) + 4c_1 Z^2) = 0 \tag{3-23}$$

$$\frac{1}{2}E_L A(\frac{\pi}{L})^2 d\sum_{n=2}^{\infty} c_n n^2 + \frac{1}{8}E_L AL(\frac{\pi}{L})^4 (c_1^2\sum_{n=2}^{\infty} c_n n^2 + \sum_{n=2}^{\infty} c_n^3 n^4) + \frac{1}{2}E_L IL(\frac{\pi}{L})^4 \sum_{n=2}^{\infty} c_n n^4$$

$$-\frac{5}{8}E_L IL(\frac{\pi}{L})^6 (c_1^2\sum_{n=2}^{\infty} c_n n^2(1+n^2) + \sum_{n=2}^{\infty} c_n^3 n^6 + 4Z^2\sum_{n=2}^{\infty} c_n n^4) = 0 \quad m = 2,3,4,\cdots \tag{3-24}$$

$$P + \frac{E_L A}{L}d(1 - \frac{61}{63}\pi^2(\frac{Z}{L})^2) + \frac{1}{4}E_L A(\frac{\pi}{L})^2(c_1^2 + \sum_{n=2}^{\infty} c_n^2 n^2) = 0 \tag{3-25}$$

There are two possible cases that result from equations (3-23), (3-24) and (3-25).

Case I: $c_1 \neq 0$ and $c_n = 0$ for n=2,3,4,$\cdots$

Case II: $c_1 \neq 0$, $c_m \neq 0$ and $c_n = 0$ for n=2,3,4,$\cdots$ except n=m.

Case I: Substituting $c_n = 0$ for n=2,3,4,$\cdots$ into equations (3-23) and (3-25) and rearranging them, one obtains

$$\frac{P}{\pi^2 E_L I/L^2} = (1 - \frac{5}{4}(\frac{\pi}{L})^2(c_1^2 + 4Z^2))(1 - \frac{61}{63}\pi^2(\frac{Z}{L})^2) - \frac{61}{252}\frac{E_L A}{E_L I}(\frac{\pi}{L})^2 Z^2 c_1^2 \tag{3-26}$$

The load reaches maximum when c_1 approaches zero. The buckling load for this case is

$$\frac{P_{cr1}}{\pi^2 E_L I/L^2} = 1 - \frac{376}{63}\pi^2(\frac{Z}{L})^2 + \frac{305}{63}\pi^4(\frac{Z}{L})^4 \tag{3-27}$$

Case II: Eliminating d and c_m from equations (3-23) through (3-25) and rearranging them, one obtains

$$\begin{aligned}\frac{P}{\pi^2 E_L I/L^2} &= (1-\frac{61}{63}\pi^2(\frac{Z}{L})^2)(m^4 - \frac{5}{4}\pi^2((1+m^2+m^4)(\frac{c_1}{L})^2 + 4(\frac{Z}{L})^2 m^4)) \\ &-\frac{61}{252}\frac{E_L A Z^2}{E_L I}\pi^2((1+m^2)(\frac{c_1}{L})^2 + 4(\frac{Z}{L})^2(m^2-1)) - \frac{61}{315}\frac{E_L A Z^2}{E_L I}(1-m^2)\end{aligned} \tag{3-28}$$

The maximum load corresponds to a_1 approaching zero. This yields

$$\frac{P}{\pi^2 E_L I/L^2} = m^4(1-5\pi^2(\frac{Z}{L})^2)(1-\frac{61}{63}\pi^2(\frac{Z}{L})^2) + \frac{61}{63}\frac{E_L A Z^2}{E_L I}(m^2-1)(\frac{1}{5}-\pi^2(\frac{Z}{L})^2) \tag{3-29}$$

The lowest value of P with respect to values of integer m corresponds to m=2 and

$$\frac{P_{crm}}{\pi^2 E_L I/L^2} = 16(1-5\pi^2(\frac{Z}{L})^2)(1-\frac{61}{63}\pi^2(\frac{Z}{L})^2) + \frac{61}{21}\frac{E_L A Z^2}{E_L I}(\frac{1}{5}-\pi^2(\frac{Z}{L})^2) \tag{3-30}$$

Comparing Case I with Case II, the critical load should be the smaller one of them, which is given by equation (3-27).

From equation (3-27), two observations can be seen: first, the change of buckling load for a curved beam with respect to the Euler buckling load for straight beam is proportional to the square of the initial rise of the beam. Second, when the initial rise, Z, of the beam is very small, i.e., $Z \ll 1$, one obtains from equation (3-27) by neglecting the last two terms that the buckling load is the same as the Euler's buckling load for a straight beam. This means that the buckling load for a curved beam is the same as the one for a straight beam. Actually, a beam with small initial rise corresponds to a shallow

curved beam. In this case, the initial deflection may be considered as a kind of small imperfection of the beam. As we know the small imperfection due to a small deflection does not change the Euler buckling load.

Substituting Z=0.133 mm and L=4.58 mm into equation (3-27) in the present case, one obtains

$$\frac{P_{cr}}{\pi^2 E_L I / L^2} = .9507 \tag{3-31}$$

It is seen that there is 4.93% decrease for the buckling load with respect to the Euler buckling load.

3.2 Two intersected half sinusoidal beam structure

A simply-supported two-intersected half sinusoidal beam structure is shown in Fig. 3.2. It is constituted by two half-sinusoidal beams and resin, which bonds the beams together at their midpoints, and it is loaded at its roller-supported ends along the local longitudinal axis of each beam.

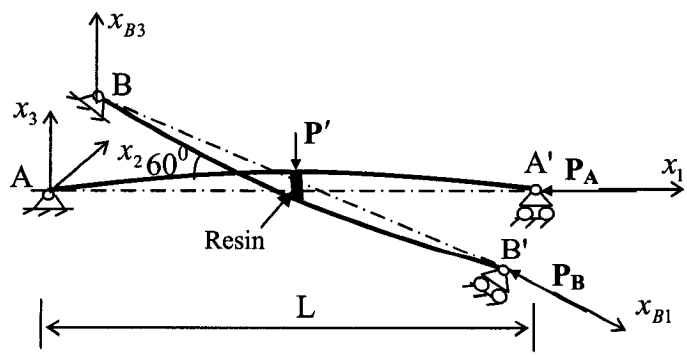

Fig. 3. 2: Tri-axial tow structure with two intersected curved tows

The total potential is given by

$$U_T = U_{AT} + U_{BT} + U_R \tag{3-32}$$

where the total potentials of beams AA' and BB' are given, respectively, by

$$U_{AT} = \frac{1}{2}\int_0^{L_A} (E_{LA} A_A \varepsilon_{A0}{}^2 + E_{LA} I_A \kappa_A{}^2)\, dx_1 + P_A u_1 \Big|_0^{L_A} \tag{3-33}$$

$$U_{BT} = \frac{1}{2}\int_0^{L_B} (E_{LB} A_B \varepsilon_{B0}{}^2 + E_{LB} I_B \kappa_B{}^2)\, dx_{B1} + P_B u_{B1} \Big|_0^{L_B} \tag{3-34}$$

The total potential of the resin is given by, assuming that the resin acts like a stretching spring and its shear effect is neglected due to its small order of magnitude,

$$U_R = \frac{1}{2} E_R \frac{a_R b_R}{t_R} (\Delta u_{A3}(\frac{L_A}{2}) - \Delta u_{B3}(\frac{L_B}{2}))^2 \tag{3-35}$$

where

$$\begin{cases} \Delta u_{A3}(\frac{L_A}{2}) = u_{A3}(\frac{L_A}{2}) - u_{A30}(\frac{L_A}{2}) \\ \\ \Delta u_{B3}(\frac{L_A}{2}) = u_{B3}(\frac{L_B}{2}) - u_{B30}(\frac{L_B}{2}) \end{cases} \tag{3-36}$$

are the displacements of the beams AA' and BB' at their midpoints.

W is the work done by the external forces, which is given in the present case by

$$W = -P_A u_{A1}(L_A) - P_B u_{B1}(L_B) \tag{3-37}$$

The formulae for strain and change of curvature of the reference line are given by equations (3-5) and (3-7). Substituting equations (3-5), (3-7), (3-33) through (3-37) into equation (3-32), one can obtain the formula for the total potential in the same form as equation (3-16).

Boundary conditions:

Beam AA': $\Delta u_{A3}(0) = \Delta u_{A3}(L_A) = 0$; $\Delta u''_{A3}(0) = \Delta u''_{A3}(L_A) = 0$; $u_{A1}(0) = 0$ (3-38)

Beam BB': $\Delta u_{B3}(0) = \Delta u_{B3}(L_B) = 0$; $\Delta u''_{B3}(0) = \Delta u''_{B3}(L_B) = 0$; $u_{B1}(0) = 0$ (3-39)

Initial shape:

Beam AA': $u_{A30} = Z_A \sin(\frac{\pi}{L_A} x_{A1})$ $0 \le x_{A1} \le L_A$ (3-40)

Beam BB': $u_{B30} = Z_B \sin(\frac{\pi}{L_B} x_{B1})$ $0 \le x_{B1} \le L_B$ (3-41)

where Z_A and Z_B are initial parameters of beams AA' and BB', respectively.

Deflections:

Beam AA': $u_{A3} = u_{A30} + \sum_{n=1}^{\infty} c_{An} \sin(\frac{n_A \pi}{L_A} x_{A1})$ $0 \le x_{A1} \le L_A$ (3-42)

Beam BB': $u_{B3} = u_{B30} + \sum_{n=1}^{\infty} c_{Bn} \sin(\frac{n_B \pi}{L_B} x_{B1})$ $0 \le x_{B1} \le L_B$ (3-43)

where c_{An} and c_{Bn} ($n = 1,2, \ldots \infty$) are the undetermined coefficients.

Axial displacement:

Beam AA: $u_{A1} = d_A(1 - \cos(\frac{\pi}{2L_A} x_{A1}))$ $0 \le x_{A1} \le L_A$ (3-44)

Beam BB: $u_{B1} = d_B(1 - \cos(\frac{\pi}{2L_B} x_{B1}))$ $0 \le x_{B1} \le L_B$ (3-45)

where d_A and d_B are the undetermined coefficients.

Substituting all the assumed initial shapes, deflections and axial displacements into total potential expression, using the same material properties and geometries for the two beams but different initial rise parameters, i.e. Z_A and Z_B, setting $Z_B = -Z_A = -Z$ and performing the same procedure of operation as in Section 3.1, one obtains the buckling loads as follows:

$$\frac{P_{cr}}{E_L I(\frac{\pi}{L})^2} = 1 - \frac{13}{60}\pi^2(\frac{Z}{L})^2 + \frac{\pi^2}{8}(\frac{Z}{L})^2\left[\frac{169}{1800}(\frac{E_L A}{E_L I})^2 Z^4 + 11(1 - \frac{13}{60}\pi^2(\frac{Z}{L})^2)^2\right.$$

$$\left. + \frac{143}{60}\frac{E_L A}{E_L I}Z^2(1 - \frac{13}{60}\pi^2(\frac{Z}{L})^2)\right] \Big/ \left[\frac{13}{60}\frac{E_L A}{E_L I}Z^2 + 5(1 - \frac{13}{60}\pi^2(\frac{Z}{L})^2)\right] \tag{3-46}$$

For accuracy to the second order of the initial rise, buckling load in equation (3-46) can be approximated by

$$\frac{P_{cr}}{E_L I(\frac{\pi}{L})^2} \approx 1 + \frac{7}{120}\pi^2(\frac{Z}{L})^2 \tag{3-47}$$

If the beam is very flat and the initial rise has the same order as the height of the cross-section of the beam, the factor, $E_L AZ^2/E_L I$, will not be a small quantity. In this case the buckling load can be approximated by

$$\frac{P_{cr}}{E_L I(\frac{\pi}{L})^2} = 1 + (\frac{\pi Z}{2L})^2\left\{-\frac{13}{15} + \frac{1}{2}\left[\frac{169}{1800}(\frac{E_L AZ^2}{E_L I})^2 + 11 + \frac{143}{60}\frac{E_L AZ^2}{E_L I}\right] \Big/ \left[\frac{13}{60}\frac{E_L AZ^2}{E_L I} + 5\right]\right\} \tag{3-48}$$

Substituting Z=0.133 mm and L=2.29 mm into equations (3-46), (3-47) and (3-48) in the present case, one obtains the non-dimensional buckling loads in these three cases, respectively, as follows

$$\frac{P_{cr}}{\pi^2 E_L I/L^2} = 1.0105,\ 1.0019 \text{ and } 1.0106 \tag{3-49}$$

It is seen that equation (3-48) is a very good approximation.

From equation (3-46) or (3-48) one observes that the buckling load of two intersected half-sinusoidal beam structure with flat cross-section not only depends on the factor of initial rise parameter, $(Z/L)^2$, but also depends on the ratio of the tension stiffness ($E_L A$) to the bending stiffness ($E_L I$) of the beam. The relation between buckling

load and ratio of tension stiffness and bending stiffness, $E_LA/\ E_LI$, based on equation (3-46) is plotted in Fig. 3.3. The value of the stiffness ratio, $E_LA/\ E_LI$, shown in Fig. 3.3 is obtained by changing the thickness of the beam from 0.16 *mm* to 0.24 *mm*, of which 0.22 *mm* is the real thickness of the beam. The selected thicknesses at five different points which correspond to the values of the stiffness ratio at these points shown in Fig. 3.3 are

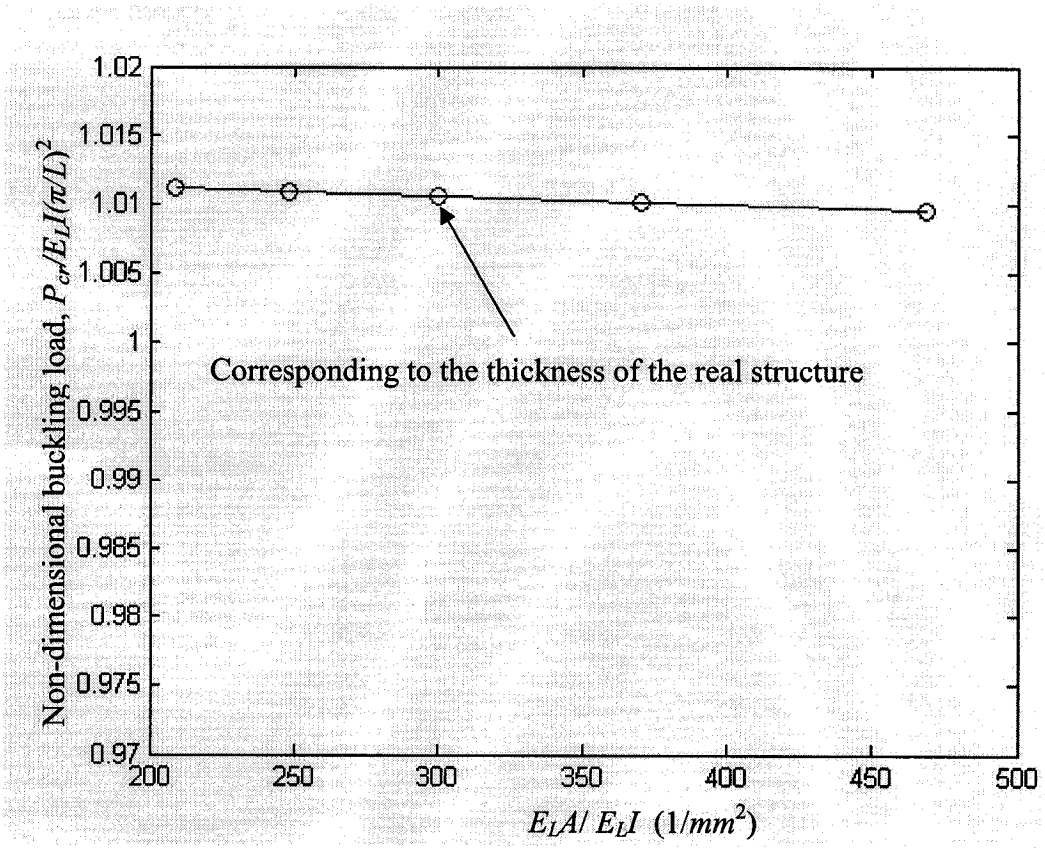

Fig. 3. 3: Curve of non-dimensional buckling load versus stiffness ratio $E_LA/\ E_LI$ for two intersected curved beam structure

uniformly distributed over the range of [0.16, 0.24]. Actually, substituting the area and moment of inertia of the cross-section of the beam, that is, $A = ab$ and $I = \frac{1}{12}ba^3$, into stiffness ratio and canceling the similar factors, one obtains $E_LA/\ E_LI = 12/a^2$. This equation shows that the stiffness ratio is a function depending on the thickness of the

beam only. It also shows that the larger thickness of the beam corresponds to the smaller stiffness ratio. Therefore, smaller value of the stiffness ratio corresponding to horizontal coordinate in Fig. 3.3 corresponds to larger thickness of the beam.

3.3 Three intersected full sinusoidal beam structure

A simply-supported three-intersected full sinusoidal beam structure is shown in Fig. 3.4. This structure is a unit cell of the tri-axial woven fabric composite structure. It is made of three full sinusoidal composite tows woven at angles of 0°, 60°and -60° with each other and bonded together by resin and is loaded at its three roller-supported ends along the local longitudinal axis of each beam.

The total potential of unit cell is given by

$$U_T = U_A + U_B + U_C + U_R - W \tag{3-50}$$

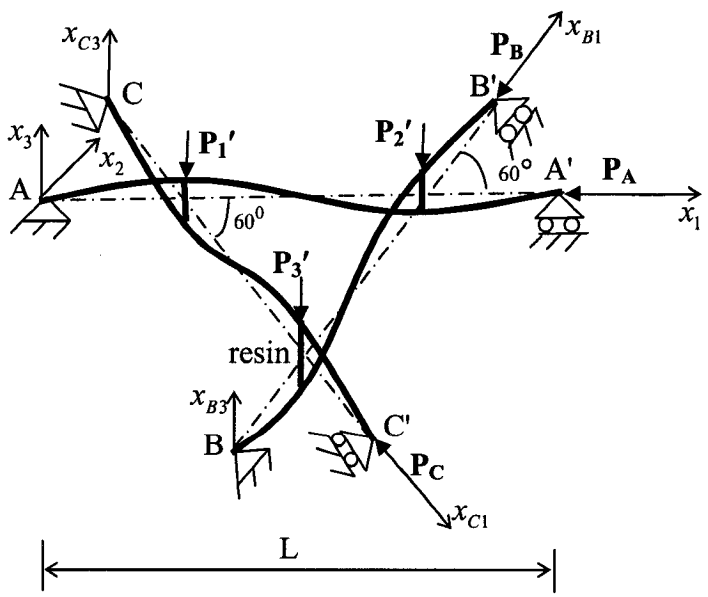

Fig. 3. 4: Woven tri-axial tow structure with three intersected curved tows

where U_A, U_B, U_C are strain energies of beams AA', BB' and CC', respectively. U_A is given by

$$U_A = \frac{1}{2}\int_0^{L_A}(E_{LA}A_A\varepsilon_{A0}^2 + E_{LA}I_A\kappa_A^2)dx_1 \tag{3-51}$$

U_B and U_C can be obtained simply by changing the subscript A in equation (3-51) into B and C.

U_R is the strain energy of the resin, which is given by

$$\begin{aligned} U_R = {} & \frac{1}{2}E_R\frac{a_R b_R}{t_R}(\Delta u_{A3}(\frac{L}{4}) - \Delta u_{B3}(\frac{L}{4}))^2 + \frac{1}{2}E_R\frac{a_R b_R}{t_R}(\Delta u_{C3}(\frac{3L}{4}) - \Delta u_{A3}(\frac{3L}{4}))^2 \\ & + \frac{1}{2}E_R\frac{a_R b_R}{t_R}(\Delta u_{B3}(\frac{3L}{4}) - \Delta u_{C3}(\frac{L}{4}))^2 \end{aligned} \tag{3-52}$$

W is the work done by the external forces, which is given in the present case by

$$W = -P_A u_{A1}(L_A) - P_B u_{B1}(L_B) - P_C u_{C1}(L_C) \tag{3-53}$$

Boundary conditions:

Beam AA': $\Delta u_{A3}(0) = \Delta u_{A3}(L_A) = 0$; $\Delta u''_{A3}(0) = \Delta u''_{A3}(L_A) = 0$; $u_{A1}(0) = 0$ (3-54)

Beam BB': $\Delta u_{B3}(0) = \Delta u_{B3}(L_B) = 0$; $\Delta u''_{B3}(0) = \Delta u''_{B3}(L_B) = 0$; $u_{B1}(0) = 0$ (3-55)

Beam CC': $\Delta u_{C3}(0) = \Delta u_{C3}(L_C) = 0$; $\Delta u''_{C3}(0) = \Delta u''_{C3}(L_C) = 0$; $u_{C1}(0) = 0$ (3-56)

Initial shape:

Beam AA': $u_{A30} = Z_A \sin(\frac{2\pi}{L_A}x_{A1})$ $\quad 0 \le x_{A1} \le L_A$ (3-57)

Beam BB': $u_{B30} = Z_B \sin(\frac{2\pi}{L_B}x_{B1})$ $\quad 0 \le x_{B1} \le L_B$ (3-58)

Beam CC': $u_{C30} = Z_C \sin(\frac{2\pi}{L_C}x_{C1})$ $\quad 0 \le x_{C1} \le L_C$ (3-59)

where Z_A, Z_B and Z_C are initial parameters.

Deflections:

$$\text{Beam AA': } u_{A3} = u_{A30} + \sum_{n=1}^{\infty} c_{An} \sin(\frac{n_A \pi}{L_A} x_{A1}) \qquad 0 \le x_{A1} \le L_A \tag{3-60}$$

$$\text{Beam BB': } u_{B3} = u_{B30} + \sum_{n=1}^{\infty} c_{Bn} \sin(\frac{n_B \pi}{L_B} x_{B1}) \qquad 0 \le x_{B1} \le L_B \tag{3-61}$$

$$\text{Beam CC': } u_{C3} = u_{C30} + \sum_{n=1}^{\infty} c_{Cn} \sin(\frac{n_C \pi}{L_C} x_{C1}) \qquad 0 \le x_{C1} \le L_C \tag{3-62}$$

where c_{An}, c_{Bn} and c_{Cn} (n = 1,2, ... ∞) are the undetermined coefficients.

Axial displacement:

$$\text{Beam AA': } u_{A1} = d_A(1 - \cos(\frac{\pi}{2L_A} x_{A1})) \qquad 0 \le x_{A1} \le L_A \tag{3-63}$$

$$\text{Beam BB': } u_{B1} = d_B(1 - \cos(\frac{\pi}{2L_B} x_{B1})) \qquad 0 \le x_{B1} \le L_B \tag{3-64}$$

$$\text{Beam CC': } u_{C1} = d_C(1 - \cos(\frac{\pi}{2L_C} x_{C1})) \qquad 0 \le x_{C1} \le L_C \tag{3-65}$$

where d_A, d_B and d_C are the undetermined coefficients.

Substituting all the assumed initial shapes, deflections and axial displacements into total potential expression, equation (3-50) using the same material properties and geometries for the three beams but different initial parameters, i.e. Z_A, Z_B and Z_C, setting $Z_C = Z_B = -Z_A = -Z$ and performing the same procedure of operation as in the Section 3.1, one obtains the buckling load

$$\frac{P_{cr}}{\pi^2 E_L I / L^2} = 1 - \frac{376}{63}\pi^2(\frac{Z}{L})^2 + \frac{305}{63}\pi^4(\frac{Z}{L})^4 \tag{3-66}$$

Substituting Z=0.133 mm and L=4.58 mm into equation (3-66) in the present case, one obtains

$$\frac{P_{cr}}{\pi^2 E_L I / L^2} = 0.9507 \tag{3-67}$$

It is seen that nearly 5% decrease for the critical load with respect to the Euler critical load for single straight beam case is predicted.

3.4 Conclusion

The approximate analytical solutions for buckling loads of some simple configurations such as a simply-supported curved composite beam, a simply-supported tow structure with two intersected beams and a simply-supported tow structure with three intersected curved beams have been presented by using the energy method. They can be used as confirmation of the numerical non-linear finite element solution obtained in the next Chapter for these configurations.

Chapter 4

Finite element buckling analysis of curved beam structures

Using the formulation derived in Chapter 2, the buckling behavior of a few simple configurations of the curved composite beam will be presented in the following. These simple configurations include a straight composite beam, a curved composite beam, tow structures with two intersected curved beams and a tri-axial tow structure with three intersected curved beams. The material properties of the tow (beam) and resin used in this Chapter and the following Chapters are given in the Table below:

Table 4. 1: Material properties of tri-axial composite tow and resin*

Material	E_L (GPa)	E_T (GPa)	G_{LT} (GPa)	G_{TT} (GPa)	v_{LT}
Composite tow	500.0	40.0	24.0	14.3	0.26
Resin	3.5	3.5	1.3	1.3	0.35

* Subscript L denotes longitudinal direction; Subscript T denotes transverse direction.

where E is Young's modulus, G is shear modulus and v is Poisson's ratio.

The geometric parameters of the tow are as follows:

Height of cross-section of tow $a = 0.2\ mm$

Width of cross-section of tow $b = 0.84\ mm$

The geometric parameters of the resin are

Width×Length×Thickness = 0.87×0.87×0.067 *mm*

Transverse loads used in the following case $P' = 0.005\ N$

4.1 Buckling behavior of single isotropic arch beam with clamped ends

The single isotropic circular arch beam is shown in Fig. 4.1. It is clamped at both ends with a single load at the apex. The material of the arch is assumed to be isotropic

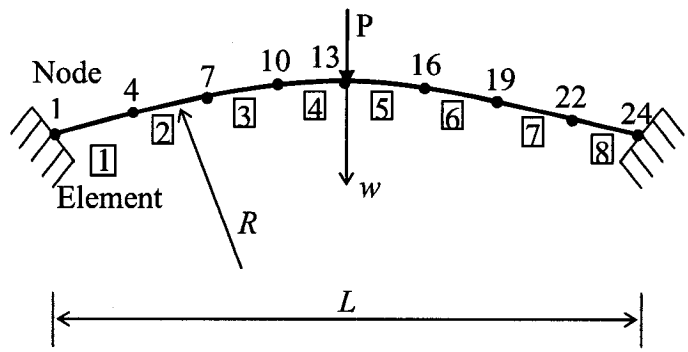

Fig. 4. 1: Arch beam with clamped ends

and linearly elastic. The arch is idealized using 8 equal curved beam elements. The maximum deflection w is measured from the apex of the configuration before loading.

Geometry and material properties of the beam are as follows [64]:

The radius of the arch	$R = 3381\ mm$
Height of the cross-section	$a = 4.8\ mm$
Width of the cross-section	$b = 25.4\ mm$
Length of the arch	$L = 863.6\ mm$
Young's modulus of elasticity	$E = 68.95\ GPa$
Poison's ratio	$\nu = 0.2$
Number of elements	$N = 8$

Comparison of the results with the one given in the Ref. [64] is shown in Fig.4.2. It can be seen that very good agreement is obtained, proving the accuracy of the formulation and also of the computer program developed for the analysis.

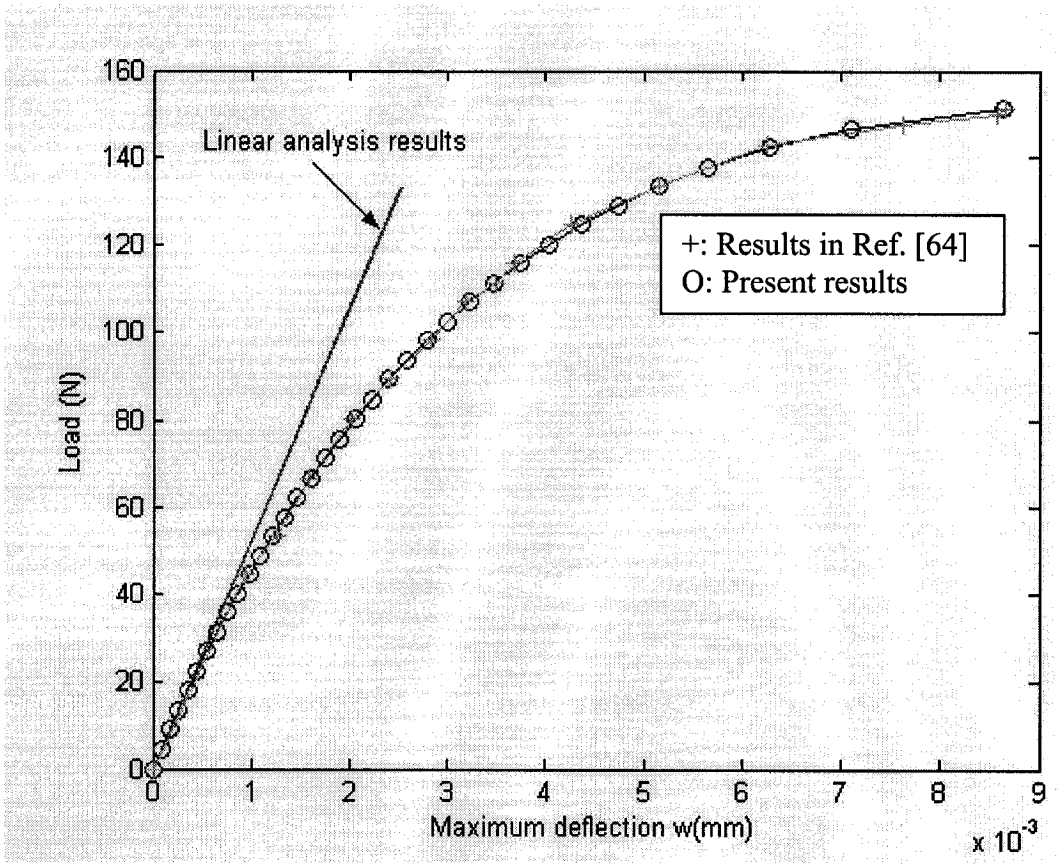

Fig. 4. 2: Load versus maximum deflection curve for the arch—Curve I

Since this is a well known structure, its buckling behavior has been studied by many researchers such as Bathe [64], Surana [62], Dupuis [66], Hu [48], etc. One of the most important characteristics of its buckling behavior is that it undergoes snap-through during deformation while loading. In order to check if the present formulation and software can predict this nature of the buckling behavior of the structure and their effectiveness for large deformation of a structure, further loading is made by increasing the value of the load from the level of the situation shown in Fig. 4.2. The result is shown

in Fig. 4.3. In this figure, one can clearly see that there is a big jump of deflection when the load reaches a certain value. This shows that a snap-through exists in this case. Thus, the accuracy and effectiveness of the present model and software has been confirmed.

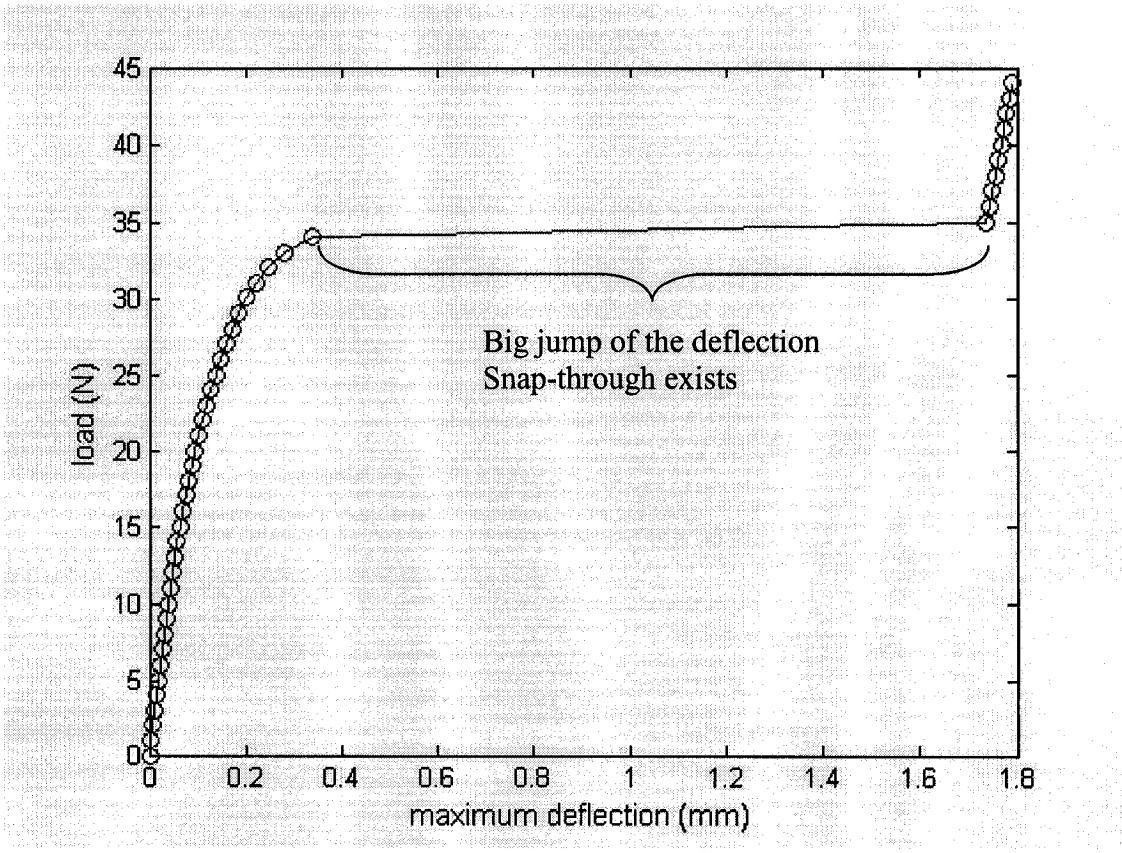

Fig. 4. 3: Load versus maximum deflection curve for the arch—Curve II

4.2 Simply-supported straight beam made of individual composite tow

A simply-supported straight composite beam with a static compressive load at the roller-supported end and a small lateral downward static load at the center, which is employed to initiate the instability, is shown in Fig. 4.4. The beam is composed of an individual composite tow which is assumed to be orthotropic and linearly elastic. The

same assumption holds in the following sections. The length of the beam is 4.58 *mm*. It is analyzed using 4 4-node elements. The maximum deflection $u_{3\max}$ was measured from the center corresponding to the unloaded configuration along x_3 direction.

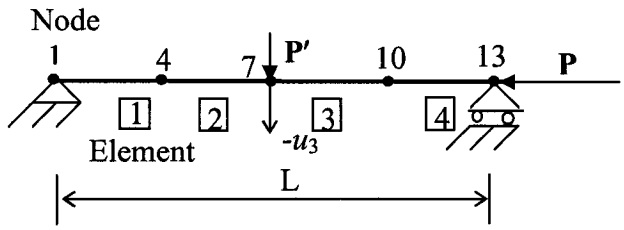

Fig. 4. 4: Simply-supported straight tri-axial composite beam

The non-dimensional load versus maximum non-dimensional deflection curve of the beam in non-linear analysis is shown in Fig.4.5.

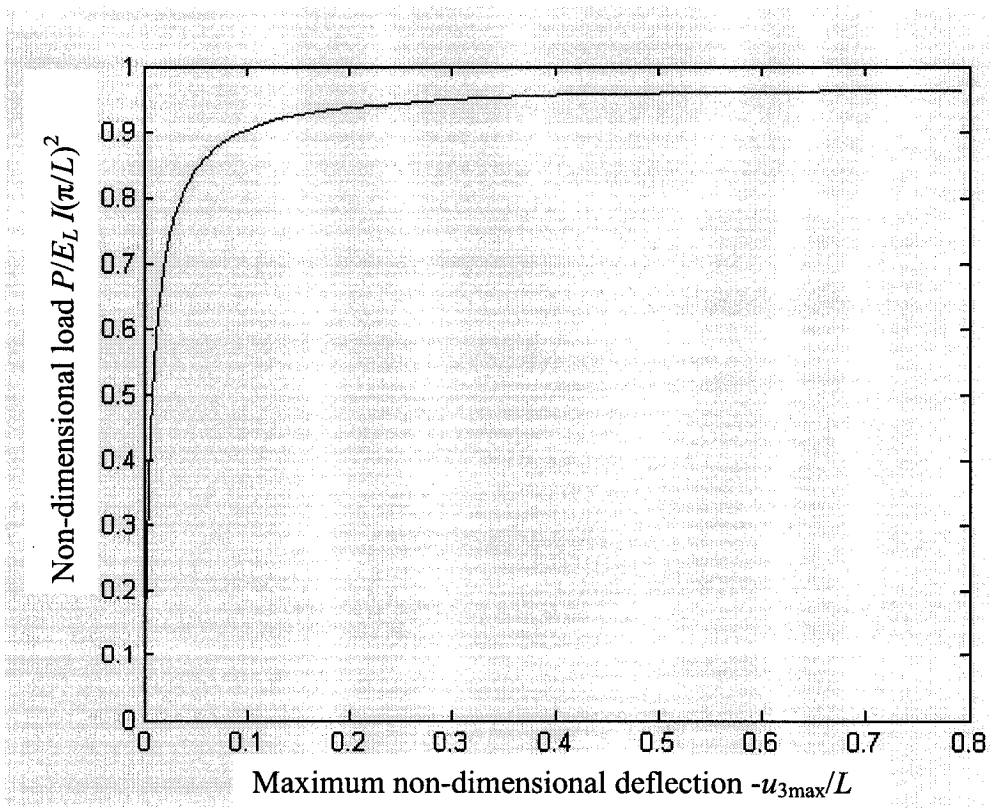

Fig. 4. 5: Load versus deflection curve for simply-supported straight tow.

The non-linear finite element solution obtained for the non-dimensional buckling load in this case is $P_{cr}/(\pi^2 E_L I/L^2) = 0.9648$. This result is very close to the result obtained using well known Euler's beam-column formula, that is, $P_{cr}/(\pi^2 E_L I/L^2) = 1$. There is about 3.5% difference that is predicted. The reason for this is that the shear effect is included in the present case while the shear effect is not considered in the Euler case. Since the present beam is a thin beam, the shear effect will "soften" the beam and decrease the value of its buckling load. Therefore, very good consistency is obtained.

4.3 Straight cantilever beam made of tri-axial composite

A straight cantilever composite beam with an individual static compressive load at the free end and a small lateral downward static load, which is employed to initiate the instability, at the same end is shown in Fig. 4.6. It is analyzed using 4 4-node elements. The length of the beam is 4.58 *mm*. The maximum deflection u_3 is measured from the free end corresponding to the unloaded configuration. The non-dimensional load versus maximum non-dimensional deflection curve of the beam in non-linear finite element analysis is shown in Fig. 4.7.

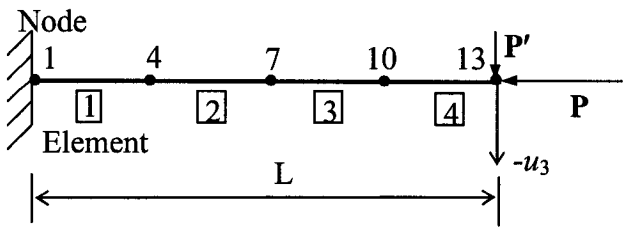

Fig. 4. 6: Straight cantilever composite beam made of individual tow

The non-linear finite element solution obtained for the non-dimensional buckling load in this case is $P_{cr}/(\pi^2 E_L I/L^2) = 0.2429$. This result is very close to the result obtained using Euler's beam-column theory given by $P_{cr}/(\pi^2 E_L I/L^2) = 0.25$. There is about 2.84% difference between them. The reason for this is also the shear effect. The difference has the same order as the simply-supported straight beam. It can be seen that excellent agreement is also obtained.

It is worthy to mention that the ratio of the critical loads corresponding to the simply-supported beam and cantilever beam obtained using Euler's theory is 4. In the present non-linear finite element analysis the ratio is 3.972, which is very close to 4. The agreement is therefore confirmed. This further proves the accuracy of the formulation and the computer program developed for the analysis.

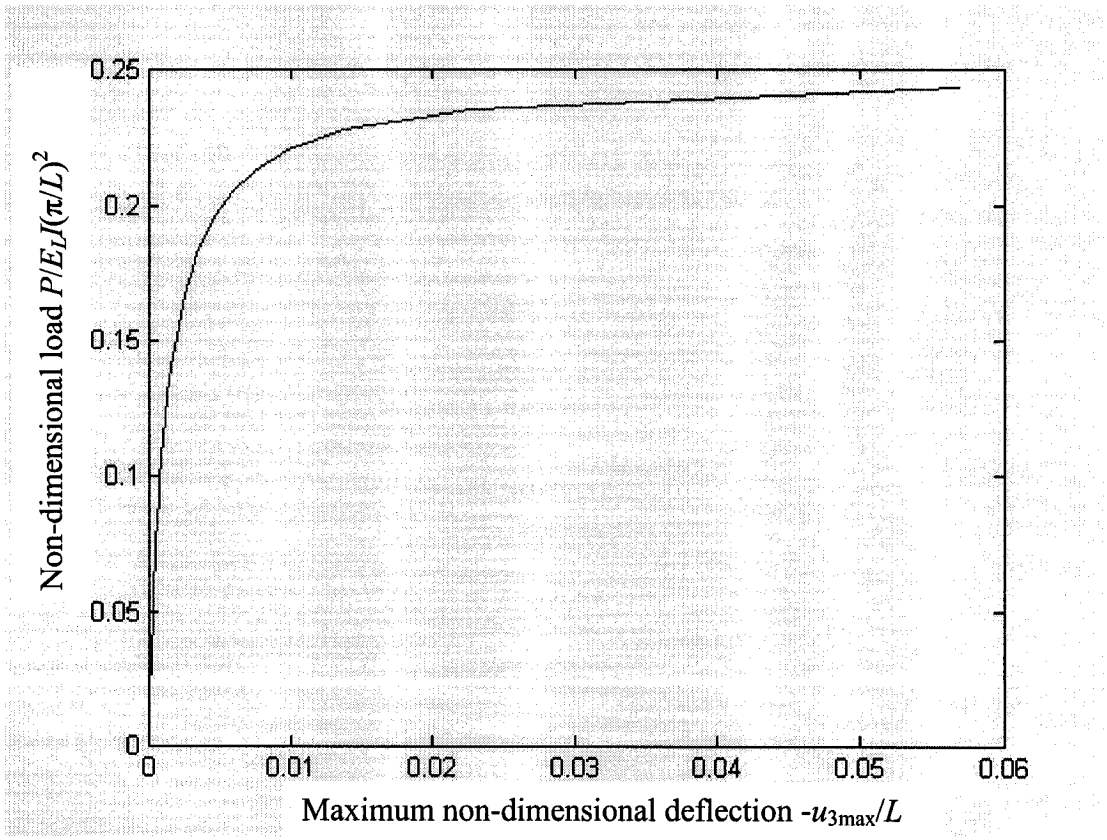

Fig. 4. 7: Load versus deflection curve for clamped straight tow

4.4 Simply-supported curved beam made of individual composite tow

A simply-supported curved composite beam with a static compressive load at the roller-supported end and a small lateral downward static load, which is used to initiate the instability, at the middle of the beam is shown in Fig. 4.8. It is analyzed using 4 4-node elements. The span of the beam is 4.58 *mm*. The maximum deflection u_3 is measured from its center line corresponding to the unloaded configuration. The curved beam is on ox_1x_3 plane and the equation of its center line can be expressed as:

$$\begin{cases} x_3 = Z\sin(2\pi x / L) \\ x_2 = 0 \end{cases} \tag{4-1}$$

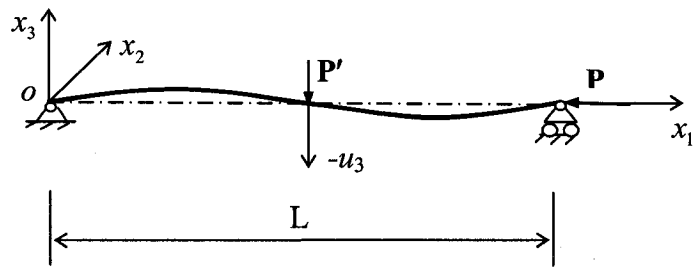

Fig. 4. 8: Simply-supported curved composite beam

where the maximum value of the co-ordinate in x_3 direction is $Z = 0.133\,mm$. This value is obtained from observation of the microphotograph of a section of the individual tow in a tri-axial structure as shown in Fig. 4.9.

Non-dimensional load versus maximum non-dimensional deflection curve of simply-supported individual curved composite beam is shown in Fig. 4.10.

Fig. 4. 9: Configuration of the fiber tow and resin.

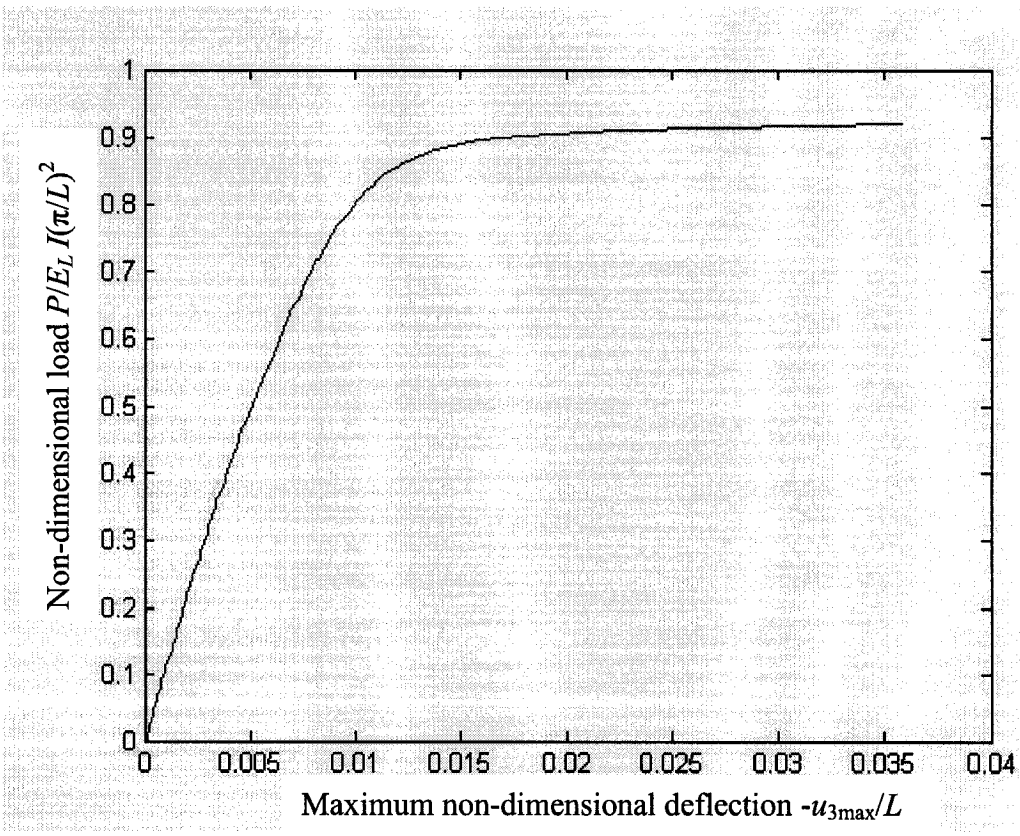

Fig. 4. 10: Load versus deflection curve for simply-supported curved tow

The non-linear finite element solution obtained for the non-dimensional buckling load of a simply-supported individual curved tow is $P_{cr}/(\pi^2 E_L I/L^2) = 0.9185$. It is 4.8% less than the finite element result in straight beam case and 3.4% less than analytical result. It is also worthy to note that the difference (4.8%) of the non-linear finite element solution for buckling loads between straight beam and curved beam almost has the same amount of difference (4.9%) from analytical solution for the two beams. It shows that the change of the buckling load due to curving the beam in finite element solution obeys the same law given by equation (3-27) if the buckling load is measured based on the straight beam buckling load. Next, from figures 4.5 and 4.10 we can see that the slope of the load versus maximum-deflection curve of a curved beam before buckling is less than the slope of the load versus maximum-deflection curve of a straight beam before buckling. It means that curving the beam will increase the deforming rate of the beam before buckling and as a result, as we have expected, the deformation of a curved beam will be larger than the deformation of a straight beam at the same amount of axial compressive load. Therefore, good agreement is thus confirmed.

Deformed and undeformed shapes of simply-supported single curved composite tow are shown in Fig. 4.11 when load is equal to 120 *N*.

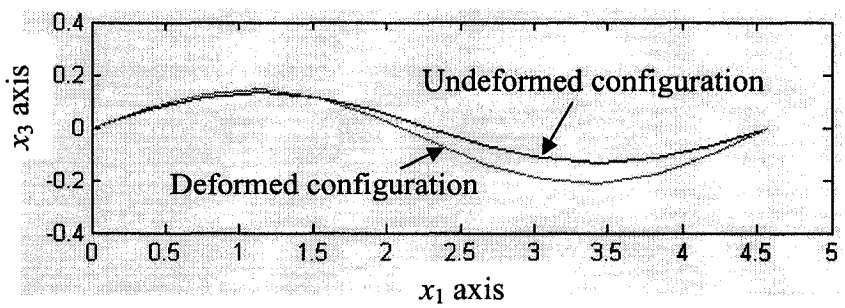

Fig. 4. 11: Deformed and undeformed shapes of simply-supported curved composite tow

4.5 Cantilever curved composite beam

Using the same beam configuration, the same material properties and the same finite element mesh as that of the simply-supported curved composite beam in Section 4.4, but different boundary conditions, that is, the clamped boundary condition at the left end of the beam and free end condition at the other end, and different load condition with a compressive load and a small lateral downward static load to initiate the instability at the free end and performing the non-linear finite element analysis, one obtains the load versus maximum deflection curve as shown in Fig. 4.12. We can see from Fig. 4.12 that a

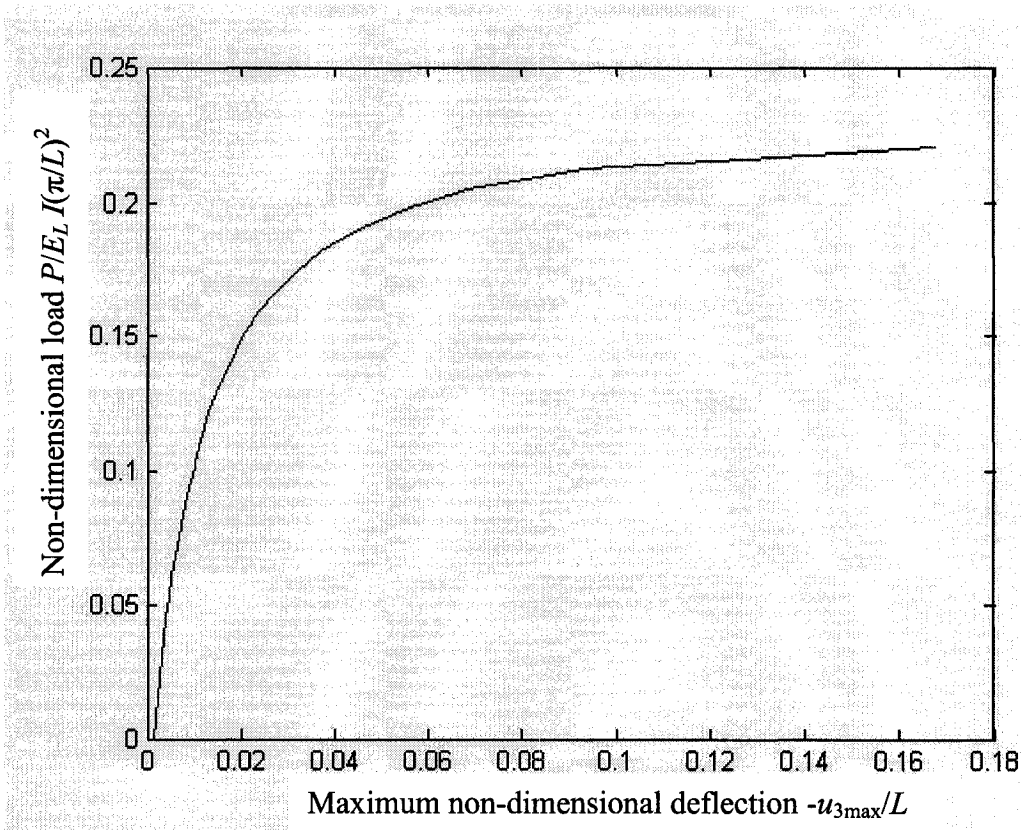

Fig. 4. 12: Load versus maximum deflection curve for cantilever curved tow

much larger deflection and much larger deformation rate of the curved beam compared with the cantilever straight beam case in Section 4.3 at a certain amount of axial compressive load are predicted.

We did not draw this curve together with the curves of other cases due to this reason. This further confirms the observations made in Section 4.4.

The non-linear finite element solution thus obtained for the non-dimensional buckling load of a cantilever individual curved tow is $P_{cr}/(\pi^2 E_L I/L^2) = 0.2201$. The ratio of the buckling load for simply-supported curved beam to the one in the present case is 4.17. It is very close to 4. It shows that the Euler buckling load relation between a simply-supported beam and a cantilever beam also holds for the present case. Deformed and undeformed shapes of cantilever individual curved composite tow are shown in Fig. 4.13 when load is equal to 27 *N*. It may be noted here that for the curved beam the original configuration is oriented at an angle with respect to x_1-axis at both the fixed and free ends.

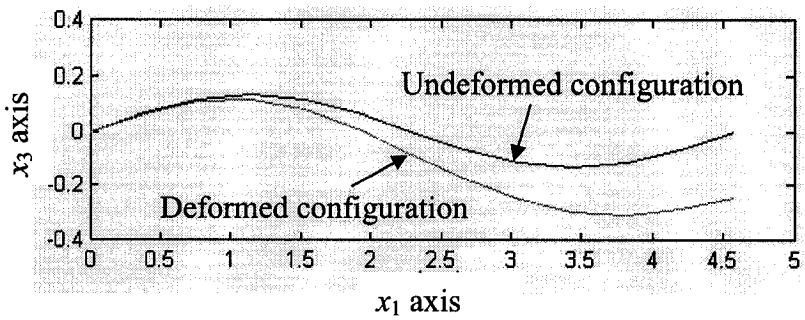

Fig. 4. 13: Deformed and undeformed shapes of cantilever curved beam

4.6 Simply-supported two intersected curved composite tow structure

A simply supported curved tri-axial composite tow structure is shown in Fig. 3.2. This structure is made of two intersected curved composite tows at angle of 60°, which

are bonded together by resin at the midpoints of each tow for the sake of symmetry. The initial configurations of the beams follow half of a sine curve. Thus, the curvature of the tow is maintained. The resin layer at the cross over of the tows can be represented by bars as modeled in Chapter 2. The ends of the tows are represented by pins at one end of the tow and by pin-on-rollers at the other end of the tow. The tows are constrained at the ends such that the reaction forces at the constraints are perpendicular to the orientation of the tows at these ends. Two static compressive loads along the connection lines of corresponding supported ends and a small lateral downward static load at the apex are applied. The small lateral load **P'** is employed to initiate the instability and it is kept to be constant. The values of the axial loads for the two beams, which are $\mathbf{P}_A$ and $\mathbf{P}_B$, will be kept to be the same. The structure is analyzed using 4 4-node elements with two elements for each tow. The maximum deflection u_3 is measured from its central line corresponding to its unloaded configuration. The dotted lines in the figure constitute the x_1x_2 plane of co-ordinate system. The length of the beam is 2.29 *mm*. Geometries of the structure are as follows:

The beam AA' is in x_1x_3 plane and the equation of its central line is given by

$$\begin{cases} x_3 = Z\sin(\dfrac{\pi}{L}x_1) \\ x_2 = 0 \end{cases} \tag{4-2}$$

The beam BB' is in $x_{B1}x_{B3}$ plane, where x_{B3} is parallel to x_3 axis and x_{B1} is in ox_1x_2 plane and is intersected with ox_1 axis at angle of 60^0, as shown in Fig. 3.2. The equation of central line of beam BB' is as follows:

$$x_{B3} = -Z\sin(\frac{\pi}{L}x_{B1}) \tag{4-3}$$

Load versus maximum deflection curve is plotted in Fig. 4.14. The non-dimensional buckling load obtained from the non-linear finite element analysis in

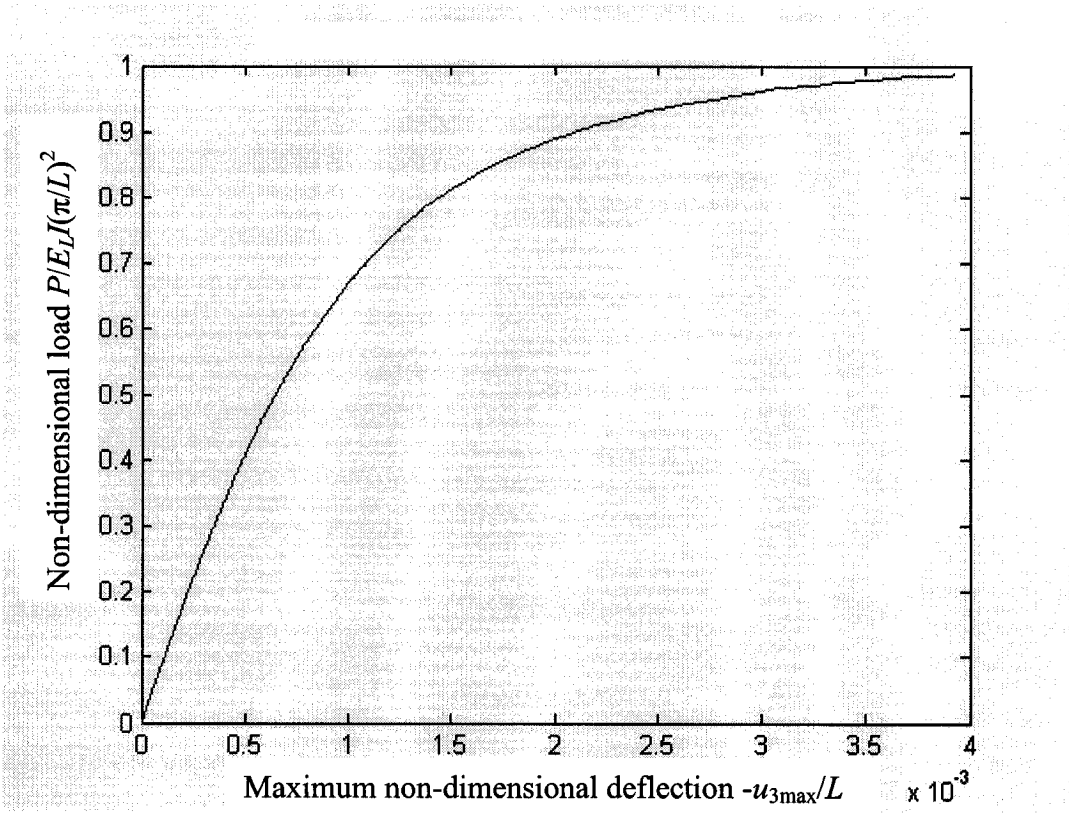

Fig. 4. 14: Load versus maximum deflection curve of simply-supported two intersected tow structure

this case is $P_{cr}/(\pi^2 E_L I/L^2) = 0.9862$. It is 6.86% larger than the individual curved beam case and 2.22% larger than the individual straight beam case. It shows that the resin used for bonding two oppositely curved tows may have the effect to resist further deformation of the structure. The result obtained from the approximation solution given in Section 3.2 is 1.01. It is 1% larger than the Euler buckling load in straight beam case. This further confirms the effect of the resin on resisting the deformation of the structure. Comparing

the two results, the non-linear finite element solution is seen to be 2.36% less than the approximate solution. It is a very good agreement. The reason for the difference between the two solutions is the shear effect of the beams. Non-linear finite element solution takes the shear effect into consideration while the analytical approximate solution does not.

In order to know the effect of the resin on the buckling behavior of simply-supported two oppositely curved tow structure, ten times of variation, both increasing and decreasing, of Young's modulus of resin is made. Buckling loads at different Young's modulus values are plotted in Fig. 4.15. From this figure one observes that buckling load increases as the Young's modulus becomes smaller - this is because smaller Young's modulus leads to smaller stiffness of the resin as a bar, correspondingly, the resin is deformed more easily. This leads to further increase in curvature of each beam when loads are smaller. Note that each beam is curved along different directions. In order to

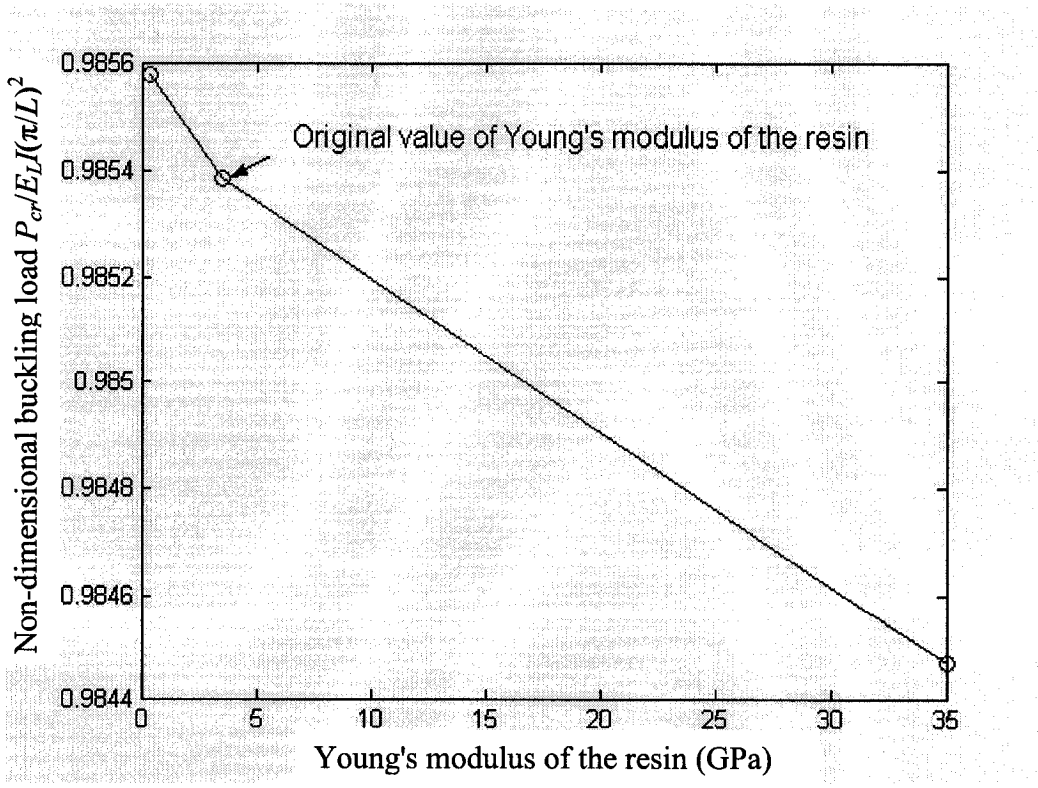

Fig. 4. 15: Buckling load for two-tow structure versus Young's modulus of the resin

make the two beams to buckle together, great effort needs to be exerted in order to reverse the curvature of one beam. Therefore, larger value of load **P** is needed to buckle the structure if the two beams are to buckle on the same side, either up or down. For the case of stiff resin, the two tows are held together more rigidly. As such they tend todeform together at the initial low loads, that makes buckling easier. This procedure can be described by Fig. 4.16. The structure in Fig. 4.16 is buckled downward due to a downward small transverse load **P′**.

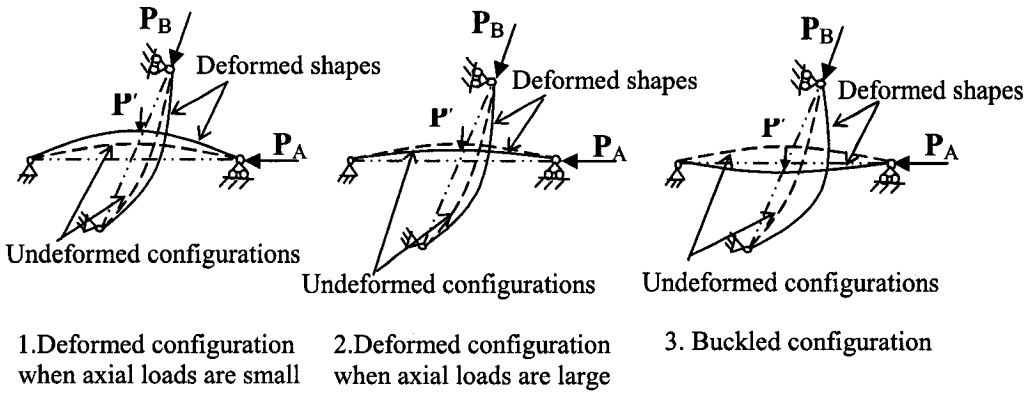

Fig. 4. 16: Deformation patterns of two-tow structure

Non-linear finite element solution for the relation of buckling load and ratio of tension stiffness and bending stiffness, E_LA/E_LI, is plotted in Fig. 4.17. For comparison purpose the analytical solution shown in Fig. 3.3 is also plotted in Fig. 4.17. The values of the stiffness ratio at different points shown in Fig. 4.17 are obtained in the same way as in Fig. 3.3. For clarity the values shown in Fig. 4.17 are also listed in Table 4.2. From both the table and the figure one can observe that the value of the buckling load obtained from either non-linear finite element solution or approximate analytical solution tends to increase as the thickness of the beam becomes larger, but the differences between the two

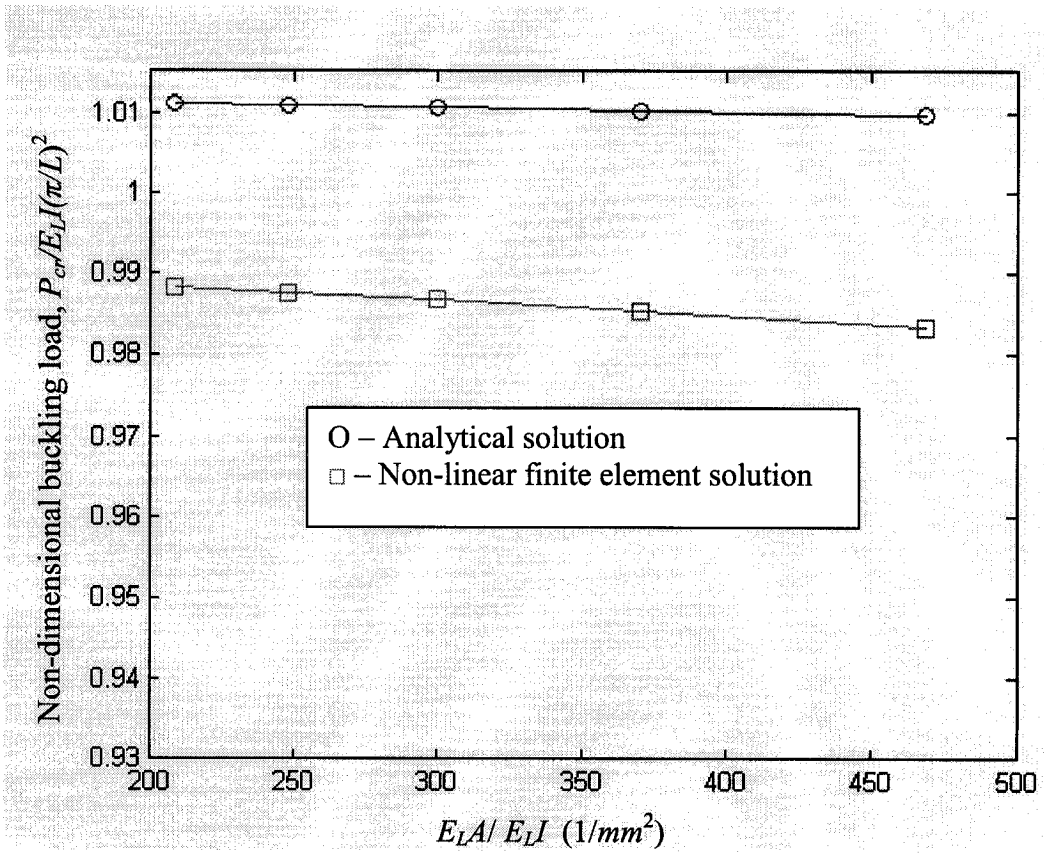

Fig. 4. 17: Curve of non-dimensional buckling load versus stiffness ratio E_LA/E_LI for two intersected curved beam structure

Table 4. 2: List of non-dimensional buckling loads of NFES[1] and AAS[2]

Stiffness ratio ($1/mm$)	208.33	247.93	300.00	370.37	468.75
Thickness of the beam (mm)	0.24	0.22	0.20	0.18	0.16
NBLNFES[3]	0.9882	0.9876	0.9862	0.9853	0.9834
NBLAAS[4]	1.0111	1.0109	1.0105	1.0101	1.0096
Relative error[5] (%)	2.26	2.30	2.38	2.46	2.60

1. NFES – Non-linear finite element solution.
2. AAS – Approximate analytical solution
3. NBLNFES – Non-linear finite element solution for non-dimensional buckling load.
4. NBLAAS – Approximate analytical solution for non-dimensional buckling load.

5. The error of non-linear finite element solution relative to approximate analytical solution.

solutions tends to decrease. This is because of the shear effect of the beam. For a thin beam, when it gets thinner, it will be easier to be deformed and the value of its buckling load will tend to be smaller.

4.7 Simply-supported three intersected curved tri-axial composite structure

A simply supported curved tri-axial composite tow structure, the so-called unit cell, is shown in Fig. 3.4. This tri-axial structure is made of three composite tows woven at angles of 0°, 60°and -60° with each other and bonded together by resin at locations situated at 1/4 and 3/4 of the length of each beam. There are three connections among the three beams. The initial configurations of the beams follow full sine curve. The structure is loaded with three static compressive loads at three roller-supported ends and three small lateral downward static loads at the three apexes shown in Fig. 3.4. The small lateral load $\mathbf{P'_1}$, $\mathbf{P'_2}$ and $\mathbf{P'_3}$ at apex are still used to initiate the instability. The values of the axial loads for the three beams, which are $\mathbf{P_A}$, $\mathbf{P_B}$ and $\mathbf{P_C}$, will be kept the same.

The structure is modeled using 12 4-node elements with 4 elements for each tow. The maximum deflection u_3 is measured from its central line corresponding to its unloaded configuration. The dotted lines in the figure constitute the x_1x_2 plane of co-ordinate system. Geometries of the structure shown in Fig. 3.4 are as follows:

The beam AA' is in x_1x_3 plane and the equation of its central line is given by

$$x_3 = Z\sin(\frac{2\pi}{L}x_1) \tag{4-4}$$

$$x_2 = 0 \tag{4-5}$$

The beam CC' is in $x_{C1}x_{C3}$ plane, where x_{C3} is parallel to x_3 axis and x_{C1} is in ox_1x_2 plane and is intersected with ox_1 axis at angle of -60^0. The equation of central line of beam CC' is given by

$$x_{C3} = -Z\sin(\frac{2\pi}{L}x_{C1}) \tag{4-6}$$

The beam BB' is in $x_{B1}x_{B3}$ plane, where x_{B3} is parallel to x_3 axis and x_{B1} is in ox_1x_2 plane and is intersected with ox_1 axis at angle of 60^0. The equation of central line of beam BB' is given by

$$x_{B3} = -Z\sin(\frac{2\pi}{L}x_{B1}) \tag{4-7}$$

The load and maximum deflection curve of the structure is shown in Fig. 4.18. The buckling load from non-linear finite element solution in this case is $P_{cr}/(\pi^2 E_L I/L^2)$ = 0.9564. The result obtained from approximate analytical solution in Section 3.3 is 0.9507. Comparing the two solutions, the difference of the buckling load for a unit cell between them is 0.6%. It is an excellent agreement.

The effect of the resin on three-intersected-tow structure is shown in Fig. 4.19. It can be seen that the effect of the resin on the three-intersected-tow structure looks the same as the two-intersected-tow structure, except the slope of the curve for the three-intersected-tow structure is less than that of the two-intersected-tow structure. This reveals that the more tows are involved in the tow structure by weaving, the less effects the resin has on the buckling behavior of the structure.

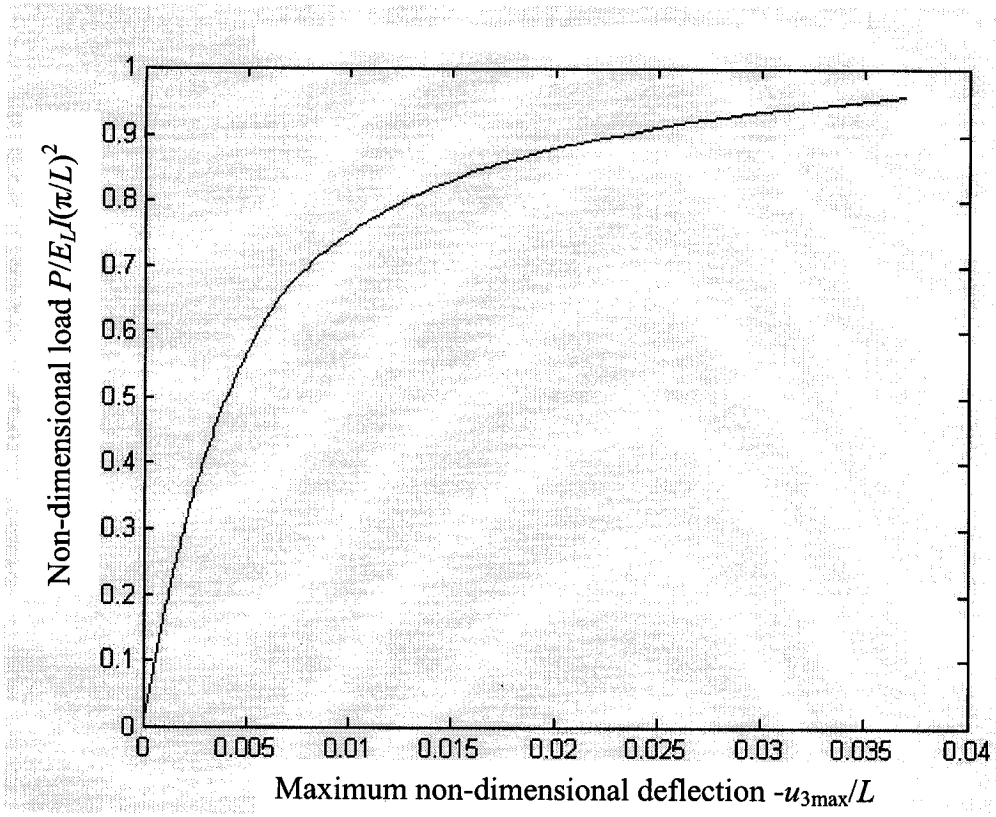

Fig. 4. 18: Load versus maximum deflection curve of simply-supported three intersected tow structure

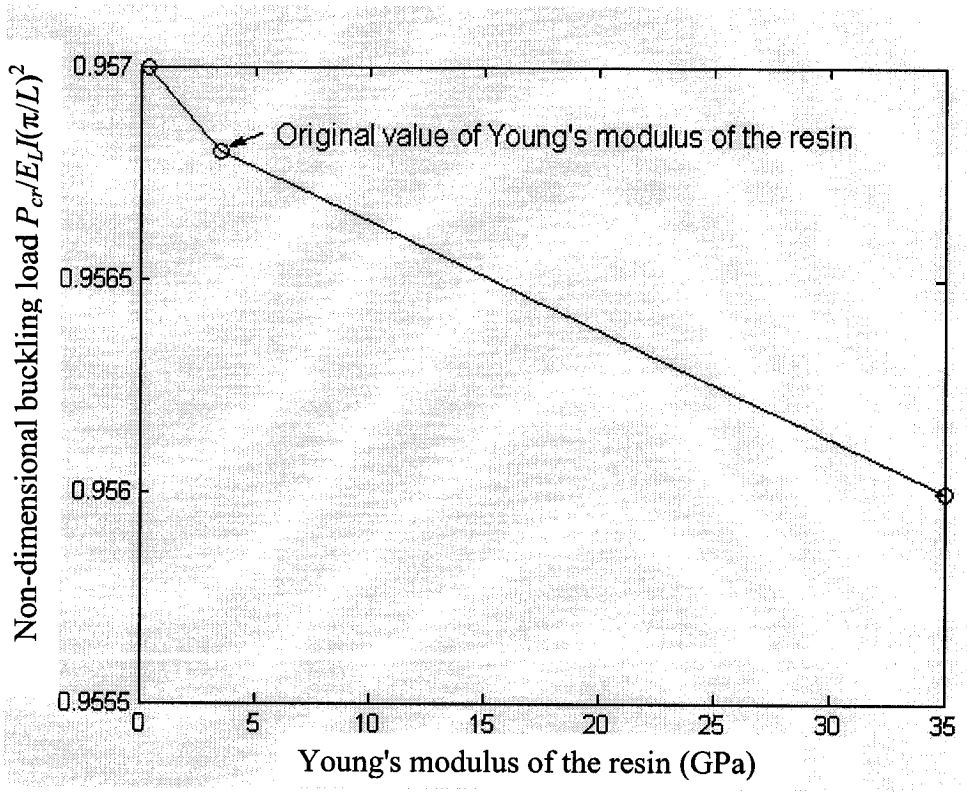

Fig. 4. 19: Buckling load for three-tow structure versus Young's modulus of the resin

4.8 Conclusion

A non-linear finite element analysis for the buckling behavior of several simple curved composite beam structures has been performed. These structures include individual straight and curved composite beam, composite tow structure with two intersected curved beams and tow structures with three intersected curved beams. Comparisons between present numerical solution and approximate analytical solutions obtained in Chapter four for the corresponding structures are also made. The accuracy of the numerical solutions has been confirmed by the approximate analytical solutions for corresponding structures. Therefore, the non-linear finite element formulation can be used for analyzing the buckling behavior of the complicated tri-axial woven fabric composite tow structures, which will be presented in the next Chapter.

Chapter 5

Buckling analysis of more complicated tri-axial structures

Buckling of a structure may cause structural instability or collapse. The maximum load that a structure can support prior to failure has to be estimated. In this Chapter, the buckling analysis for more complicated tri-axial structures will be conducted. The tri-axial structures are restrained either along upper and lower edges or only along left and right edges or all four edges and are subjected to a uni-directional or bi-directional loading. These cases will be studied separately.

The typical configuration of the tri-axial tow structure under investigation is the basic composite structure with six tri-axial woven fabric composite tows bonded at their interlaced parts by resin, as shown in Fig. 5.1. The investigation conducted involves buckling analysis, sensitivity analysis of buckling behavior to initial imperfections and to the change in boundary conditions. By adding different numbers of X-crossovers both vertically and horizontally to the basic tri-axial structure, modified basic tri-axial structures configured in the rectangular in-plane shape with different in-plane aspect ratio values are obtained. Sensitivity of buckling behavior to the in-plane aspect ratio of these structures will also be studied. Performing buckling analysis on these configurations will lead to a better understanding of the relationship between buckling loads and the size and shape of the tri-axial woven structures.

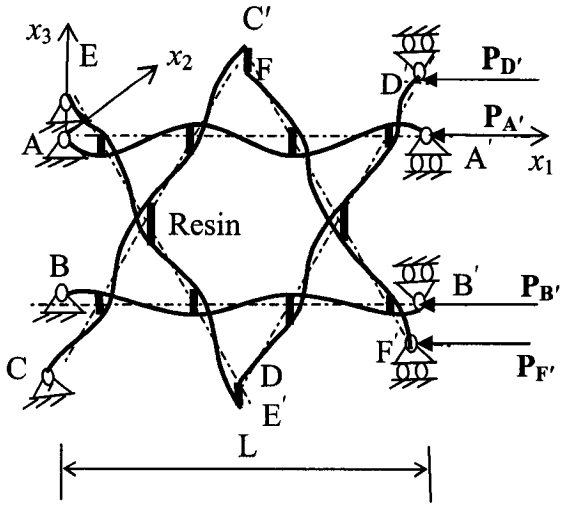

Fig. 5. 1: Basic composite structure with six woven intersected curved tows

5.1 Simply-supported basic structure subjected to uni-directional loading along x_1 direction

A simply-supported composite structure consisting of six curved tri-axial woven fabric composite tows (the so-called basic tri-axial composite structure shown in Fig. 5.1) subjected to uni-directional compressive loads $\mathbf{P}_{D'}$, $\mathbf{P}_{A'}$, $\mathbf{P}_{B'}$ and $\mathbf{P}_{F'}$ along x_1 direction at the supported ends and six small lateral downward static loads of equal magnitude denoted by dots at the six apexes, that are used to initiate the deflection, is shown in Fig. 5.2. The structures shown in Fig. 5.1 and 5.2 are the same. Both of them are the basic composite structure. Fig. 5.1 is a three dimensional view of the central line of the structure and Fig. 5.2 is a two dimensional view of the configuration. The values of the axial loads, $\mathbf{P}_{A'}$, $\mathbf{P}_{B'}$, $\mathbf{P}_{F'}$ and $\mathbf{P}_{D'}$ are kept to be equal and they are increased by the same increment each time. The values of the six transverse loads denoted by dots are kept to be equal and constant throughout. They are equal to 0.005N and this loading is kept to be the same in the following sections, unless otherwise specified.

The structure, as mentioned in the above, is made of six composite tri-axial tows that are woven at angles of 0°, 60°and 120° and bonded together by resin at the interlaced parts. The tri-axial composite tow is assumed to be orthotropic and linearly elastic. It is idealized by using 48 4-node beam elements which are distributed along the central line of every individual curved tow, as shown in Fig. 5.3. The central lines of the curved tows can be approximated by sine curves. Every element takes up a quarter of a full sine curve of the central line as shown in Fig. 5.3. The projected length, L, of the structure is equal

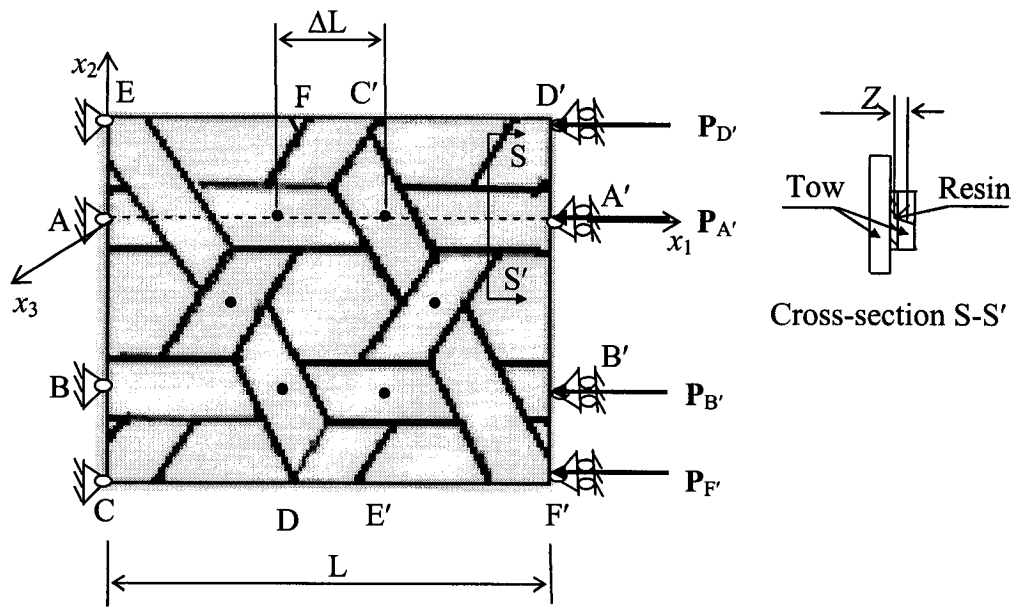

Fig. 5. 2: Basic structure with six intersected tows subjected to uni-directional loading

to 9.16 *mm*. The cross-sectional dimensions of the beam (tow) are 0.84×0.2 *mm*, which is kept the same in the following sections. The maximum deflection $u_{3\max}$ of the structure is measured from its mid surface corresponding to the unloaded configuration. The central points of the resin part that is between the interlaced tows in Fig. 5.2 constitute the x_1x_2

plane of the co-ordinate system and the x_3 co-ordinate is determined as per the right-hand-rule. The structure is simply-supported at the edges of x_1=0, L as shown in Fig. 5.2.

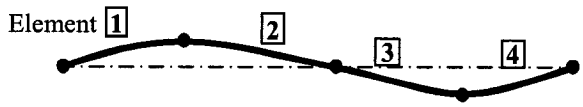

Fig. 5. 3: Central line of a full sine wave of an individual tow of the basic structure and its element meshing

The central line of beam AA′ as shown in Fig. 5.1 and 5.2 is in x_1x_3 plane and A is the origin of the co-ordinate system. The equation of its central line is given by

$$\begin{cases} x_1 = \xi \\ x_2 = 0 \\ x_3 = -Z\sin(\dfrac{\pi}{\Delta L}\xi) \end{cases} \tag{5-1}$$

where $Z = 0.133$ mm, and this value has been obtained from experimental observation of the microphotograph of a tow. Here, Z is the amplitude of the curved tow, which is equal to the distance between the centers of the resin part and tow at the interlaced cross-section as shown in Fig. 5.2; $\xi \in [0, L]$ is the independent parameter used to express a space curve in the co-ordinate system $x_1x_2x_3$ with origin at A; ΔL is the length of hexagon in the middle as shown in Fig. 5.2, $\Delta L = 2.29$ *mm*.

The beam BB′ is parallel to beam AA′ and the distance between them is $2\Delta L\sin(\dfrac{\pi}{3})$ as shown in figures 5.1 and 5.2. The equation of the central line of beam BB′ is given by

$$\begin{cases} x_1 = \xi \\ x_2 = -2\Delta L \sin(\frac{\pi}{3}) \\ x_3 = Z \sin(\frac{\pi}{\Delta L}\xi) \end{cases} \tag{5-2}$$

The beam CC′ is intersected with beam AA′ at an angle of 60° counterclockwise as shown in figures 5.1 and 5.2. The equation of its central line is given by

$$\begin{cases} x_1 = \xi \cos(\frac{\pi}{3}) \\ x_2 = (\xi - 3\Delta L)\sin(\frac{\pi}{3}) \\ x_3 = Z \sin(\frac{\pi}{\Delta L}\xi + \frac{\pi}{2}) \end{cases} \tag{5-3}$$

The beam DD′ is parallel to beam CC′ and is located at a distance of $2\Delta L \sin(\frac{\pi}{3})$ from beam CC′ as shown in figures 5.1 and 5.2. The equation of its central line is given by

$$\begin{cases} x_1 = 2\Delta L + \xi \cos(\frac{\pi}{3}) \\ x_2 = (\xi - 3\Delta L)\sin(\frac{\pi}{3}) \\ x_3 = Z \sin(\frac{\pi}{\Delta L}\xi + \frac{\pi}{2}) \end{cases} \tag{5-4}$$

The beam EE′ is intersected with beam AA′ at an angle of 120° counterclockwise as shown in figures 5.1 and 5.2. The equation of its central line is given by

$$\begin{cases} x_1 = \xi \cos(\frac{\pi}{3}) \\ x_2 = (\Delta L - \xi)\sin(\frac{\pi}{3}) \\ x_3 = Z \sin(\frac{\pi}{\Delta L}\xi - \frac{\pi}{2}) \end{cases} \tag{5-5}$$

The beam FF′ is parallel to beam EE′ and is located at a distance of $2\Delta L \sin(\frac{\pi}{3})$ from beam EE′ as shown in figures 5.1 and 5.2. The equation of its central line is given by

$$\begin{cases} x_1 = 2\Delta L + \xi \cos(\frac{\pi}{3}) \\ x_2 = (\Delta L - \xi)\sin(\frac{\pi}{3}) \\ x_3 = Z \sin(\frac{\pi}{\Delta L}\xi - \frac{\pi}{2}) \end{cases} \tag{5-6}$$

Material properties of tri-axial composite tow and resin are given in Chapter 4. The non-dimensional load versus non-dimensional maximum deflection curve of the structure obtained by performing non-linear finite element analysis developed in Chapter 2 is shown in Fig. 5.4. Note that load P in this figure refers to the load applied to each beam (tow). The symbol P will have the same meaning in the following sections, unless otherwise specified. During this analysis, the load increment is set to be equal to 1N in order to perform the static analysis. This procedure of load application is also used in the following sections.

The non-linear finite element solution for the non-dimensional buckling load of a simply-supported basic composite structure shown in Fig. 5.2 subjected to uni-directional

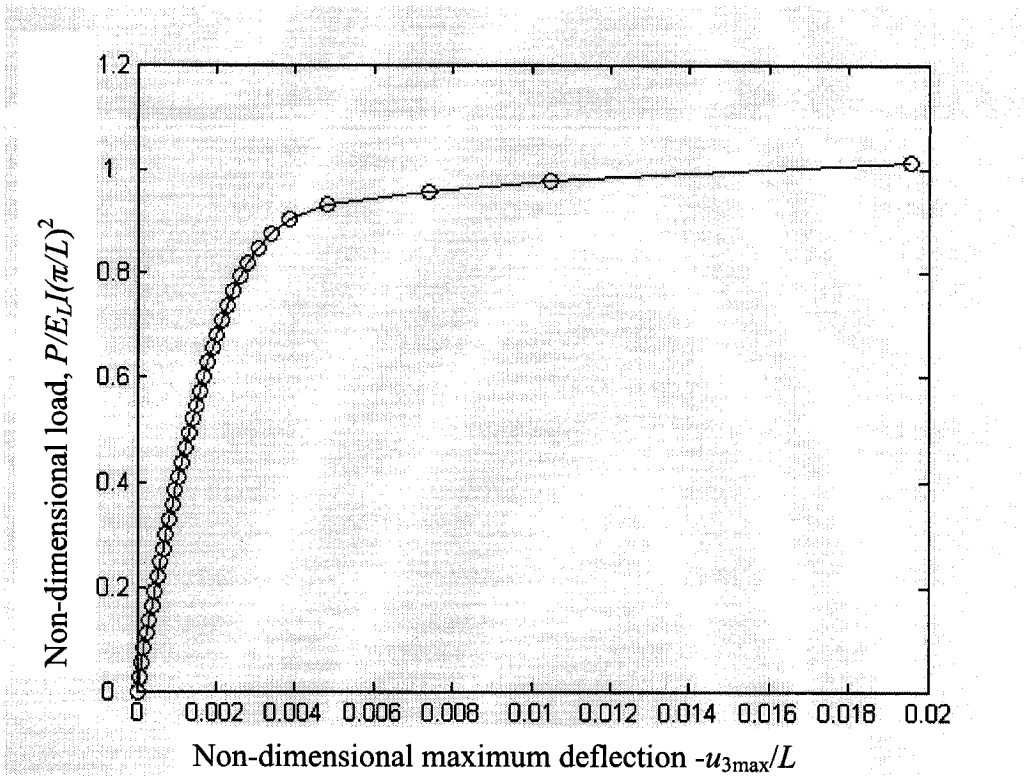

Fig. 5. 4: Load versus maximum deflection curve corresponding to the structure shown in Fig. 5.2; u_{3max} is the maximum deflection of the structure referred to the unloaded configuration

loading is $P_{cr}/(\pi^2 E_L I/L^2)=1.002$.

Comparing the value of the buckling load for the basic tri-axial structure with those of the simply-supported individual curved beam made of a tow shown in Fig. 4.8 and the simply-supported three-intersected curved tow structure shown in Fig. 3.3, it is seen that the critical buckling load of the basic structure is 9.09% higher than that of the simply-supported individual curved beam and 4.77% higher than the critical buckling load of the three-intersected curved tow structure. It shows that the basic tri-axial composite structure made by bonding and weaving many curved tows together can sustain larger compressive loads than that of the individual curved tow and that of the tri-axial woven fabric tow structure with fewer tows. Actually, when the tri-axial composite structure is fabricated by weaving and bonding tows together in the way shown in Fig.

1.2 and loaded uni-directionally, the structure is strengthened by the bonded and woven tows in the directions of 60^0 and 120^0 and resin. Therefore, the value of its buckling load should be larger than that of the individual tow and that of the structure with fewer tows.

For the purpose of application, the total non-dimensional load ($P_T/(\pi^2 E_L I/L^2)$) per unit width of the tri-axial structure versus non-dimensional maximum deflection curve of the structure is shown in Fig. 5.5. From this figure one can observe that the shape of the curve is similar to the one shown in Fig. 5.4, but the values of the buckling load shown in these two figures are different. This is because the quantity of the load shown in Fig. 5.5 is obtained by dividing the load in Fig. 5.4 by the width of the basic tri-axial structure.

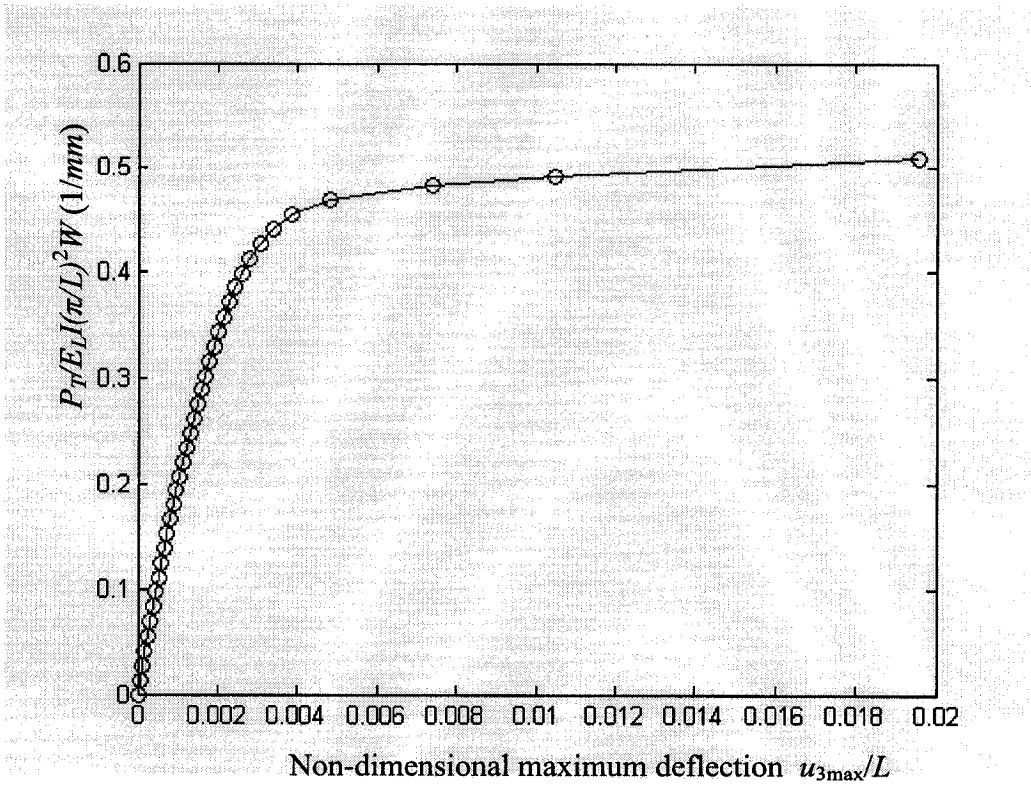

Fig. 5. 5: Total non-dimensional load per unit width of the basic tri-axial structure, $P_T/E_L I(\pi/L)^2 W$, versus non-dimensional maximum deflection curve

Effect of Young's modulus of resin

In order to know the effect of the Young's modulus of the resin on the buckling behavior of simply-supported basic tri-axial structure shown in Fig. 5.2, ten times of variation, both larger and smaller than the current Young's modulus of resin is considered. Buckling loads for different Young's modulus values are plotted in Fig. 5.6. From this figure one can observe that variation of the Young's modulus of the resin has little effect on buckling load of the basic structure. This is because the effect of the resin is diminished due to the interaction of the woven tows constituting the structure when they move up and down.

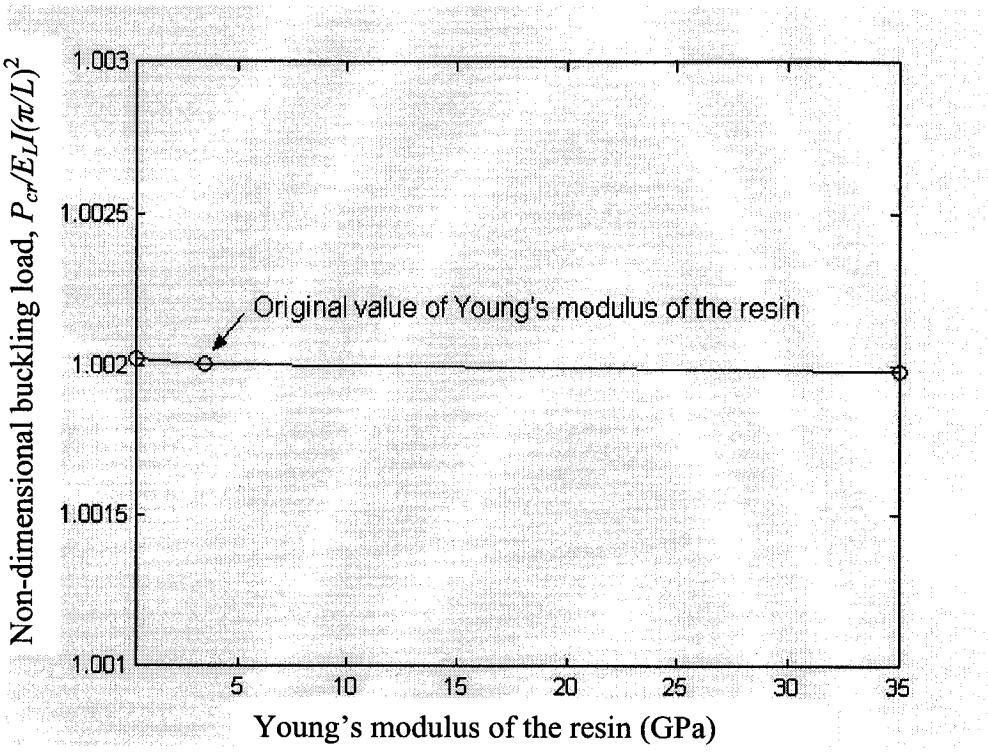

Fig. 5. 6: Buckling load for basic structure versus Young's modulus of the resin

5.2 Simply supported basic structure subject to loading along x_2 direction

In some cases, the tri-axial woven structure may sustain compressive loads in the x_2 direction. The buckling behavior may be different from that of the structures that are loaded in x_1 direction because of the apparent anisotropic nature of the structure. In order to predict the buckling behavior of the tri-axial woven structure in these cases, consider the basic tri-axial structure that is simply-supported at the edges parallel to x_1 axis and loaded in x_2 direction as shown in Fig. 5.7.

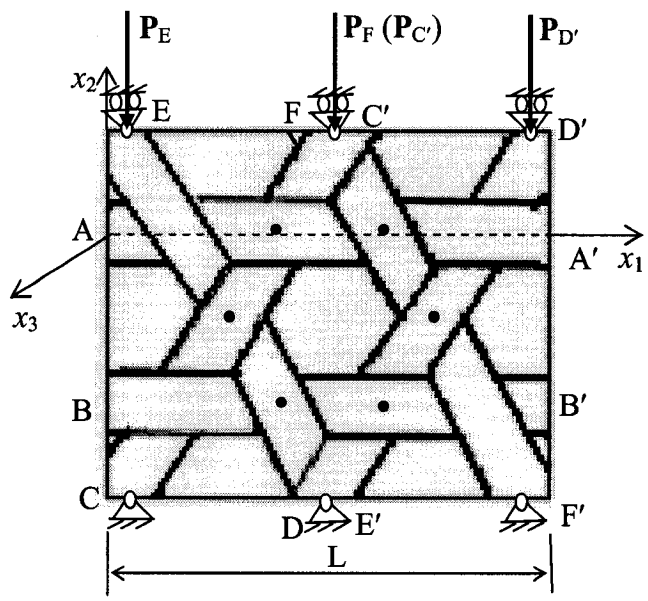

Fig. 5. 7: Basic structure with six intersected tows subjected to uni-directional loading in x_2 direction

The non-linear finite element solution for the non-dimensional buckling load of the structure shown in Fig. 5.8 subjected to uni-directional loading in x_2 direction is $P_{cr}/(\pi^2 E_L I/L^2)$=0.9217. Comparing this result with the one corresponding to the structure

as shown in figures 5.2 and 5.4, the difference between the values of the buckling loads in both cases is about 0.08. It is only 8% less in the present case than in the previous case. This shows that the tri-axial woven fabric composite structure displays in-plane isotropic properties.

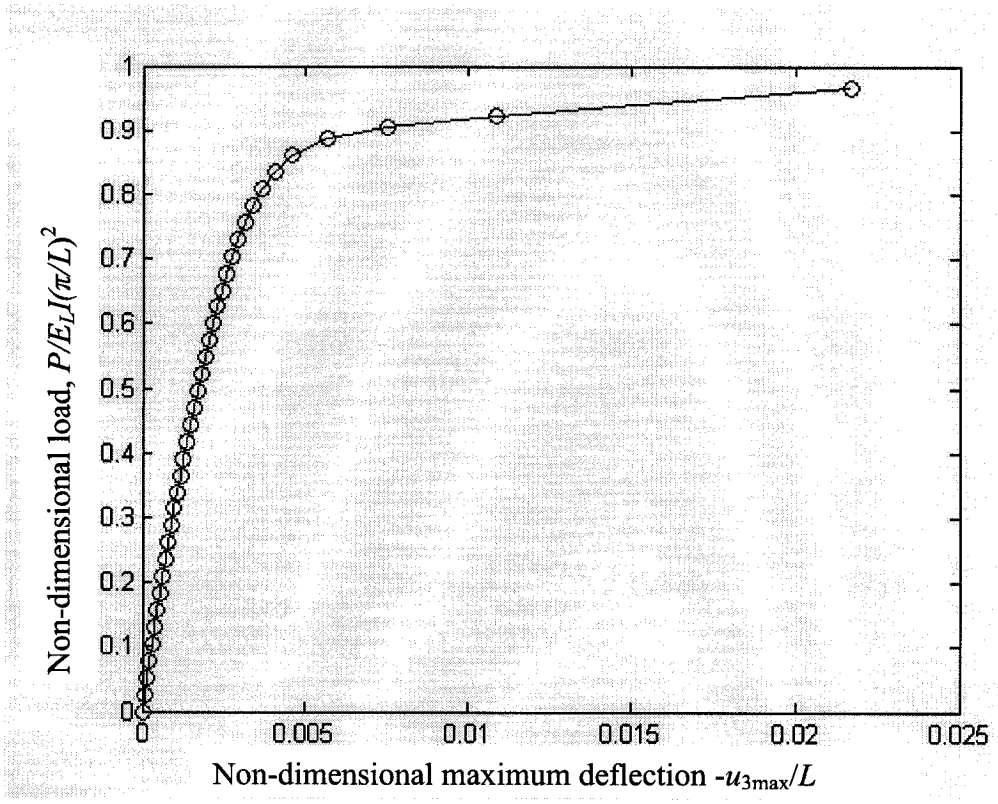

Fig. 5. 8: Load versus maximum deflection curve of the structure as shown in Fig. 5.7

5.3 Simply-supported modified basic tri-axial structure subjected to uni-directional loading along x_1 direction

Modified basic tri-axial structures are obtained by adding additional tows to the basic tri-axial structure. These structures have longer and wider in-plane dimensions than the basic tri-axial structure. Studying the buckling behavior of the modified basic tri-axial

structures can provide the sensitivity analysis for the in-plane aspect ratio of the tri-axial structures.

Two modified basic tri-axial structures will be discussed in this section. The first one (8-tow structure) corresponds to the tri-axial woven structure in which one more X-crossover is added horizontally to the basic structure as shown in Fig. 5.9. The second one (10-tow structure) corresponds to the tri-axial woven structure in which two more X-crossovers are added horizontally to the basic structure as shown in Fig. 5.10.

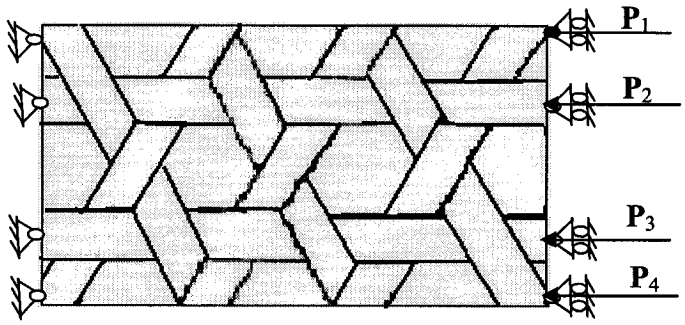

Fig. 5. 9: Tri-axial woven composite structure with eight intersected curved tows

The final configurations of the two modified tri-axial structures will have different in-plane aspect ratio values with respect to the original in-plane configuration of the basic tri-axial structure. The loading and boundary conditions are the same as the one shown in Fig. 5.2 in Section 5.1.

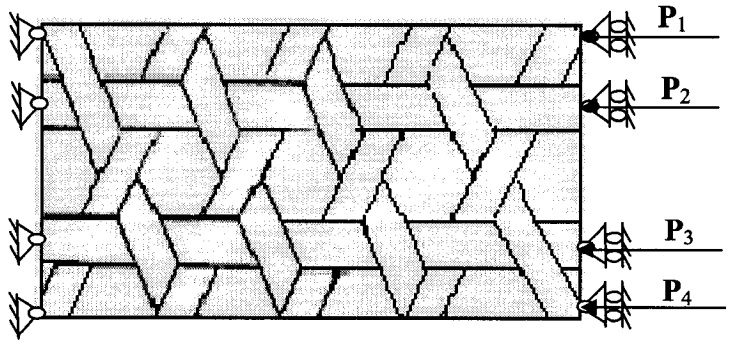

Fig. 5. 10: Tri-axial woven composite structure with ten intersected curved tows

By performing the non-linear finite element analysis, one obtains for these two structures the curves of load versus maximum deflection measured from their unloaded configurations as shown in Fig. 5.11. For convenience of comparison, the load versus maximum deflection curve for basic tri-axial structure is also shown in this figure. The values of the buckling load obtained from non-linear finite element analysis for the modified 8-tow and 10-tow structures are $P_{cr}/(\pi^2 E_L I/L^2) = 1.0034$ and 1.0049, respectively.

From this figure one can see that the buckling loads for both cases are almost the same, but the rates of their deformation are a little different. The deformation rate of

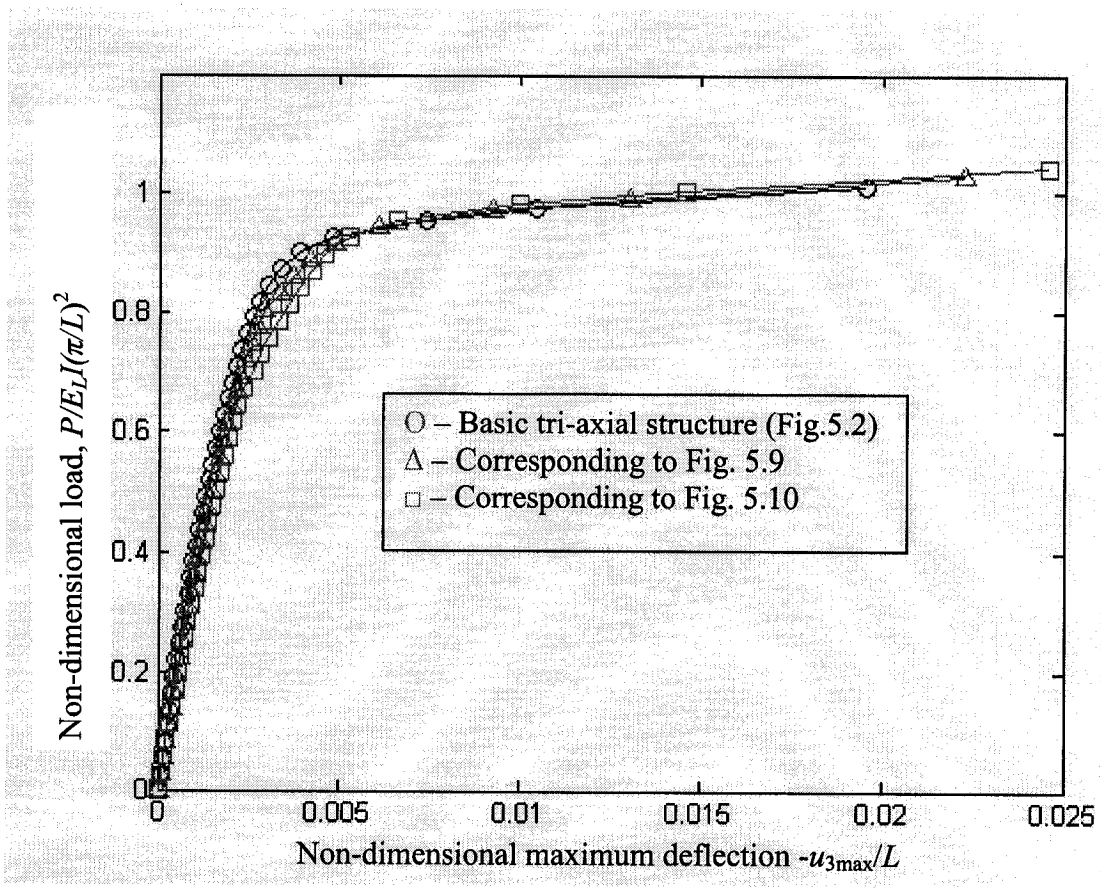

Fig. 5. 11: Load versus maximum deflection curve for tri-axial woven structures shown in figures 5.2, 5.9 and 5.10

longer sized tri-axial structure corresponding to Fig. 5.10 is a little larger than that of the shorter sized one corresponding to Fig. 5.9 after the load reaches certain value. It shows that when more X-crossovers are involved in the basic tri-axial structure in horizontal direction or the in-plane aspect ratio of the tri-axial structure becomes larger, the structure becomes less stiff, or in other words, the tri-axial structures with larger aspect ratios are easier to be deformed. The reasons for approximately the same value of the buckling loads for both structures are that first, the difference of the size between the two structures is not so much. Slight difference in the size of the structures may not result in big change in the value of their buckling loads. Second, both the structures have the same total cross-section, but different length. If the values of their buckling loads are normalized, their buckling loads may not change too much. Comparing with the load versus maximum deflection curve for the basic tri-axial structure shown in Fig. 5.11, the buckling behavior of the three cases are nearly the same. Therefore, one can conclude that changing the aspect ratio of the basic structure by adding more X-crossovers horizontally to the basic tri-axial structure will not change much of the buckling behavior of the tri-axial composite structure.

5.4 Sensitivity analysis due to the change in boundary conditions

In previous sections the structures are simply-supported. But in many situations, the structures are required to be clamped at one end and to be simply-supported or free at the other end. In these cases the boundary conditions will be different from the previous case. Therefore, the buckling behavior will also be different. It is the purpose of this

section to conduct the investigation of buckling behavior of the basic structure subjected to the change in boundary conditions. Since the tri-axial woven fabric composite structures with boundary conditions clamped at one end and free at the other end are relatively very rare in practice, the boundary condition in which the left end ($x_1 = 0$) is clamped and the right end ($x_1 = L$) simply-supported as shown in Fig. 5.12 will be studied instead. Uni-directional loading will be applied.

As for the case of the basic tri-axial structure subjected to uni-directional loading with all the four edges to be simply-supported, it is exactly the same as the case which will be studied in Case I of Section 5.7 when the loads in x_2 direction are equal to zero. Therefore, the analysis of buckling behavior for this case will not be performed in the present Section. A detailed discussion will be given in Section 5.7.

By performing the non-linear finite element analysis, one obtains for this case the curve of load versus maximum deflection measured from its unloaded configuration as shown in Fig. 5.13. From this figure one obtains that the value of the non- dimensional

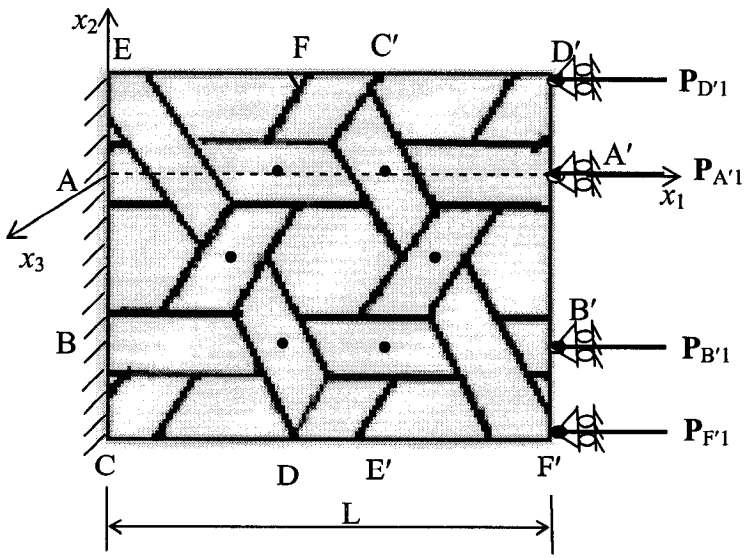

Fig. 5. 12: Basic structure with clamped and simply-supported boundary conditions under uni-directional loading

buckling load in this case is equal to 1.5110, which is 50.8% larger than that of the basic structure subjected to uni-directional loading shown in Fig. 5.2. This is because the clamped end can resist the rotation of the structure at this end and thus shorten the deformable length of the structure compared to the same configuration with simply-supported end. Smaller length of the structure corresponds to larger buckling load if the structures have the same cross-section.

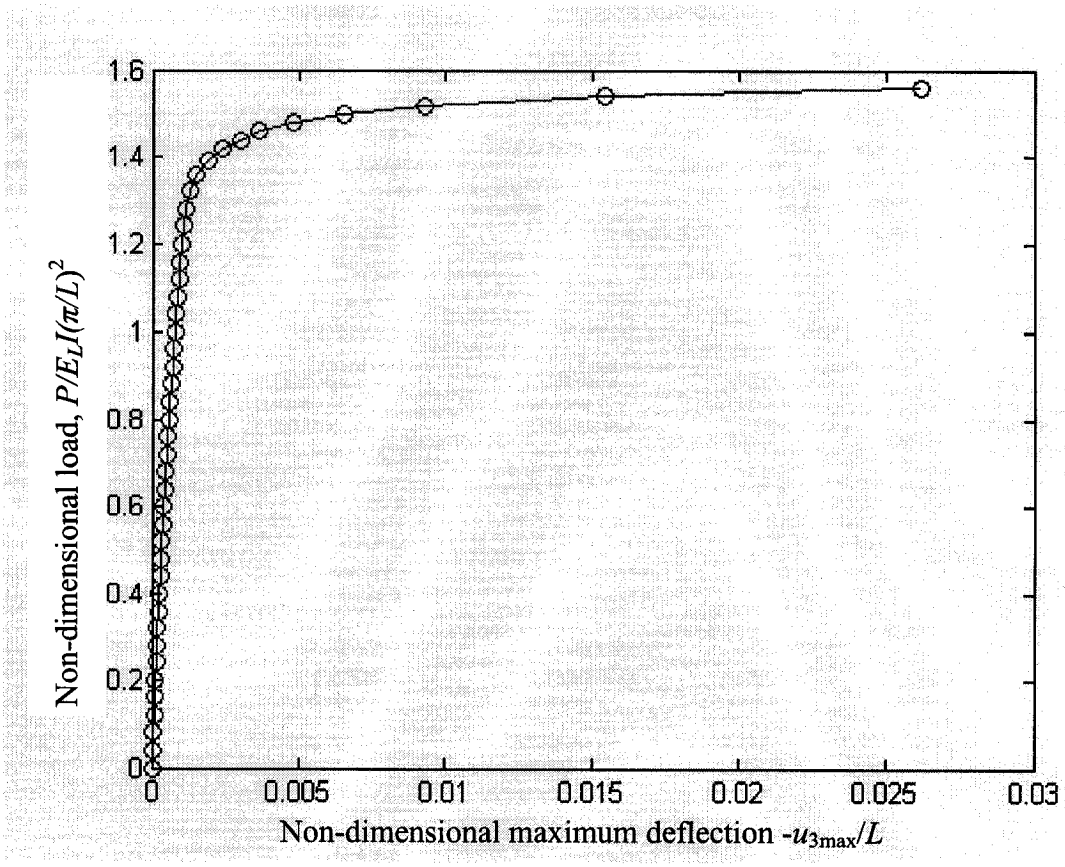

Fig. 5. 13: Load versus maximum deflection curve for basic composite structure with clamped and simply-supported boundary conditions

5.5 Buckling analysis of the basic structure with imperfection due to initial configuration

It is very common that imperfections exist in a structure either due to initial configuration or due to eccentric loading. However, since the dimensions of the cross-section, especially the thickness, of the beam (tow) of the structure are very small, the eccentricity of the loading will be very small. Therefore, imperfections due to the eccentric loading will not be investigated in this thesis. The sensitivity analysis of the buckling load of the basic structure to the imperfection due to initial configuration will be conducted in this section.

In practice, imperfections due to initial configuration are usually caused by manufacturing defects or some lateral load applied to the structure before compressive loads are applied to the structure. In order to model a more practical imperfect configuration and carry out the buckling analysis, imperfect configurations of the structure are obtained by superimposing the initial deflections caused by some lateral loads to the ideal configuration (perfect original configuration). The initial deflections of the structure are obtained by applying small concentrated lateral loads of different magnitudes in the middle of the structure and carrying out the corresponding finite element analysis. The combination of the original configuration and the initial deflection constitutes the configuration of the structure with imperfection. The buckling analysis will be conducted hereafter for these imperfect configurations. In these cases no further lateral loads are applied to initiate the deformations as in the previous cases.

The load versus maximum deflection curves for the imperfect basic tri-axial structure obtained by performing non-linear finite element analysis are shown in Fig. 5.14. For the purpose of comparison, the load versus maximum deflection curve for the

basic structure is also depicted in this figure. The maximum deflection is measured from the corresponding unloaded configuration with imperfection. From this figure following observations can be made: The value of the buckling load decreases and the curvature of the curve before buckling increases as the initial deflection of the basic structure increases. Comparing the curves for the basic tri-axial structure with imperfection with the curve for their perfect structure shown in Fig. 5.14, it can be observed that the curvatures of the curves for the configurations with imperfection before buckling are

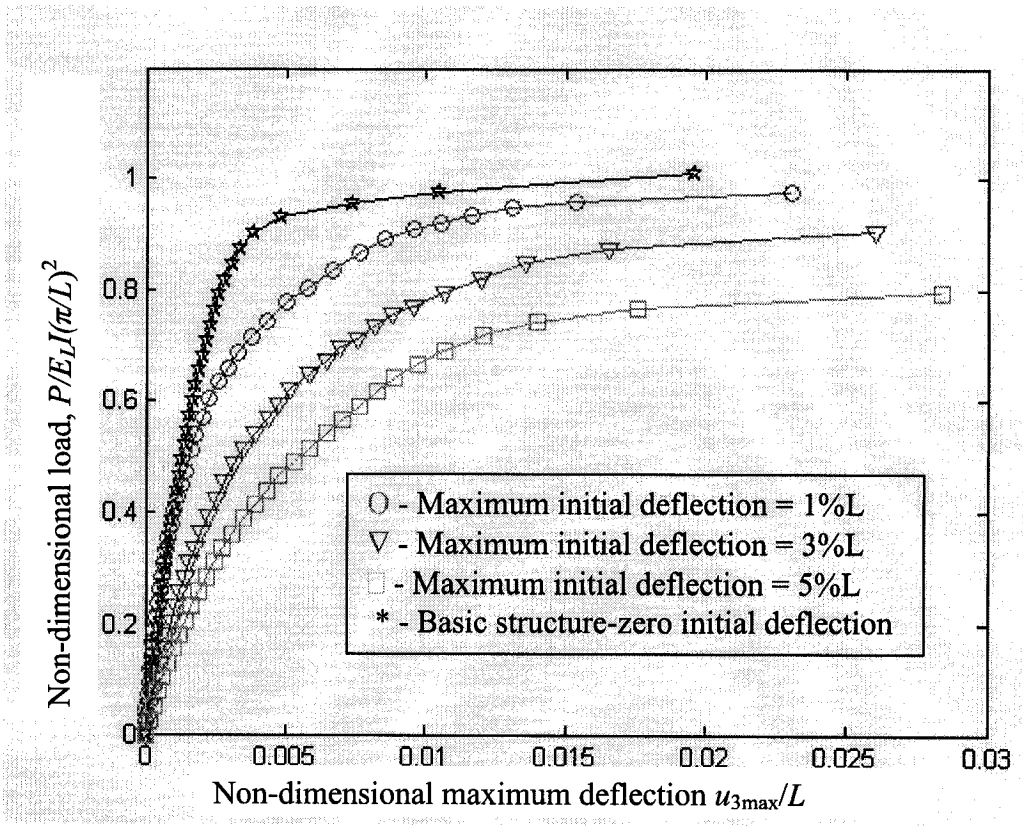

Fig. 5. 14: Load versus maximum deflection curves of the basic tri-axial structure with different initial deflections

larger than that of the perfect configuration. The larger curvature of the curve corresponds to the more pronounced effects of the non-linearity of deformation. The larger the initial deflection of the configuration is, the larger the deformation of the structure will be due to compressive loading.

5.6 Simply-supported enlarged basic structure subjected to uni-directional loading along x_1 direction

In Section 5.3 the buckling behavior of two tri-axial composite structures of rectangular in-plane shape with different aspect ratios has been analyzed. In practical applications, the configuration of the tri-axial composite structures could also be of quasi square in-plane shape, which is obtained by involving the same number of X-crossovers both in x_1 and x_2 directions. In order to carry out the buckling analysis of such configuration, the buckling behavior of the so called enlarged basic structure will be investigated in this section. The present enlarged basic structure (12-tow structure) can be obtained by adding four more X-crossovers to the basic structure, with two such X-crossovers in each of the directions of x_1 and x_2, respectively, as shown in Fig. 5.15. It is subjected to uni-

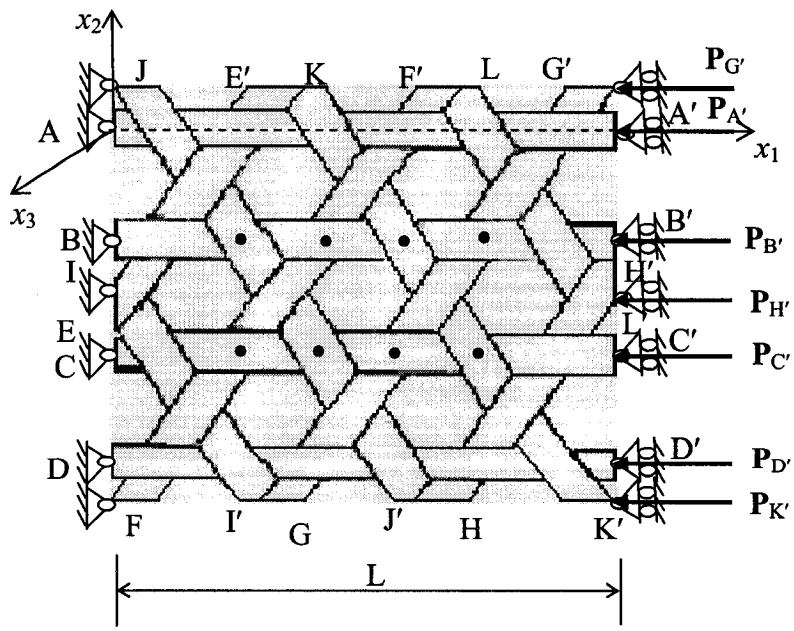

Fig. 5. 15: Simply-supported enlarged basic composite structure

directional loading and is simply-supported at both the left and right ends. Its upper and lower edges are free.

By performing the non-linear finite element analysis, one obtains the curve of load versus maximum deflection measured from the unloaded configuration as shown in Fig. 5.16. For comparison purpose, the load versus maximum deflection curve for the basic tri-axial structure is also presented in this figure.

Comparing the two curves shown in Fig. 5.16, it can be observed that the two configurations shown in Fig. 5.2 and Fig. 5.15 have little difference in their buckling behavior except the rate of deformation of the enlarged basic tri-axial structure is a little

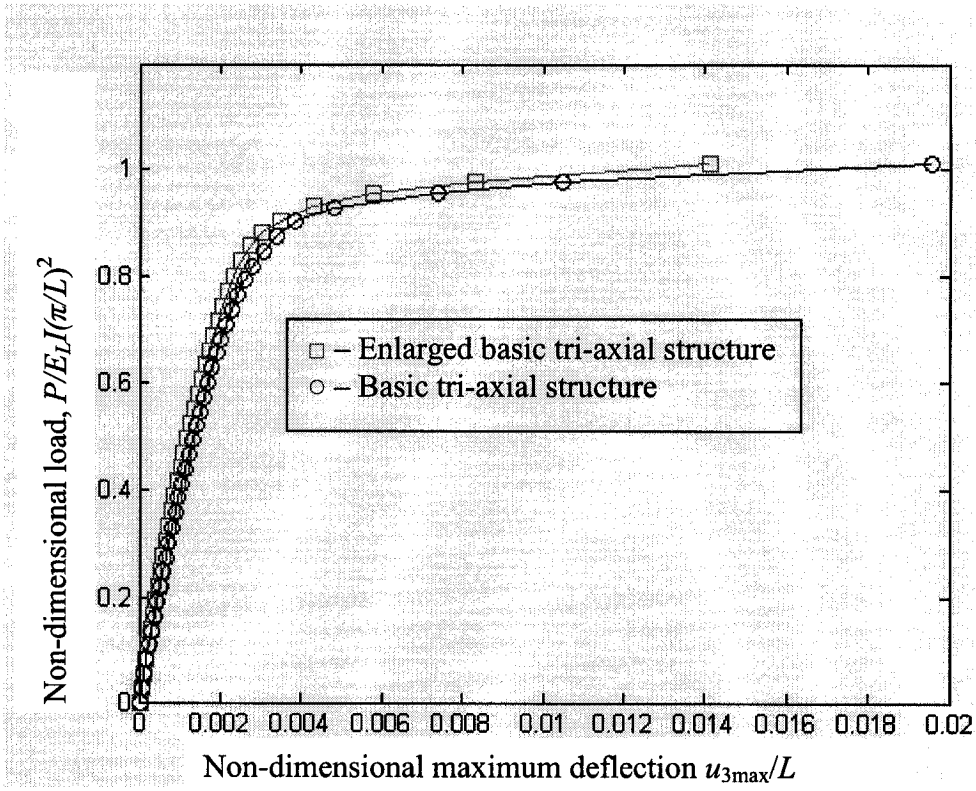

Fig. 5. 16: Load versus maximum deflection curve of the enlarged basic tri-axial structure under uni-directional loading

smaller than that of the basic tri-axial structure. It shows that the enlarged basic tri-axial structure is a little stiffer than the basic tri-axial structure. The value of the non-

dimensional buckling load of non-linear finite element solution for the enlarged tri-axial structure is $P_{cr}/(\pi^2 E_L I/L^2) = 1.008$. It is only 0.6% larger than the value of the buckling load for the basic tri-axial structure considered in Section 5.1. This is because the two tri-axial composite structures have similar cross-sectional properties along x_1 direction. That is, every cross-section of each composite structure along x_1 direction has the same number of tows in three different directions and the structures are fabricated in the same way. If they are equivalent to beam-columns, their buckling behavior should not be much different from each other. The small increment in the value of the buckling load for the enlarged tri-axial structure compared to the basic tri-axial structure shows that when the in-plane sizes of the tri-axial composite structure is relatively small, the more tows are involved in the cross-section of the tri-axial structure along the load (x_1) direction, the larger the normalized compressive load tends to be sustained by the tri-axial structure. However, the magnitude of the normalized compressive buckling load may not increase infinitely; instead it may approach a certain value as the in-plane size of the tri-axial structure increases. This will be observed using the approximate analysis later on.

As for the slight difference in stiffness (slopes of the load versus maximum deflection shown in Fig. 5.16) of the two tri-axial structures, it is because the enlarged tri-axial structure can sustain a little larger load as discussed above than the basic tri-axial structure as discussed above. Therefore, the following conclusion can be made: the basic tri-axial structure and enlarged basic tri-axial structure have little difference in their buckling behavior.

The total non-dimensional load ($P_T/(\pi^2 E_L I/L^2)$) per unit width of the enlarged tri-axial structure versus maximum deflection curve is shown in Fig. 5.17. For

convenience the same curve for basic tri-axial structure is also shown in Fig. 5.17. From this figure one can observe that the relation between the two curves of total non-dimensional load ($P_T/(\pi^2 E_L I/L^2)$) per unit width versus maximum deflection for basic and enlarged tri-axial structures is similar to those shown in Fig. 5.16, but the values of the buckling load are different from those shown in Fig. 5.16. This is because the width

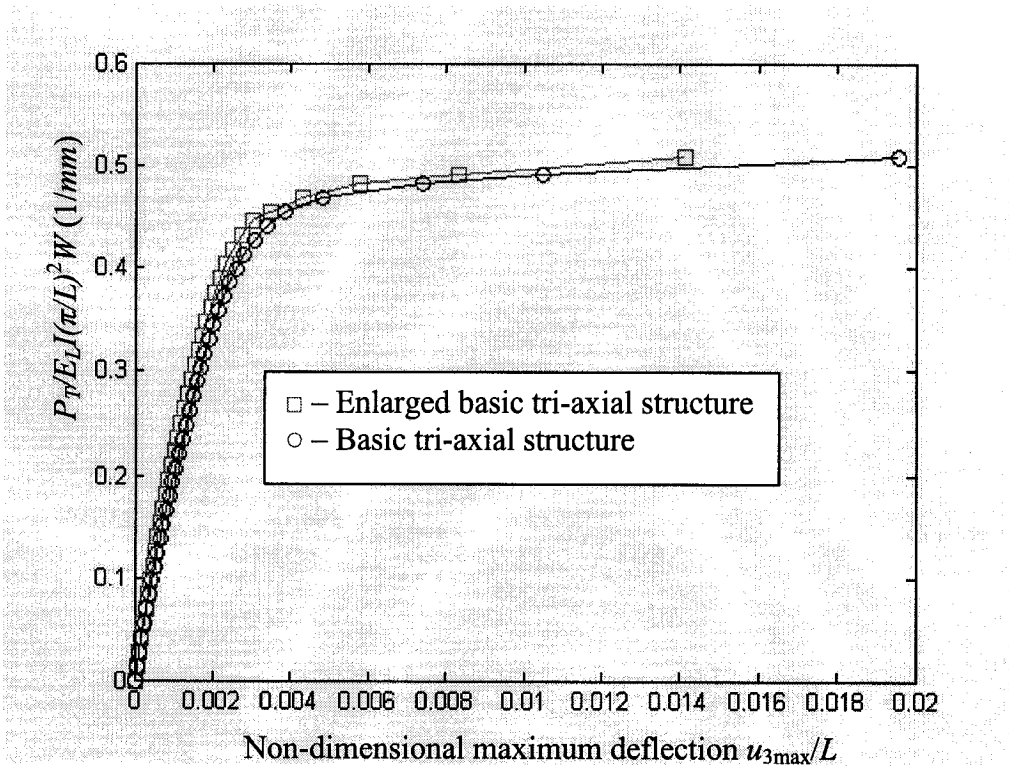

Fig. 5. 17: Total non-dimensional load per unit width of the tri-axial structure, $P_T/E_L I(\pi/L)^2 W$, versus non-dimensional maximum deflection curve

of the enlarged basic tri-axial structure is twice as much as that of the basic tri-axial structure and the total load applied to the enlarged basic tri-axial structure in x_1 direction is also two times as much as that applied to the basic tri-axial structure. The same increment ratio is applied to both the width of the structure and the axial load.

The curve of buckling load of different tri-axial structures versus the number of tows in these tri-axial structures is shown in Fig 5.18. From this figure one can see the

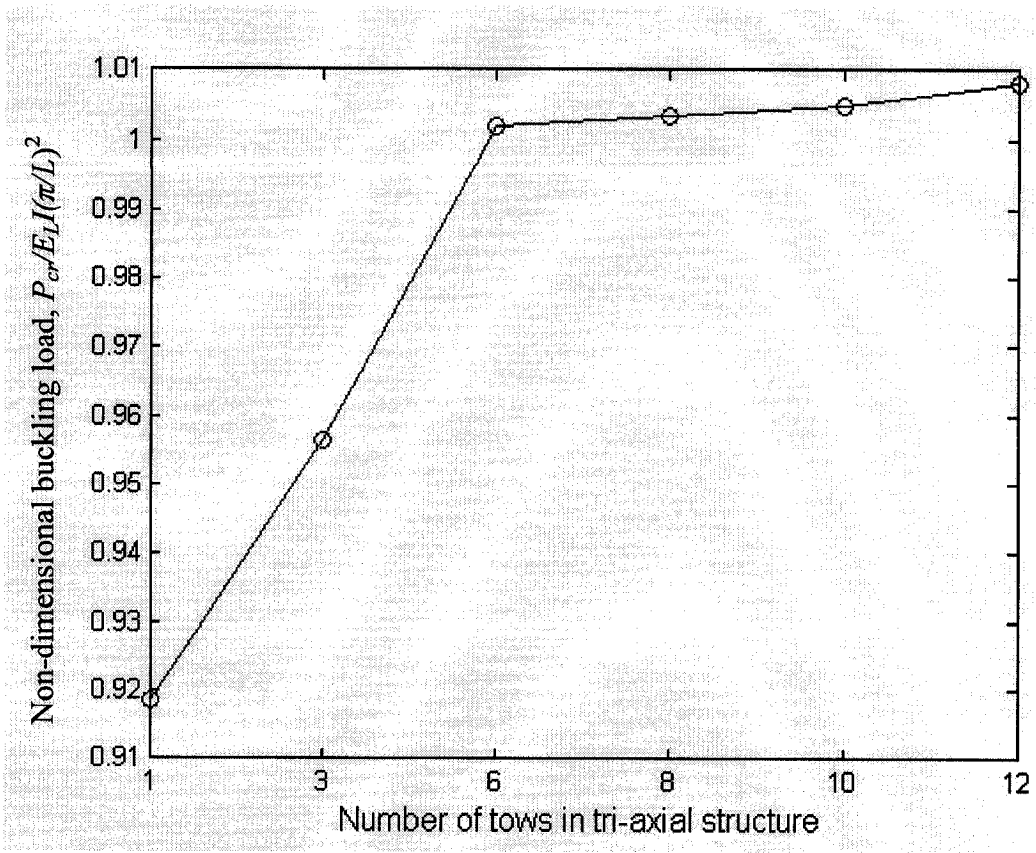

Fig. 5. 18: Buckling load versus the number of tows in tri-axial structure

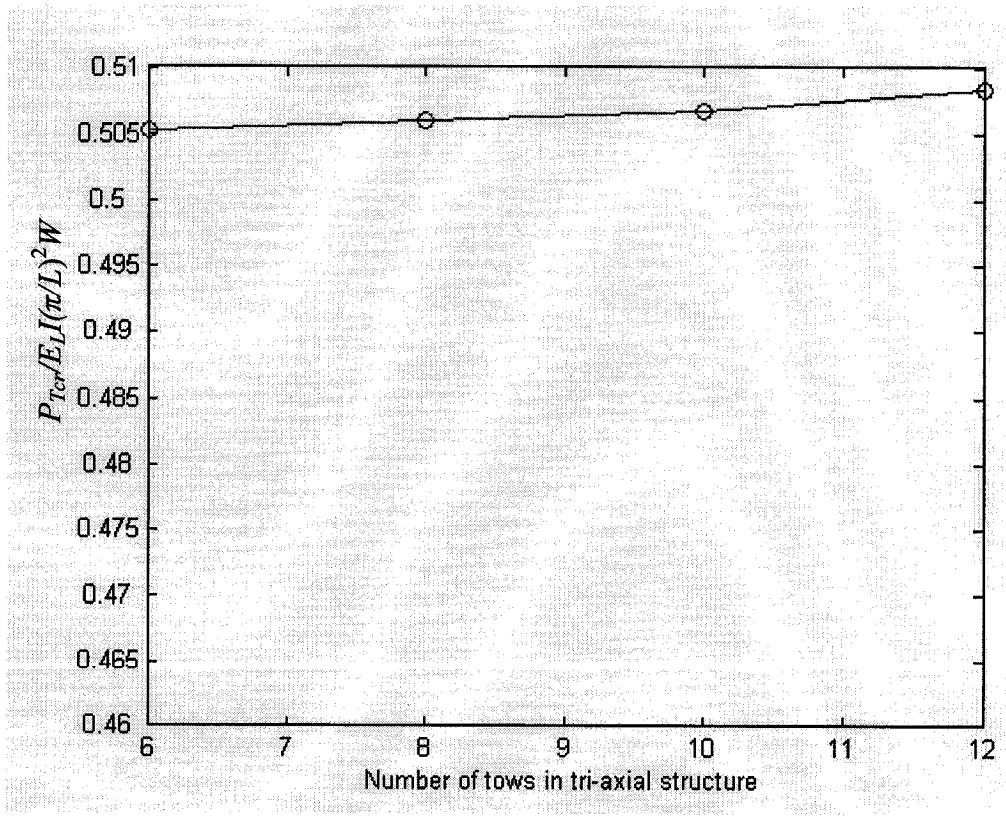

Fig. 5. 19: Total buckling load per unit width versus the number of tows in tri-axial structure

tendency of the value of the buckling load as the number of tows involved in the tri-axial structure gets larger.

The curve of non-dimensional buckling load per unit width for different tri-axial structures versus the number of tows in these tri-axial structures is shown in Fig 5.19.

5.7 Simply-supported basic tri-axial structure subjected to bi-directional loading

In many cases, the structures are loaded bi-directionally. In order to understand the buckling behavior of the tri-axial composite structure subjected to bi-directional loading, the buckling analysis of the simply-supported basic structure subjected to the bi-directional loading will be conducted next. The structure is the same as the one considered in Section 5.1, but it is subjected to bi-directional loading and is roller-supported at the upper and lower edges, as shown in Fig. 5.20. To analyze the effects of bi-directional loading on buckling behavior of basic tri-axial structure, two cases will be investigated:

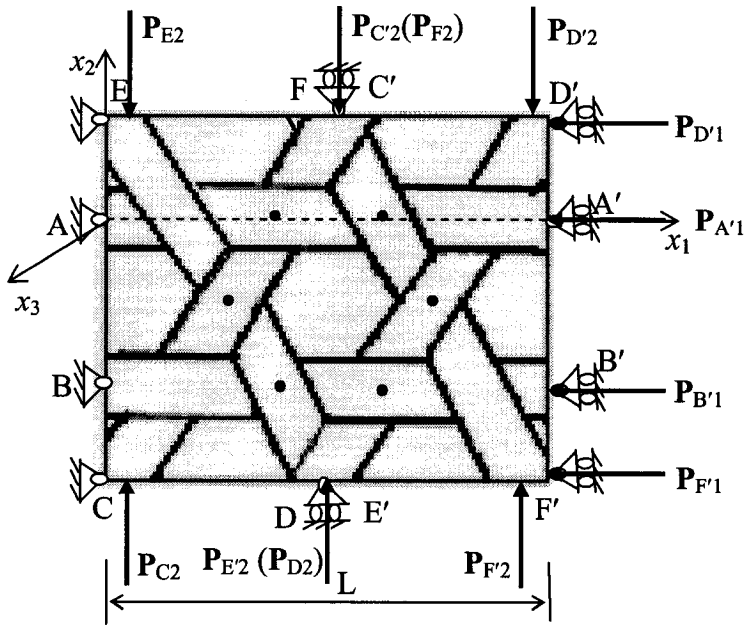

Fig. 5. 20: Basic tri-axial structure with six intersected tows subjected to bi-directional loading

Case I: The values of all the loads in x_2 direction are kept to be equal and constant throughout while the values of the loads in x_1 direction are kept to be equal and they are increased by the same increment each time.

Case II: The values of all the loads both in x_1 and x_2 directions are kept to be equal and they are increased by the same increment each time.

In both situations the values of six small lateral downward static loads denoted by dots in Fig. 5.20 at the six apexes that are used to initiate the deflection of the structure are also kept to be equal throughout.

By performing the non-linear finite element analysis as in the previous sections, one obtains the curve of non-dimensional buckling loads versus non-dimensional load in

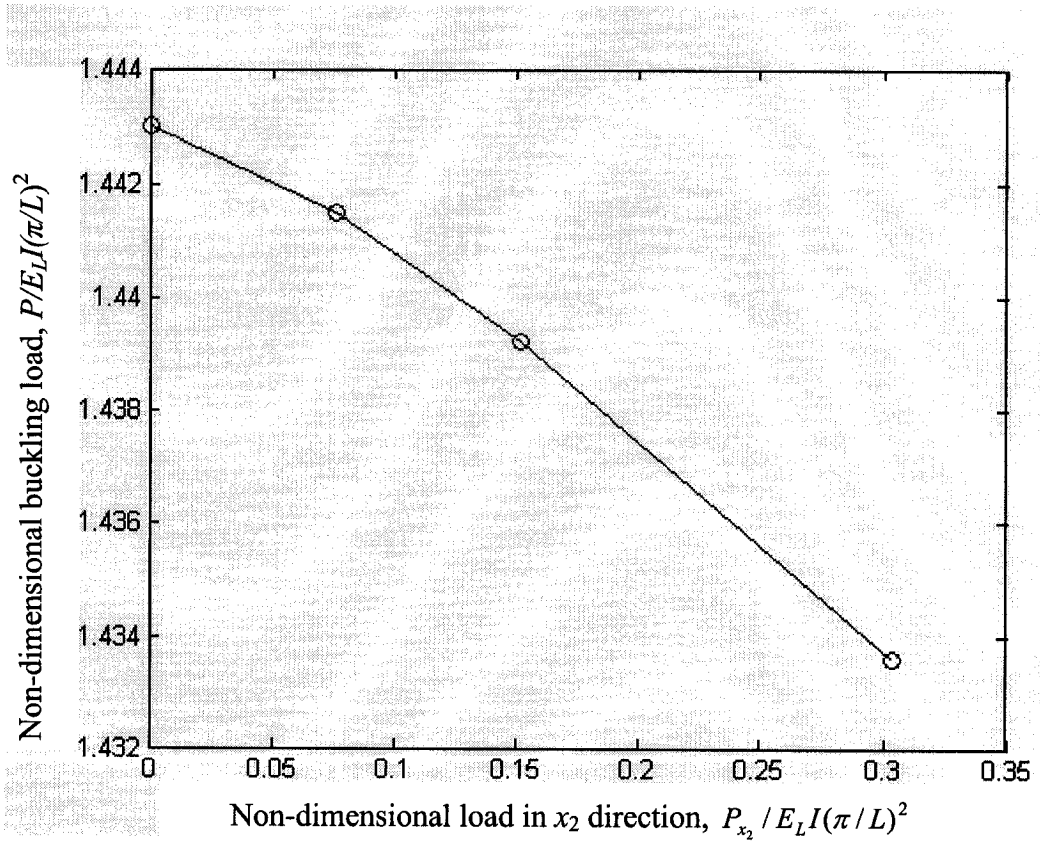

Fig. 5. 21: Curve of buckling load versus the loads in x_2 direction for Case I

x_2 direction as shown in Fig. 5.21 corresponding to case I, for which the results are also listed in Table 5.1, and the curve of the non-dimensional load versus non-dimensional maximum deflection measured from the unloaded configuration corresponding to the case II (that is, the case with the same loading in both x_1 and x_2 directions) as shown in Fig. 5.22. The non-linear finite element solution of the non-dimensional buckling load for case II is $P_{cr}/(\pi^2 E_L I/L^2) = 0.8729$.

Table 5. 1 List of FES* of basic tri-axial structure subjected to bi-directional loading**

$P_{bx_2}/(\pi^2 E_L I/L^2)$	0.000	0.0759	0.1518	0.3036
$(P_{bx_1})_{cr}/(\pi^2 E_L I/L^2)$	1.4430	1.4415	1.4392	1.4336

* FES refers to finite element solution.

** Values of both loads along x_1 and x_2 directions are normalized based on the individual beam structure.

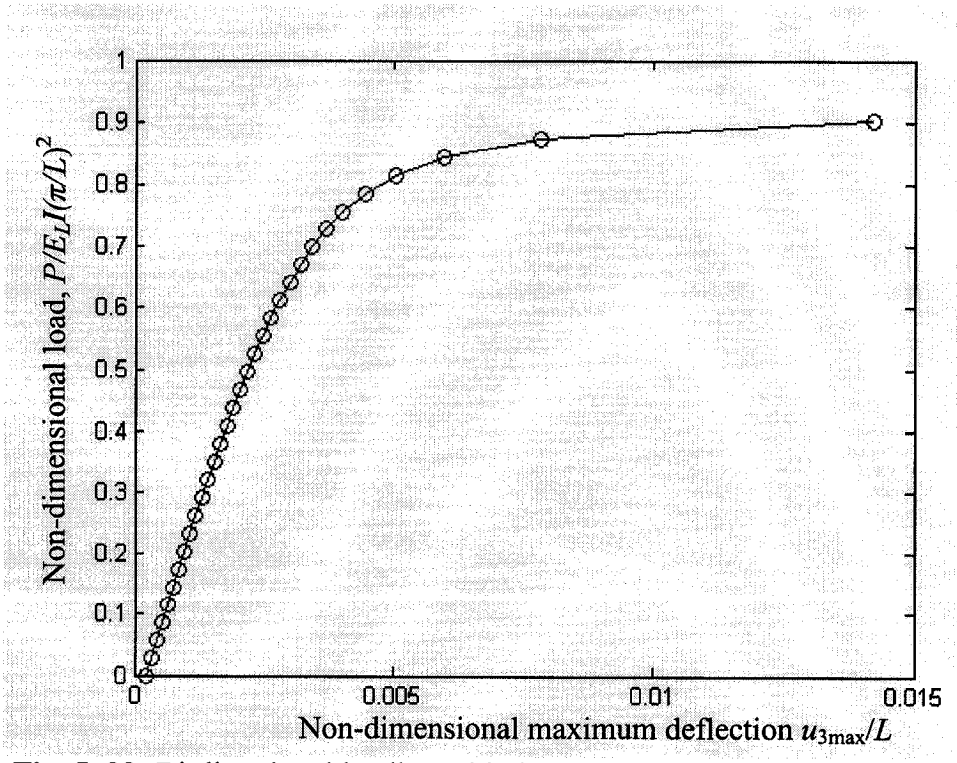

Fig. 5. 22: Bi-directional loading with the same increment of the loads both in x_1 and x_2 directions for Case II

From Fig. 5.21 two observations can be made. First, the value of the buckling load along x_1 direction decreases as the value of the load along x_2 direction increases. The decreasing rate of the value of the buckling load is larger when the value of the load in x_2 direction is getting larger. This is because the structure has been deformed due to the loads in x_2 direction before the compressive loads in x_1 direction are applied. This deformation can be considered as the initial imperfection of the configuration of the basic composite structure. When the values of the loads in x_2 direction are getting larger, the deformation or in other words the initial deflection of the configuration due to the loads in x_2 direction will be larger. On the contrary, the values of the buckling loads along x_1 direction will become smaller.

Next, simply-supporting the upper and lower edges of the basic structure increases the value of its buckling load when it is subjected to uni-directional loading. Actually, when the values of the loads in x_2 direction are equal to zero, the basic structure is subjected to uni-directional loading. The point on the vertical coordinate in Fig. 5.21 corresponds to this case. Comparing the values of the buckling loads of the uni-directionally loaded basic tri-axial structure that has free upper and lower edges as shown in Fig. 5.2 with the one that has roller supported upper and lower edges as shown in Fig. 5.20, one obtains that the buckling load of the structure with the roller supported edges is 44% larger than that of the structure with free edges. It is because restraining the unloaded edges of the basic structure may make the structure harder to deform. As a result, its buckling load becomes larger compared with the free edge case.

Fig. 5.22 shows the buckling behavior of the bi-directionally loaded basic tri-axial structure with the same increments of the loads in both x_1 and x_2 directions. Comparing

Fig. 5.22 with Fig. 5.4, following observations can be made: first, the value of the buckling load ($P_{cr}/(\pi^2 E_L I/L^2)$ = 0.8729 in this case) of the bi-directionally loaded tri-axial composite structure is smaller than that of the uni-directionally loaded basic tri-axial composite structure; second, the deflection and the rate of deformation of the bi-directionally loaded case are also a little bit larger than those of the uni-directionally loaded case. The reason for that is due to the effects of the loads in x_2 direction.

5.8 Conclusion

Buckling behavior of various forms of tri-axial woven fabric composite structure has been studied numerically using non-linear finite element formulation developed in Chapter two. The structures include the basic tri-axial structure, modified basic tri-axial structures that are obtained by adding one or two X-crossovers horizontally to the basic tri-axial structure and enlarged basic tri-axial structure that is obtained by adding more X-crossover to the basic tri-axial structure both horizontally and vertically, two each in both directions. They are subjected to either uni-directional loading or bi-directional loading. The numerical results reveal that these tri-axial composite structures subjected to uni-directional loading have a little difference in the value of their buckling loads. This shows that slight difference in the configuration of tri-axial composite structure will not result in big jump in the value of its buckling load, but the small change in the value of the buckling load does have its significance, that is, when the number of tows in tri-axial structure gets larger, the value of the buckling load of corresponding structure becomes higher. Buckling analysis of the simply-supported basic tri-axial structure with

imperfection in the form of initial deflection and basic tri-axial structure subjected to different boundary conditions is also performed. It is observed that the value of the buckling load decreases as the maximum initial deflection increases and changing the boundary conditions of the basic tri-axial structure from simply-supported ends to clamped ends will increase the value of its buckling load. The investigation of the effect of the resin on the basic tri-axial structure shows that the Young's modulus of the resin has little effect on the buckling behavior of the basic tri-axial structure due to the interaction of the woven tows constituting the structure.

Chapter 6

Approximate solutions for simply-supported basic tri-axial composite structure

In order to evaluate the numerical results obtained from non-linear finite element analysis and to provide a simpler way to validate and interpret the results, approximate analytical solution for simply-supported basic tri-axial composite structure subjected to uni-directional loading and bi-directional loading will be presented in this Chapter. The equivalent multi-layered composite plates corresponding to the uni-directionally loaded basic tri-axial composite structure and equivalent anisotropic plate corresponding to bi-directionally loaded basic tri-axial structure will be used for modeling. Plate theory will be employed to determine their buckling loads.

6.1 Basic tri-axial structure subjected to uni-directional loading

A typical simply-supported tri-axial woven fabric composite tow structure subjected to uni-directional loading is shown in Fig. 6.1. Two rigid bars served as the support fixture are bonded with the structure at the ends of x_1=0 and L. The loads are uniformly distributed at the restrained end. Considering that the thickness of the structure is very small compared with its in-plane dimensions and that the overall in-plane shape of the structure is more like a thin plate or a shell (after undergoing larger deflections) with

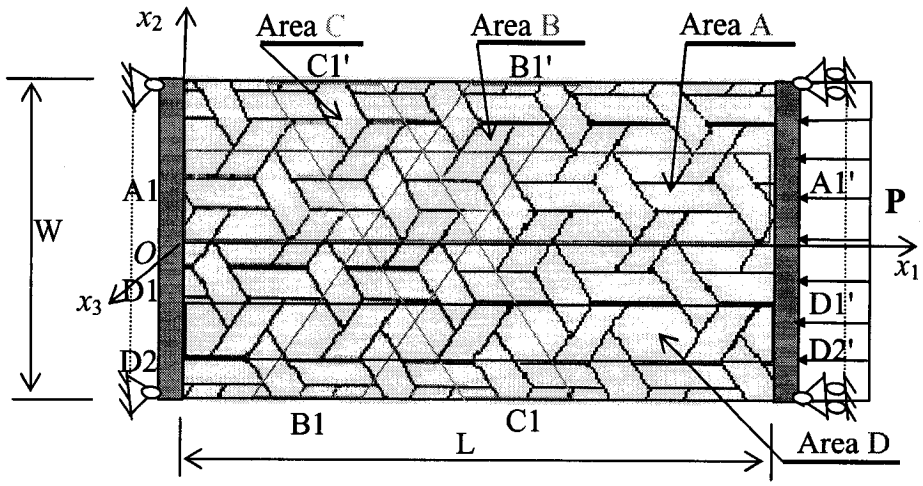

Fig. 6. 1: Typical tri-axial woven fabric composite tow structure

open holes, if the open holes of the structure are idealized to have been filled with some kind of pseudo material, the whole structure could be modeled as a plate. Therefore, it is the purpose of the present section to find out an equivalent laminated composite plate model (hereafter called "plate model") to the tri-axial composite structure (hereafter called "beam model" since it is modeled as an interconnected beam structure) to determine its buckling load. If the whole piece of the structure is taken as a thin laminated composite plate, cylindrical bending of the plate may be anticipated and the equivalent conditions between the "beam model" and the "plate model" need to be made.

The procedure to obtain an equivalent plate to the tri-axial structure is as follows:

1. The tri-axial structure consists of three types of tows: tows parallel to the loading direction, tows making an angle of 60^0 with the loading direction and tows making an angle of -60^0 with the loading direction.
2. One set of equations will be developed to establish equivalence between tows parallel to the loading direction and an equivalent plate with a principal axis parallel to the loading direction.

3. One set of equations will be developed to establish the equivalency between tows making an angle of $\pm 60^0$ to the loading direction and an equivalent skew plate with two parallel edges making an angle of $\pm 60^0$ to the loading direction.
4. The final equivalent multi-layered plate with different fiber orientations equivalent to the tri-axial structure will be made by bonding all the equivalent single layered plates corresponding to tows as discussed in item 2 and 3 above.
5. Critical buckling loads calculated using the above equivalency will be done. If good comparison is obtained, the equivalency equations will be established for approval use.

6.1.1 Equivalent conditions for a simply-supported composite beam and simply-supported single layered composite plate

Let us consider the equivalent conditions for a simply-supported composite beam and a single layered composite plate with simply-supported edges at $x_1 = 0$ and L and free edges at $x_2 = -\bar{b}/2$ and $\bar{b}/2$ as shown in Fig.6.2 (where $\bar{b}$ is the width of the plate). In this figure the geometric parameters of the single layered plate are defined symbolically with overbar.

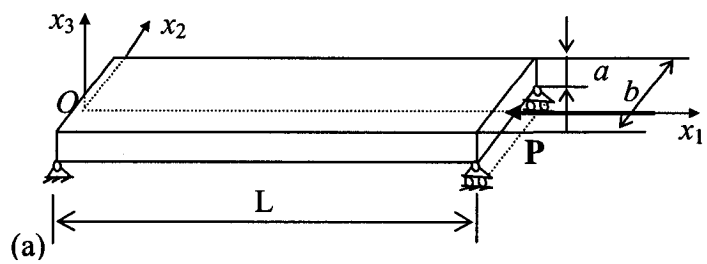

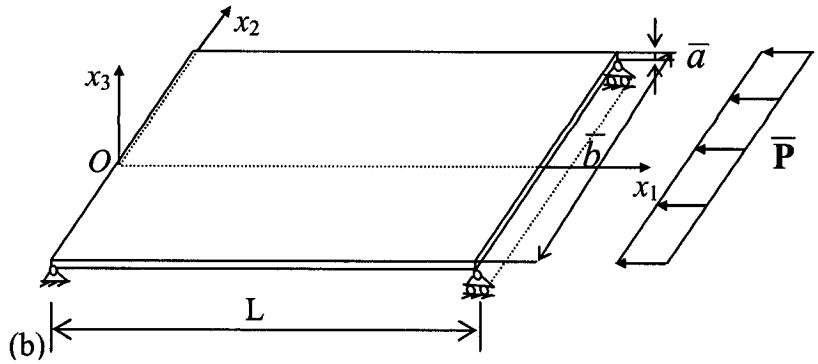

Fig. 6. 2: (a) Simply-supported beam; (b) Simply-supported rectangular plate

6.1.1.1 Equilibrium equation for a simply-supported individual composite beam

For a simply-supported straight beam (assume that the beam is made by an individual straight composite tow) and using the same assumptions made in Chapter 3, that is, plane sections remain plane after bending and the effect of transverse shear is negligible, the equilibrium equation corresponding to Fig. 6.2(a) can be written as [20]

$$E_L I_{x_2} \frac{d^4 u_{b3}}{dx_1^4} + P \frac{d^2 u_{b3}}{dx_1^2} = 0 \qquad (6\text{-}1)$$

where P is the concentrated compressive load applied at the centre of the beam and u_{b3} is the deflection of the beam and subscript b hereafter refers to the beam.

6.1.1.2 Equilibrium equation for a simply-supported rectangular single layered composite plate

Consider a rectangular plate with its left and right edges simply-supported and the other two opposite edges free, as shown in Fig. 6.2(b). If one assumes that the plate is made by using the same composite material as the composite beam (tow) but with different cross-sectional dimensions and uniformly distributed load is applied at the right

end of the plate along x_1 direction, the deflection of the plate is independent of x_2 and its equilibrium equation is given by [67]

$$D_{11}\bar{b}\frac{d^4\bar{u}_{p3}}{dx_1^4}+\bar{P}\bar{a}\bar{b}\frac{d^2\bar{u}_{p3}}{dx_1^2}=0 \tag{6-2}$$

where $D_{11}=\frac{1}{12}\frac{E_L}{1-\nu_{LT}\nu_{TL}}\bar{a}^3$ is the bending rigidity of the single layered plate per unit width in x_2 direction, ν_{LT} and ν_{TL} are the longitudinal-transverse and transverse-longitudinal Poisson's ratio of the tow, respectively, $\bar{a}$ is the thickness of the single layered plate, $\bar{b}$ is the width of the plate, $\bar{P}$ is the applied uniformly distributed pressure, $\bar{u}_{p3}$ is the deflection of the plate and subscript p and hereafter refers to the plate.

6.1.1.3 Equivalent conditions for simply-supported composite beam and simply-supported single layered rectangular composite plate

From equations (6-1) and (6-2), if the beam and the single layered rectangular plate are completely similar or equations (6-1) and (6-2) have the same solutions, the following relations must be satisfied:

$$\frac{\bar{a}^3\bar{b}}{1-\nu_{LT}\nu_{TL}}=a^3b \tag{6-3}$$

$$\bar{a}\bar{b}=ab \tag{6-4}$$

$$\bar{P}\bar{a}\bar{b}=P \tag{6-5}$$

Note that since the same material is used for the beam and the equivalent single layered plate, their material constants are the same. Therefore, the cancellations are made

for the factors with the same material constants during the derivation of equation (6-3). The same procedures are employed in the derivation used in Figure 6.3.

Equations (6-3) through (6-5) are the requirements for the availability of replacing the composite beam with an equivalent single layered composite plate, that is, the equivalent conditions for the beam and the single layered plate.

6.1.2 Equivalent conditions for a simply-supported off-axis composite beam and simply-supported off-axis single layered composite plate

Let us consider the equivalent conditions for simply-supported off-axis composite beam and off-axis single layered composite plate. Here the "off-axis beam" or "off-axis plate" means the longitudinal symmetric axis of the beam or the plate makes an angle with x_1 axis, as shown in Fig. 6.3.

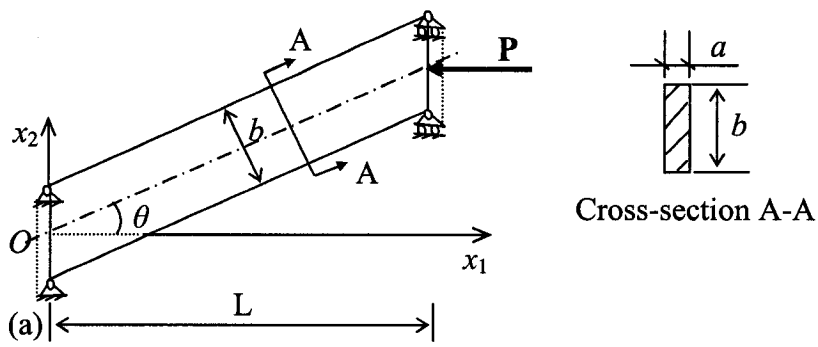

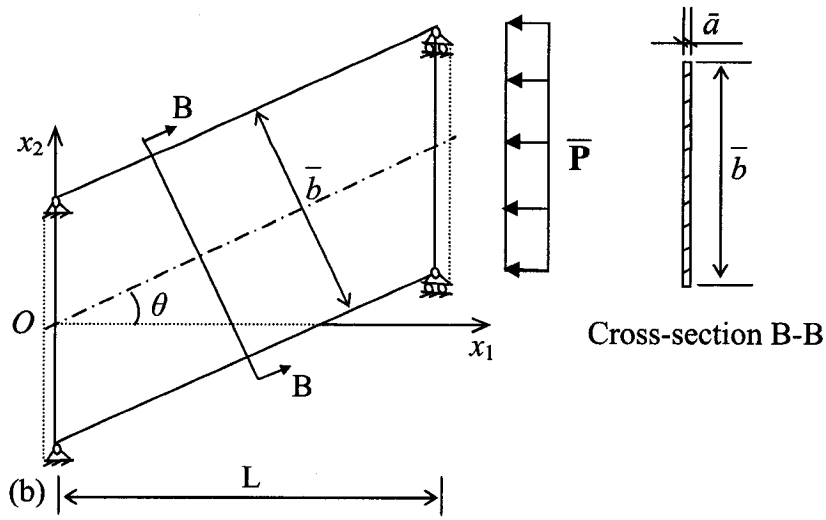

Fig. 6. 3: (a) Simply-supported off-axis composite beam;
(b) Simply-supported off-axis single layered composite plate

6.1.2.1 Equilibrium equations for simply-supported individual off-axis composite beam

For a simply-supported straight off-axis composite beam as shown in Fig. 6.3(a) (assume that the beam is made by an individual straight composite tow and its symmetric axis makes an angle of θ with x_1 axis), its equilibrium differential equation can be derived by considering an element of the beam. For clarity the center line of the beam and its corresponding beam element are shown in Fig. 6.4. Before deriving the equilibrium equation of the off-axis beam, the following assumptions are made.

Assumption 1. Apart from the force P applied in x_1 direction, there are no other external forces or moments applied to the beam.

Assumption 2. The torsional effect of the beam is small and is neglected. This is because there is no external torsional moment applied to the beam.

Assumption 3. The effects of shearing deformations and shortening of the beam axis are neglected. Therefore, plane sections remain plane after bending.

Assumption 4. Deformation of the beam is very small so that the cross-sectional rotations of the beam can be decomposed into two rotations, that is, rotation about x_2 axis and rotation about x_3 axis, and this decomposition is unique. This assumption will allow us to decompose or superimpose the rotations of the beam cross-section about x_2 and x_3 axes without considering the effect of the sequence of the rotations and to decouple the moment equilibrium equations about x_2 and x_3 axes.

Assumption 5. The shearing force V and bending moment M acting on the sides of the element are assumed positive in the directions shown in Fig. 6.4 (b) in three dimensional view. For clarity, the shearing force V and bending moment M are also shown in figures 6.4 (c) and (d) in two dimensional view.

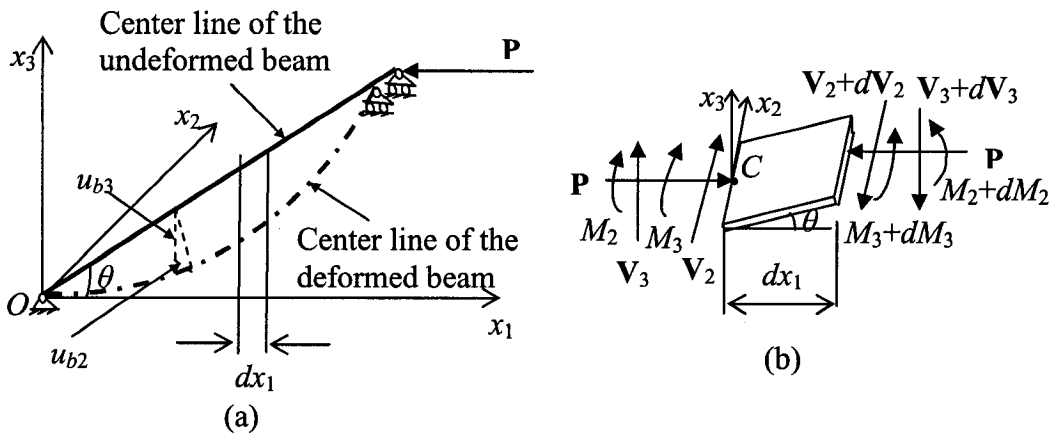

Fig. 6. 4: (a) Simply-supported off-axis beam; (b) Beam element; M is the bending moment of the cross- section and V is the shear force of the cross-section.

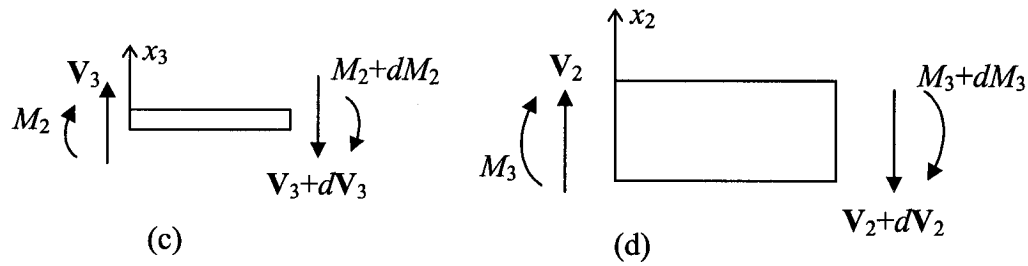

Fig. 6. 4: (c): Beam element in x_1x_3 plane; (d): Beam element in x_1x_2 plane.

The relations among the load P, shearing force V, and bending moment M are obtained from the equilibrium of the element in Fig. 6.4(b). Summing forces in the x_3 direction gives

$$V_3 - (V_3 + dV_3) = 0$$

or $$dV_3 = 0 \tag{6-6}$$

Taking moments about the central horizontal line of the left side cross-section parallel to x_2 axis at point C (center of the cross-section) gives

$$M_2 + (V_3 + dV_3)dx_1 - (M_2 + dM_2) + P\frac{du_{b3}}{dx_1}dx_1 = 0$$

or (considering equation (6-6))

$$\frac{dM_2}{dx_1} - P\frac{du_{b3}}{dx_1} = V_3 \tag{6-7}$$

where P is the equivalent concentrated compressive load applied at the centre of the beam and u_{b3} is the deflection of the beam in x_3 direction.

According to the assumptions made before that the beam undergoes small deformation (small translations and small rotations) and no torsional deformation happens, the cross-sectional rotations of the beam can be decomposed into two rotations, that is, rotation about x_2 axis and rotation about x_3 axis. In this case, the axial deformation of the element shown in Fig. 6.4(b) caused by bending can be decomposed into bending caused by moment M_2 and bending caused by M_3 and the corresponding strains and stresses can be decomposed in the same way. Therefore, the axial deformation as shown in Fig. 6.5 caused by bending, i.e. moment M_2, in the vertical plane is given by

$$u_{b1/2} = -x_3\theta_{b2} \tag{6-8}$$

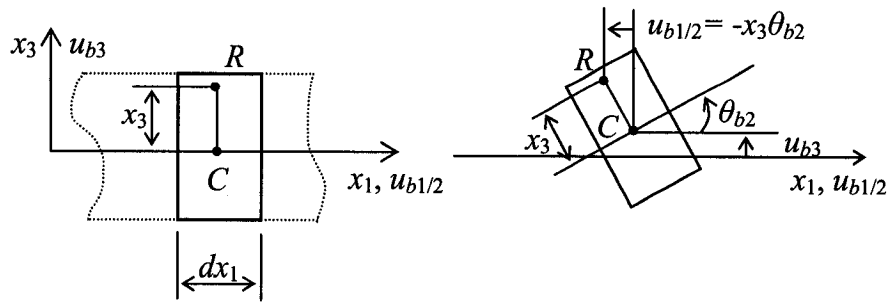

Fig. 6. 5: Differential slice of a beam before and after bending under the action of moment M_2 only

where $u_{b1/2}$ is the displacement of point R along x_1 direction due to bending caused by moment M_2 only and θ_{b2} is the cross-sectional rotation of the beam about x_2 due to bending caused by moment M_2 only.

For small deflections, the rotation of the cross-section about x_2 or the slope of the projection of the deformed central axis of the beam in Ox_1x_3 plane is given by

$$\theta_{b2} = \frac{du_{b3}}{dx_1} \tag{6-9}$$

By substituting equation (6-9) into equation (6-8), one obtains

$$u_{b1/2} = -x_3 \frac{du_{b3}}{dx_1} \tag{6-10}$$

The strain in x_1 direction caused by bending moment M_2 is given by

$$\varepsilon_{1/2} = \frac{du_{b1/2}}{dx_1} = -x_3 \frac{d^2u_{b3}}{dx_1^2} \tag{6-11}$$

The stress corresponding to this strain can be written as

$$\sigma_{1/2} = E_{x_1}\varepsilon_{1/2} = -E_{x_1}x_3 \frac{d^2u_{b3}}{dx_1^2} \tag{6-12}$$

where E_{x_1} is the Young's modulus of the composite beam along x_1 direction and is given by [68]

$$\frac{1}{E_{x_1}} = \frac{m^2}{E_L}(m^2 - n^2\nu_{LT}) + \frac{n^2}{E_T}(n^2 - m^2\nu_{TL}) + \frac{n^2 m^2}{G_{LT}} \tag{6-13}$$

where $m = \cos\theta$ and $n = \sin\theta$, θ is the orientation of the fiber.

Over a cross-section, the moment corresponding to this stress as shown in Fig. 6.6, M_2, is given by

$$M_2 = -\int_A \sigma_{1/2} x_3 dA \tag{6-14}$$

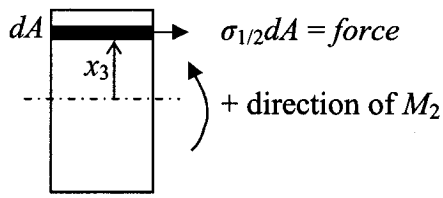

Fig. 6. 6: Moment and stress relation over a cross-section

Substituting for $\sigma_{1/2}$ from equation (6-12), one obtains

$$M_2 = -\int_A E_{x_1} x_3^2 \frac{d^2 u_{b3}}{dx_1^2} dA = -E_{x_1} \frac{d^2 u_{b3}}{dx_1^2} \int_A x_3^2 dA = -E_{x_1} \frac{d^2 u_{b3}}{dx_1^2} I_{x_2} \tag{6-15}$$

where the cross-sectional moment of inertia of the composite beam about x_2 axis

$$I_{x_2} = \frac{1}{12}\frac{ba^3}{\cos\theta} \tag{6-16}$$

Substituting equation (6-15) into (6-7) and differentiating it with respect to x_1, one obtains the moment equilibrium equation about x_2 axis as follows

$$E_{x_1} I_{x_2} \frac{d^4 u_{b3}}{dx_1^4} + P\frac{d^2 u_{b3}}{dx_1^2} = 0 \tag{6-17}$$

In the same way, one can derive the moment equilibrium equation about x_3 axis. Summing forces in the x_2 direction gives

$$V_2 - (V_2 + dV_2) = 0$$

or $dV_2 = 0$ (6-18)

Taking moments about the central vertical line of the left side cross-section parallel to x_3 axis at point C (center of the cross-section) gives

$$M_3 + (V_2 + dV_2)dx_1 - (M_3 + dM_3) + P(\frac{du_{b2}}{dx_1} - \tan\theta)dx_1 = 0$$

or (considering equation (6-18))

$$\frac{dM_3}{dx_1} - P\frac{du_{b2}}{dx_1} + P\tan\theta = V_2 \tag{6-19}$$

where u_{b2} is the deflection of the beam in x_2 direction and θ is the off-axis angle of the beam axis.

Performing the same procedures or derivation as used in deriving equation (6-15), one obtains the bending moment about x_3 axis as follows:

$$M_3 = -E_{x_1}\frac{d^2u_{b2}}{dx_1^2}I_{x_3} \tag{6-20}$$

where the cross-sectional moment of inertia of the composite beam about x_3 axis

$$I_{x_3} = \frac{1}{12}\frac{ab^3}{\cos^3\theta} \tag{6-21}$$

Substituting equation (6-20) into (6-19) and differentiating it with respect to x_1, one obtains the moment equilibrium equation about x_3 axis as follows

$$E_{x_1}I_{x_3}\frac{d^4u_{b2}}{dx_1^4} + P\frac{d^2u_{b2}}{dx_1^2} = P\tan\theta \tag{6-22}$$

Equations (6-17) and (6-22) together constitute the equilibrium equations of the off-axis composite beam.

Since the cross-section of the beam is very flat and the moment of inertia of the cross-section of the beam about x_2 axis (I_{x_2}) is much smaller than the moment of inertia

of the cross-section of the beam about x_3 axis (I_{x_3}), that is, $I_{x_2} << I_{x_3}$ (I_{x_2}/I_{x_3} =1/70.56. This number is obtained by substituting the cross-sectional dimensions of the beam, which are $a = 0.2\ mm$ and $b = 0.84\ mm$, and the off-axis orientation, $\theta = 60^0$, into equations (6-16) and (6-21), that is, $I_{x_2} = \frac{0.84 \times 0.2^3}{12 \times \cos 60^0} = 1.12 \times 10^3 mm^4$ and $I_{x_3} = \frac{0.84^3 \times 0.2}{12 \times \cos^3 60^0} = 79.03 \times 10^3 mm^4$, and dividing I_{x_3} by I_{x_2}). Also there may be transverse loads to initiate the deflection in x_3 direction in practice. Furthermore, the cylindrical bending of the composite beam is assumed, that is, the symmetrical axis of the cylindrical shape of the beam is assumed to parallel to x_2 axis, the deflection, u_{b2}, in x_2 direction may be very small and can be neglected compared with the deflection, u_{b3}, in x_3 direction. In this case, equation (6-22) can be removed from the equilibrium equations and the equilibrium equation of the off-axis beam is approximately given by equation (6-17).

6.1.2.2 Equilibrium equation for simply-supported off-axis single layered composite plate

Consider the off-axis plate (in order to match the off-axis beam, off-axis plate is used instead of skew plate in this thesis) with its left and right edges simply-supported and the other two opposite edges free, as shown in Fig. 6.3(b). If one assumes that the plate is made by using the same composite material as the off-axis composite beam shown in Fig. 6.3(a) but with different cross-sectional dimensions, the load is applied at the right end of the plate along x_1 direction and is uniformly distributed over the right side

cross-section of the plate, its equilibrium equation in Cartesian coordinate system is given by [67]

$$D_{11}\frac{\partial^4 \bar{u}_{p3}}{\partial x_1^4}+4D_{16}\frac{\partial^4 \bar{u}_{p3}}{\partial x_1^3 \partial x_2}+2(D_{12}+2D_{66})\frac{\partial^4 \bar{u}_{p3}}{\partial x_1^2 \partial x_2^2}+4D_{26}\frac{\partial^4 \bar{u}_{p3}}{\partial x_2^3 \partial x_1}+D_{22}\frac{\partial^4 \bar{u}_{p3}}{\partial x_2^4}-B_{11}\frac{\partial^3 \bar{u}_{p1}^0}{\partial x_1^3}$$

$$-3B_{16}\frac{\partial^3 \bar{u}_{p1}^0}{\partial x_1^2 \partial x_2}-(B_{12}+2B_{66})\frac{\partial^3 \bar{u}_{p1}^0}{\partial x_2^2 \partial x_1}-B_{26}\frac{\partial^3 \bar{u}_{p1}^0}{\partial x_2^3}-B_{16}\frac{\partial^3 \bar{u}_{p2}^0}{\partial x_1^3}-(B_{12}+2B_{66})\frac{\partial^3 \bar{u}_{p2}^0}{\partial x_1^2 \partial x_2} \tag{6-24}$$

$$-3B_{26}\frac{\partial^3 \bar{u}_{p2}^0}{\partial x_2^2 \partial x_1}-B_{22}\frac{\partial^3 \bar{u}_{p2}^0}{\partial x_2^3}+\bar{P}\bar{a}\frac{\partial^2 \bar{u}_{p3}}{\partial x_1^2}=0$$

where $\bar{u}_{p1}^0$ and $\bar{u}_{p2}^0$ are the in-plane displacements of the mid-plane of the off-axis plate and definitions of the coefficients B_{ij} and D_{ij} are given in Reference [67]. In the present case, the coefficients

$$B_{ij} = 0 \ (i,j = 1,2,6). \tag{6-25}$$

Since the plate has been assumed to undergo cylindrical bending, the deflection of the plate is independent of x_2, that is, the deflection $\bar{u}_{p3}$ is the function of x_1 only. Therefore, all orders of the derivatives of $\bar{u}_{p3}$ with respect to x_2 are equal to zero, that is,

$$\frac{\partial^4 \bar{u}_{p3}}{\partial x_1^3 \partial x_2}=\frac{\partial^4 \bar{u}_{p3}}{\partial x_1^2 \partial x_2^2}=\frac{\partial^4 \bar{u}_{p3}}{\partial x_2^3 \partial x_1}=\frac{\partial^4 \bar{u}_{p3}}{\partial x_2^4}=0 \tag{6-26}$$

Substituting equations (6-25, 6-26) into equation (6-24), one obtains the cylindrical bending equation for the composite plate as follows:

$$\frac{D_{11}\bar{b}}{\cos\theta}\frac{d^4 \bar{u}_{p3}}{dx_1^4}+\frac{\bar{P}\bar{a}\bar{b}}{\cos\theta}\frac{d^2 \bar{u}_{p3}}{dx_1^2}=0 \tag{6-27}$$

Equation (6-27) is obtained by multiplying $\bar{b}/\cos\theta$ on both sides of equation (6-24) for the sake of comparison with equation (6-17) using same unit.

In equation (6-27) the bending rigidity of the off-axis single layered plate per unit width in x_2 direction $D_{11} = \frac{1}{12} Q_{x_1x_1} \overline{a}^3$ and the related engineering constants are given by reference [68]

$$\begin{cases} Q_{x_1x_1} = m^4 Q_{11} + n^4 Q_{22} + 2m^2 n^2 Q_{12} + 4m^2 n^2 Q_{66} \\ Q_{11} = \dfrac{E_L}{1 - \nu_{LT}\nu_{TL}} \\ Q_{22} = \dfrac{E_T}{1 - \nu_{LT}\nu_{TL}} \\ Q_{12} = \dfrac{\nu_{TL} E_L}{1 - \nu_{LT}\nu_{TL}} \\ Q_{66} = G_{LT} \end{cases} \tag{6-28}$$

Note that if the common factor $\cos\theta$ in equation (6-27) is cancelled, the equilibrium equation for the off-axis single layered composite plate will have the same form as equation (6-2) for the rectangular single layered composite plate. The difference is that their coefficients or bending rigidities D_{11} are different from each other.

6.1.2.3 Equivalent conditions for the simply-supported off-axis composite beam and the simply-supported off-axis single layered composite plate

From equations (6-17) and (6-27), if the off-axis composite beam and the off-axis single layered composite plate are completely similar, the following relations must be satisfied:

$$Q_{x_1x_1} \overline{a}^3 \overline{b} = E_{x_1} a^3 b \tag{6-29}$$

$$\bar{a}\bar{b} = ab \tag{6-30}$$

$$\bar{P}\bar{a}\bar{b}/\cos\theta = P \tag{6-31}$$

Equations (6-30) through (6-31) are the requirements for replacing the off-axis composite beam with an equivalent off-axis single layered composite plate, that is, the equivalent conditions for the off-axis composite beam and the off-axis single layered composite plate.

6.1.3 Discussion of the equivalent conditions for the composite beam and single layered composite plate

Comparing equations (6-29)-(6-31) it can be seen that equations (6-3)-(6-5) are the special case of equations (6-29)-(6-31) at $\theta = 0^0$. Therefore, equations (6-29)-(6-31) are the general equivalent conditions for a simply-supported beam and a simply-supported cylindrical bending plate. Of these, equations (6-29) and (6-31) ensure the similarity of the buckling behaviors of the two structures, while all of the three equations (6-29)-(6-31) ensure both the similarity of the buckling behavior and stress distributions of the two structures.

When equations (6-29)-(6-31) are satisfied, the beam and the plate are of complete similarity. When at least one of equations (6-29)-(6-31) can not be satisfied, the beam and the plate are of partial similarity. In the present case the buckling behavior of the tri-axial woven composite structures is of concern. Therefore, equation (6-30) will be discarded in the equivalent conditions for the two structures in order to build a laminated composite plate with uniform thickness in later sections.

It is also worthy to note that equations (6-29)-(6-31) are derived by referring to Fig. 6.3, in which off-axis angle θ is counterclockwise from horizontal line corresponding to 60^0 tows in tri-axial composite structure. These equations can also be used in the case of $\theta = -60^0$ corresponding to 120^0 tows in the tri-axial structure because no specific requirements for the off-axis angle θ are employed during their derivation.

6.1.4 Determination of the geometric parameters of the equivalent single layered plates

In order to obtain an equivalent laminated composite plate which has the same in-plane dimensions as the tri-axial composite structure, the widths of the equivalent single layered composite plates for the beams will be assumed as the distances between central lines of the two neighboring parallel strips formed by neighboring parallel beams. As shown in figures 6.1 and 6.7, for example, Area D formed by two neighboring parallel beams D1-D1' and D2-D2' is a strip. Area A, B and C are the areas surrounded by the edges of the structure and central lines of the neighboring strips parallel to beams A1-A1', B1-B1' and C1-C1', respectively, in directions of 0^0, 60^0 and 120^0. Therefore, the width of Area *A* shown in figures 6.1 and 6.7 corresponds to the width of the equivalent single layered composite plate for beam A1-A1'. Since all the beams with 0^0 orientation are distributed uniformly in the tri-axial structure along x_2 direction, the width of Area A is also the width of other equivalent single layered plates for beams with 0^0 orientation. Similarly, widths of Areas *B* and *C* in figures 6.1 and 6.7 correspond to the widths of the equivalent single layered composite plates for beams with 60^0 and 120^0 orientations, respectively. For clarity, these areas of the corresponding equivalent plates and strips are

shown in Fig. 6.7. The tows of the structure are not shown in this figure. The same symbols as in Fig. 6.1 are used in Fig. 6.7.

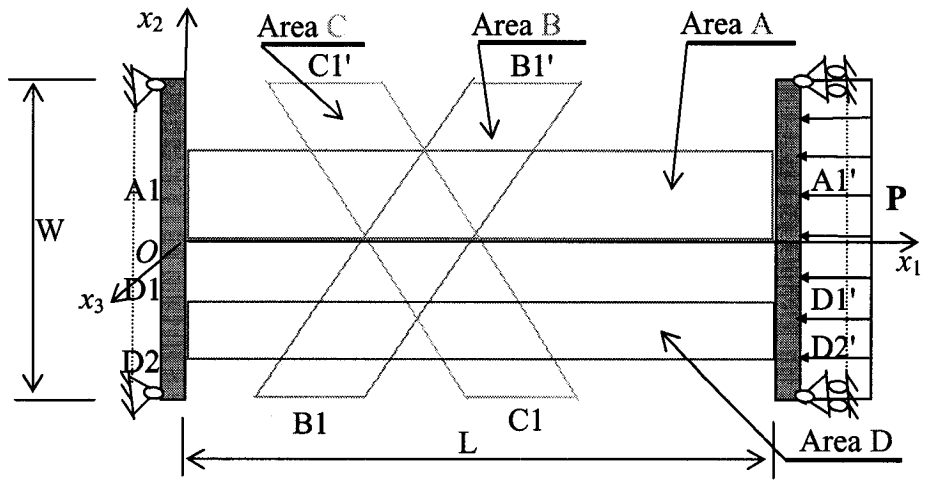

Fig. 6. 7: Equivalent plates to the corresponding beams and strip

In the present case, because the distances between the two neighboring parallel beams in all directions of 0^0, 60^0 and 120^0 are the same, the equivalent single layered composite plates for the beams in three different directions have the same width, that is,

$$\bar{b} = 3.97\ mm \tag{6-32}$$

Solving equation (6-29) for $\bar{a}$, one obtains the thickness of the equivalent single layered composite plate as follows:

$$\bar{a}_i = a\left(\frac{b}{\bar{b}}\frac{E_{x_1}}{Q_{x_1x_1}}\right)^{\frac{1}{3}} \tag{6-33}$$

where the subscript i that can be 60^0, 0^0 or -60^0 refers to the orientation of the beams.

Note that E_{x_1}, $Q_{x_1x_1}$ given by equations (6-13) and (6-28) are functions of θ. Therefore, the thickness of the single layered equivalent composite plate will be different with different orientations of the beams.

Substituting the corresponding geometric parameters and material constants of the beams and plates into equation (6-33), one finds that all the thicknesses of the equivalent single layered composite plates for the beams with different orientations are approximately equal to each other and have the value of

$$\bar{a}_i = 0.1\ mm \qquad (i = 0^0, 60^0, -60^0) \qquad (6\text{-}34)$$

6.1.5 Equivalent multi-layered composite plate and its equilibrium equation and buckling analysis

Now all the beams in the tri-axial woven fabric composite structure are replaced by their corresponding approximate equivalent single layered composite plates, for which their cross-sections are determined by equations (6-32) and (6-34). Also their lengths and fiber orientations are the same as the corresponding beams, as shown in figures 6.1 and 6.7. In addition, the equivalent single layered composite plates with the same fiber orientation are put in a plane at their corresponding beam location and bonded by resin. These plates with the same fiber orientation will form a thin layer of the composite laminate. For example, putting and bonding all the equivalent single layered plates for beams with orientation of 0^0 (all "A" areas as shown in figures 6.1 and 6.7) in the structure in parallel order in the same plane will constitute a composite laminate with 0^0 of fiber orientation. Similarly, putting and bonding all the equivalent single layered plates for beams with orientations of 60^0 and 120^0 (all "B" and "C" areas shown in figures 6.1

and 6.7) in parallel order in their corresponding planes will constitute two thin laminates with 60^0 and 120^0 of fiber orientations, respectively. Their in-plane dimensions are exactly the same as those of the tri-axial woven fabric composite structure shown in Fig. 6.1 and their thicknesses are determined by equation (6-33). Stacking and bonding with resin the three plies of the laminate in the sequence of $/60^0/0^0/-60^0/$ will form a multi-layered composite plate. This plate is used to replace the whole tri-axial woven fabric composite structure. Note that in this equivalent replacement all beams oriented at 60^0, 0^0 and 120^0 in the structure are replaced by plies with fiber orientations at 60^0, 0^0 and -60^0, respectively, and "woven fabrication and bonding with resin at the interlaced parts" of the structure is replaced by bonding with resin the laminates that form a plate structure. If they are loaded uni-directionally, both the original tri-axial woven composite structure and the new multi-layered composite plate structure will have the similar buckling behavior.

The equilibrium differential equation for the new multi-layered composite plate structure as shown in Fig. 6.8 with cylindrical bending is given by [67]

$$D_{p11}\frac{d^4u_{p3}}{dx_1^4}-B_{p11}\frac{d^3u_{p1}^0}{dx_1^3}-B_{p16}\frac{d^3u_{p2}^0}{dx_1^3}+P_pa_p\frac{d^2u_{p3}}{dx_1^2}=0 \qquad (6\text{-}35)$$

where u_{p1}^0 and u_{p2}^0 are the in-plane displacements of the mid-plane of the equivalent multi-layered plate, P_p is the distributed axial load applied to the structure in x_1 direction and $a_p=\bar{a}_{60}+\bar{a}_0+\bar{a}_{-60}$ is the total thickness of the equivalent plate structure, and the bending rigidity of the equivalent multi-layered plate structure,

$$D_{p11}=\frac{1}{3}(Q_{x_1x_1}^{-60}((-\frac{\bar{a}_0}{2})^3-(-\bar{a}_{-60}-\frac{\bar{a}_0}{2})^3)+Q_{x_1x_1}^{0}((\frac{\bar{a}_0}{2})^3-(-\frac{\bar{a}_0}{2})^3)+Q_{x_1x_1}^{60}((\bar{a}_{60}+\frac{\bar{a}_0}{2})^3-(\frac{\bar{a}_0}{2})^3)) \qquad (6\text{-}36)$$

where $Q^{i}_{x_1x_1}$ is given by equation (6-28) and the superscript i refers to the fiber orientation.

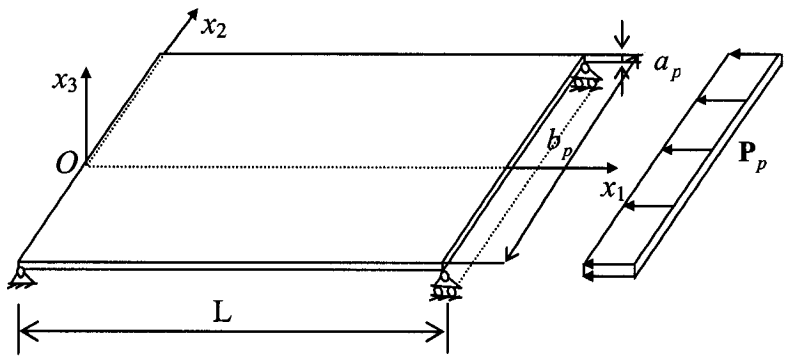

Fig. 6. 8: Simply-supported equivalent rectangular composite plate

The coefficients B_{p11} and B_{p16} in equation (41) are given by

$$B_{p11} = \frac{1}{2}(Q^{-60}_{x_1x_1}((-\frac{\bar{a}_0}{2})^2 - (-\bar{a}_{-60} - \frac{\bar{a}_0}{2})^2) + Q^{0}_{x_1x_1}((\frac{\bar{a}_0}{2})^2 - (-\frac{\bar{a}_0}{2})^2) + Q^{60}_{x_1x_1}((\bar{a}_{60} + \frac{\bar{a}_0}{2})^2 - (\frac{\bar{a}_0}{2})^2)) \quad (6\text{-}37)$$

$$B_{p16} = \frac{1}{2}(Q^{-60}_{x_1x_2}((-\frac{\bar{a}_0}{2})^2 - (-\bar{a}_{-60} - \frac{\bar{a}_0}{2})^2) + Q^{0}_{x_1x_2}((\frac{\bar{a}_0}{2})^2 - (-\frac{\bar{a}_0}{2})^2) + Q^{60}_{x_1x_2}((\bar{a}_{60} + \frac{\bar{a}_0}{2})^2 - (\frac{\bar{a}_0}{2})^2)) \quad (6\text{-}38)$$

$$Q_{x_1x_2} = (Q_{11} - Q_{12} - 2Q_{66})nm^3 + (Q_{12} - Q_{22} + 2Q_{66})mn^3 \quad (6\text{-}39)$$

Substituting the geometric parameters and material constants of the equivalent multi-layered plate into equations (6-37) and (6-38), the coefficients B_{p11} and B_{p16} are thus obtained as $B_{p11} = B_{p16} = 0$. Therefore, the equilibrium equation (6-35) for the equivalent multi-layered plate can be further simplified as

$$D_{p11}\frac{d^4u_{p3}}{dx_1^4} + P_pa_p\frac{d^2u_{p3}}{dx_1^2} = 0 \quad (6\text{-}40)$$

The critical load or buckling distributed load of the multi-layered plate structure for unit width shown in Fig. 6.8 is given by [67] as follows

$$(P_pa_p)_{cr} = D_{p11}\frac{\pi^2}{L^2} \quad (6\text{-}41)$$

The total critical load is given by

$$(P_p a_p b_p)_{cr} = D_{p11} b_p \frac{\pi^2}{L^2} \tag{6-42}$$

where b_p is the width of the equivalent plate.

Let us consider the basic structure shown in Fig. 5.2. For the basic structure, its in-plane projected width on x_2 axis is given by

$$b_b = \frac{3}{4} L \sin\frac{\pi}{3} \tag{6-43}$$

Since the equivalent multi-layered plate has the same width as the basic tri-axial structure, the width of the plate can be determined by

$$b_p = b_b \tag{6-44}$$

Substituting equation (6-44) and other material constants and geometric parameters of the equivalent multi-layered composite plate into equation (6-42), the buckling load for the plate is thus obtained as follows:

$$(P_p a_p b_p)_{cr} = 144.5 \ N \tag{6-45}$$

$(P_p a_p b_p)_{cr}$ is the total load applied to the equivalent multi-layered composite plate.

Considering the buckling load defined in the basic tri-axial woven fabric composite structure shown in Fig. 5.2, the buckling load of the equivalent multi-layered plate equivalent to that of the basic tri-axial woven composite structure is given by

$$(P_p a_p b_p)_{cr}^{eq} = (P_p a_p b_p)_{cr} / 4 = 36.1 \ N \tag{6-46}$$

where the denominator 4 corresponds to the 4 equal axial loads applied to the basic tri-axial composite structure as shown in Fig. 5.2.

The normalized non-dimensional equivalent buckling load based on the same factor as used in the basic tri-axial composite structure, that is, $\frac{\pi^2 E_L I}{L^2}$, is given by

$$\frac{(P_p a_p b_p)_{cr}^{eq}}{\pi^2 E_L I / L^2} = 1.09 \qquad (6\text{-}47)$$

This result is 8.78% larger than the value of the non-linear finite element solution given in Section 5.1 corresponding to the basic tri-axial structure shown in Fig. 5.2. It is 8.13% larger than the value of the non-linear finite element solution given in Section 5.6 corresponding to the enlarged tri-axial structure shown in Fig. 5.15. In other words, the value of the buckling load of the non-linear finite element solution for the basic tri-axial structure is 8.07% less than that of the approximate analytical solution for the equivalent multi-layered composite plate. The value of the buckling load of the non-linear finite element solution for the enlarged basic tri-axial structure shown in Fig. 5.15 is 7.52% less than that of the approximate analytical solution for the equivalent multi-layered plate.

The reason for this discrepancy is that the approximate solution for the equivalent multi-layered composite plate does not consider the shear deformation of the plate while the non-linear finite element solution for the beam does. Because this is a very thin plate, shear deformation will "soften" the structure. As a result, the value of the buckling load of the structure will be decreased due to the shear deformation. The decrease of the value may be around 3.5% referring to the difference between the analytical approximate solution and non-linear finite element solution for the thin beam given in Chapter 4.

Comparing the differences of the buckling loads of the non-linear finite element solution for the basic and enlarged basic tri-axial woven structures relative to the approximate analytical solution, one finds that difference for the buckling load of the enlarged basic tri-axial structure is smaller than that for the basic tri-axial structure. This is because the basic tri-axial structure is only a small part of the tri-axial woven fabric structure and it has lower in-plane load transferability due to the edge effect of the tri-

axial woven fabric structure. As more tows are involved in the tri-axial woven fabric composite structure and the in-plane size of the tri-axial structure gets larger, the edge effect will be weakened and load transferability will be improved. As a result, the tri-axial structure with more tows and larger in-plane size will sustain larger in-plane load. However, the load sustained by the tri-axial woven structure cannot be increased infinitely as the in-plane size of the structure increases. It has to approach a certain value. The analytical method reveals that this value has to be less than the approximate analytical solution for the buckling load of the equivalent multi-layered plate because the equivalent multi-layered plate has a better replacement or better approximation to the tri-axial woven structure when the tri-axial structure gets larger, that is, the larger the size of the tri-axial structure is, the higher accuracy the approximate analytical solution can predict.

Thus, it can be concluded that the numerical non-linear finite element solution for basic tri-axial structure subjected to uni-directional loading is confirmed by approximate analytical solution.

For convenience the results for the values of the buckling load obtained by both non-linear finite element analysis and approximate analytical method are listed in the following table 6.1 and figure 6.9. One can see either from the table or from the figure that the difference between the approximate analytical solution and non-linear finite element solution becomes smaller as the size of the tri-axial structure gets larger.

Table 6. 1: List of the non-dimensional buckling loads for the simply-supported tri-axial woven fabric composite structures

Structures	Non-linear FE solution	Approximate analytical solution	Differences relative to the analytical solution
Basic tri-axial structure with 6 tows	1.0020	1.0900	8.07%
Modified basic tri-axial structure with 8 tows	1.0034	1.0900	7.94%
Modified basic tri-axial structure with 10 tows	1.0049	1.0900	7.81%
Enlarged basic tri-axial structure with 12-tows	1.0080	1.0900	7.52%

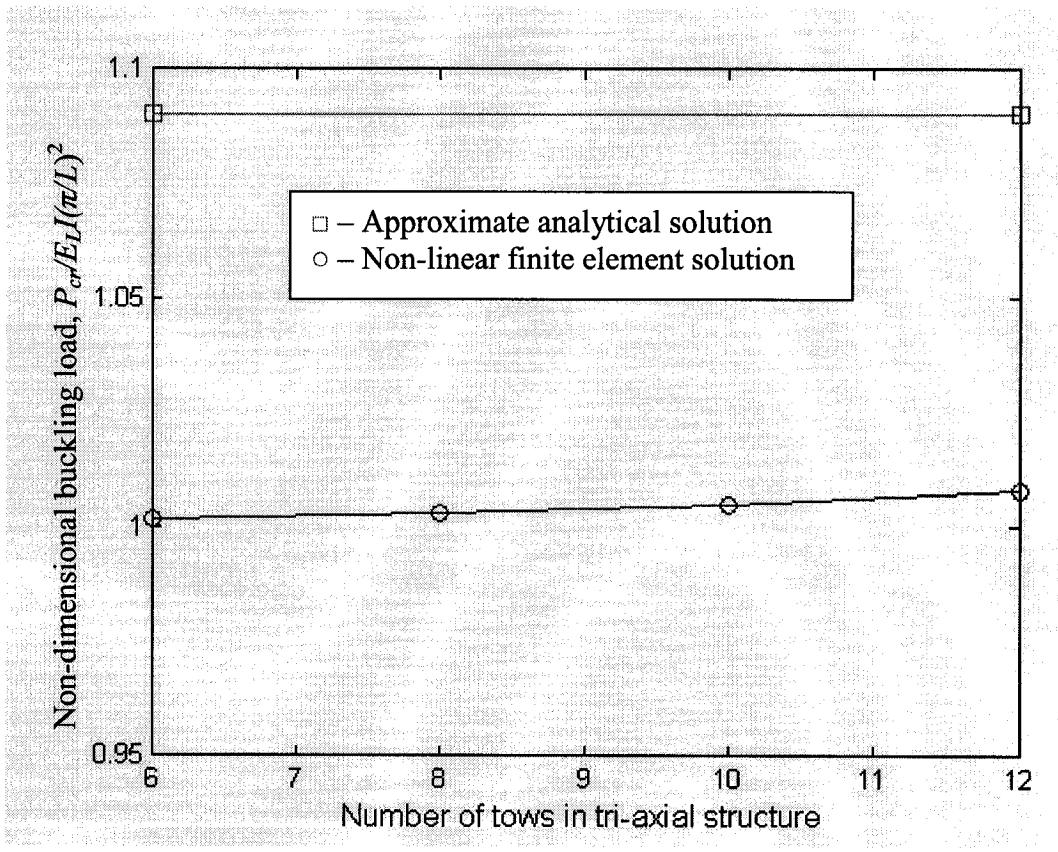

Fig. 6. 9: Comparison of buckling load between numerical solution and analytical solution

Therefore, one can further conclude that for design purpose, the value of buckling load for a large sized tri-axial structure can be obtained approximately by subtracting from the value of the approximate analytical solution by 8%. Thus determined value of buckling load for a large sized tri-axial structure is on the safe side.

6.2 Basic tri-axial structure subjected to bi-directional loading

Approximate analytical solution for buckling analysis of bi-directionally loaded tri-axial woven fabric composite structures will be more complicated than that of uni-directionally loaded tri-axial woven fabric composite structures since the bi-directionally loaded tri-axial woven structures no longer take the form of cylindrical bending as the uni-directionally loaded tri-axial woven structures do. Therefore, the multi-layered plate theory developed in the last section can not be used to predict the buckling load of a bi-directionally loaded tri-axial woven structure. New methodology has to be developed to determine the buckling load of the bi-directionally loaded tri-axial woven structure.

First, the following assumptions are made in order to find an equivalent plate of the bi-directionally loaded basic tri-axial structure. Assume that:

1. The bi-directionally loaded simply-supported basic tri-axial woven composite structure can be replaced by an equivalent anisotropic single layered plate with the same loading. Boundary conditions and in-plane sizes are the same as the basic tri-axial structure, but with different material properties.

2. Both the central planes of the equivalent plate and the basic tri-axial structure have the same deformed shape. This assumption is based on the conclusions made and numerical results obtained by Zhao and Hoa [2] and [3].

Next, determine the equivalent conditions for the equivalent plate and the basic tri-axial structure. The equivalent conditions include determination of the material properties and the thickness of the equivalent plate as well as the loading. The material constants obtained by Zhao and Hoa [2] and [3] will be used as the material properties of the equivalent plate. They are listed in the following table.

Table 6. 2: Material properties of the tri-axial woven fabric composite structure [2,3]

Young's modulus E_{p1}(GPa)	Young's modulus E_{p2}(GPa)	Poisson's ratio v_{p12}	Poisson's ratio v_{p21}
30	26.5	0.58	0.56

Though these material constants were obtained by modeling bigger in-plane size of tri-axial woven fabric composite structures than the basic tri-axial structure, they can still be used as an approximation for the basic tri-axial structure because it will be seen later in the present section that one of the most sensitive parameters for buckling load, the thickness of the equivalent plate, a_p, is a function of these constants. Different material constants will produce different thicknesses of the equivalent plate. More accurate material constants will result in more accurate thickness. Less accurate material constants will lead to less accurate thickness. However, the final buckling loads thus obtained will approximately be the same for different sets of material constants and thickness of the

plate because of their interaction and their compensation for each other. This can be seen in related equations developed in later part of the present Section.

The thickness of the equivalent plate can be determined by using energy method, that is, if a plate is equivalent to the basic tri-axial structure, its strain energy should be equal to the strain energy of the basic tri-axial structure, i.e.,

$$U_p = U_b \tag{6-48}$$

where U_p is the strain energy of the plate and U_b is the strain energy of the basic tri-axial structure; subscript p refers to plate and subscript b refers to the basic tri-axial structure.

Bi-directionally loaded simply-supported anisotropic plate is shown in Fig. 6.10. The x_1x_2 plane is the mid-plane of the rectangular plate. Its in-plane dimensions are the same as the basic tri-axial structure.

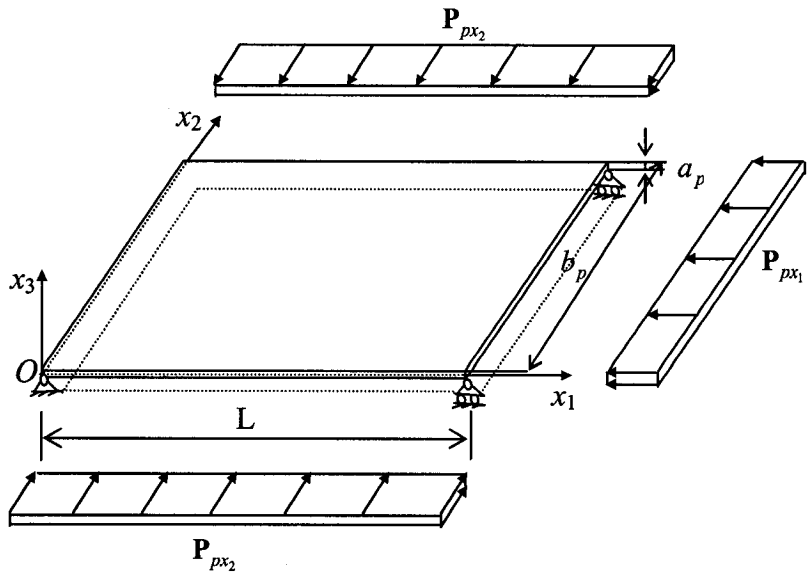

Fig. 6. 10: Bi-directionally loaded simply-supported rectangular plate

If the in-plane displacements of the plate are neglected and plane stress assumption is employed, the strain energy of the plate can be written as [67]

$$U_p = \frac{1}{2}\int_{V_p} (\sigma_{px_1}\varepsilon_{px_1} + \sigma_{px_2}\varepsilon_{px_2} + 2\sigma_{px_1x_2}\varepsilon_{px_1x_2})dV_p \tag{6-49}$$

where $\sigma_{Px_1}, \sigma_{Px_2}, \sigma_{Px_1x_2}$ and $\varepsilon_{px_1}, \varepsilon_{px_2}, \varepsilon_{px_1x_2}$ are stress components and Lagarangian strain components of the plate, respectively, and V_p is the volume of the plate.

For an anisotropic plate, its constitutive equation is given by [67]

$$\begin{bmatrix} \sigma_{px_1} \\ \sigma_{px_2} \\ \sigma_{px_1x_2} \end{bmatrix} = \begin{bmatrix} Q_{p11} & Q_{p12} & 0 \\ Q_{p12} & Q_{p22} & 0 \\ 0 & 0 & Q_{p66} \end{bmatrix} \begin{bmatrix} \varepsilon_{px_1} \\ \varepsilon_{px_2} \\ 2\varepsilon_{px_1x_2} \end{bmatrix} \tag{6-50}$$

where the elements of the stiffness matrix are given by [67]

$$\begin{cases} Q_{p11} = \dfrac{E_{p1}}{1 - \nu_{p12}E_{p2}/E_{p1}} \\ Q_{p22} = \dfrac{E_{p2}}{1 - \nu_{p12}E_{p2}/E_{p1}} \\ Q_{p12} = \dfrac{\nu_{p12}E_{p2}}{1 - \nu_{p12}E_{p2}/E_{p1}} \\ Q_{p66} = G_p = \dfrac{E_{p1}}{2(1+\nu_{p12})} \end{cases} \tag{6-51}$$

If one assumes that linear elements perpendicular to the mid-plane (x_1x_2 plane) of the plate before bending remain straight and normal to the deflection surface of the plate after bending, the components of strain can be written as:

$$\begin{cases} \varepsilon_{px_1} = -x_3 \dfrac{\partial^2 u_3}{\partial x_1^2} \\ \varepsilon_{px_2} = -x_3 \dfrac{\partial^2 u_3}{\partial x_2^2} \\ \varepsilon_{px_1x_2} = -x_3 \dfrac{\partial^2 u_3}{\partial x_1 \partial x_2} \end{cases} \tag{6-52}$$

Substituting equations (6-50) through (6-52) into equation (6-49), one obtains the strain energy of the plate as follows

$$U_p = \frac{1}{2}\int_{V_p} (Q_{p11}x_3^2(\frac{\partial^2 u_3}{\partial x_1^2})^2 + 2Q_{p12}x_3^2 \frac{\partial^2 u_3}{\partial x_1^2}\frac{\partial^2 u_3}{\partial x_2^2} + Q_{p22}x_3^2(\frac{\partial^2 u_3}{\partial x_2^2})^2 + 4Q_{p66}x_3^2(\frac{\partial^2 u_3}{\partial x_1 \partial x_2})^2) dV_p \tag{6-53}$$

For a plate being simply-supported on all four edges, its deflection may be assumed as [67]

$$u_3 = A_{mn} \sin\frac{m\pi x_1}{L} \sin\frac{n\pi x_2}{b_p} \tag{6-54}$$

where A_{mn} is an arbitrary constant, m and n are integers.

Differentiating equation (6-54) with respect to x_1 and x_2 and substituting back into equation (6-53), performing the integration to equation (6-53), one obtains the strain energy of the plate as follows

$$U_p = \frac{1}{96} A_{mn}^2 a_p^3 L b_p \left[Q_{p11}(\frac{m\pi}{L})^4 + 2Q_{p12}(\frac{m\pi}{L})^2(\frac{n\pi}{b_p})^2 + Q_{p22}(\frac{n\pi}{b_p})^4 + 4Q_{p66}(\frac{m\pi}{L})^2(\frac{n\pi}{b_p})^2 \right] \tag{6-55}$$

Considering that the lowest buckling load corresponds to the first mode deflection in both directions of x_1 and x_2, that is, $m = n = 1$, and the width of the plate $b_p = L\sin\frac{\pi}{3} = \frac{\sqrt{3}}{2}L$, the strain energy of the plate of equation (6-55) can be written as

$$U_p = \frac{1}{96}\frac{\sqrt{3}}{2} A_{11}^2 L^2 (\frac{\pi}{L})^4 a_p^3 (Q_{p11} + \frac{8}{3}Q_{p12} + \frac{16}{9}Q_{p22} + \frac{16}{3}Q_{p66}) \tag{6-56}$$

For the bi-directionally loaded simply-supported basic tri-axial structure as shown in Fig. 5.20, if its shear deformations are also neglected and the same deformation assumptions are employed as the plate deformation, namely, the plane sections originally normal to the centerline axis remain plane and undistorted under deformation and normal to this axis, the strain energy of the basic tri-axial tow structure can be written as

$$U_b = \frac{1}{2}\int_{V_b} \sigma_{x_1'} \varepsilon_{x_1'} dV_b \tag{6-57}$$

where $\sigma_{x_1'}$ and $\varepsilon_{x_1'}$ are stress and strain in local coordinate system of each tow, in which its origin of the local coordinate system corresponding to each tow is put at the end of the each tow on the left side of the structure denoted by a capital letter without prime; x_1' axis of the coordinate system is along that tow and directs toward the other end; x_2' axis is in x_1x_2 plane and directs to the upward; x_3' axis is determined by the right hand rule. An example of the local coordinate system of tow BB′ in Fig. 5.20 is shown in Fig. 6.11.

Fig. 6. 11: Local coordinate system of tow BB' in Fig. 5.20

The relation of the local stress and local strain is given by

$$\sigma_{x_1'} = E_L \varepsilon_{x_1'} \tag{6-58}$$

where the local strain $\varepsilon_{x_1'}$ is given by

$$\varepsilon_{x_1'} = -x_3' \frac{\partial^2 u_3'}{\partial x_1'^2} \tag{6-59}$$

According to the basic assumption 2 made at the beginning of this section, if the curvatures of the tows are neglected compared to the length of the tows in the structure, the deflection equation of any tow in Fig. 5.20 can be approximated in global coordinate system as (first mode deflection at $m = n = 1$)

$$\begin{cases} u_3 = A_{11} \sin\dfrac{\pi x_1}{L} \sin\dfrac{\pi x_2}{b_p} \\ \\ x_2 = k x_1 + c \end{cases} \tag{6-60}$$

The second equation given above is the equation of local coordinate axis x_1' in $O x_1 x_2$ plane, in which k and c are constants to be determined in the following and depend on the location of the tows in the structure shown in Fig. 5.20. They are given as follows:

Tow AA′ in Fig. 5.20 $k = 0$ and $c = \dfrac{3\sqrt{3}}{8} L$;

Tow BB′ $k = 0$ and $c = \dfrac{\sqrt{3}}{8} L$;

Tow CC′ $k = \sqrt{3}$ and $c = 0$; (6-61)

Tow DD′ $k = \sqrt{3}$ and $c = -\dfrac{\sqrt{3}}{2} L$;

Tow EE′ $k = -\sqrt{3}$ and $c = \dfrac{\sqrt{3}}{2} L$;

Tow FF′ $k = -\sqrt{3}$ and $c = \sqrt{3} L$;

Substituting the corresponding parameters of the tow given in equation (6-61) into equation (6-60), deflection equation of that tow can be obtained. For example, for tow

DD′, after substitution of the parameters k and c from equation (6-61), deflection equation of tow DD′ can be written as

$$\begin{cases} u_3 = A_{11} \sin\dfrac{\pi x_1}{L} \sin\dfrac{\pi x_2}{b_p} \\ \\ x_2 = \sqrt{3}\, x_1 - \dfrac{\sqrt{3}}{2} L \end{cases} \tag{6-62}$$

All the rest of the deflection equations of the tows in the structure shown in Fig. 5.20 can be obtained in the same way.

The relation between local and global coordinate systems is given by

$$\begin{cases} x_1' = (x_1 + d_1)\cos\theta + (x_2 + d_2)\sin\theta \\ \\ x_2' = -(x_1 + d_1)\sin\theta + (x_2 + d_2)\cos\theta \\ \\ x_3' = x_3 \end{cases} \tag{6-63}$$

where θ is the angle of the rotation of the local coordinate system about global coordinate system, d_1 and d_2 are constants to be determined in the following and they represent x_1 and x_2 coordinates of the origins of the local coordinate systems in global coordinate system.

The origin of the local coordinate system of tows is given as follows:

AA′ in Fig. 5.20 $\quad (d_1, d_2) = (0, 0)$

BB′ $\quad (d_1, d_2) = (0, -\dfrac{\sqrt{3}}{4} L)$

CC′ $\quad (d_1, d_2) = (0, -\dfrac{3\sqrt{3}}{8} L)$

DD′ $\quad (d_1, d_2) = (\dfrac{L}{2}, -\dfrac{3\sqrt{3}}{8} L)$ (6-64)

EE′ $$(d_1, d_2) = (0, \frac{\sqrt{3}}{8}L)$$

FF′ $$(d_1, d_2) = (\frac{L}{2}, \frac{\sqrt{3}}{8}L)$$

The displacement relation of local and global coordinate systems is given by

$$u_3' = u_3 \tag{6-65}$$

Substituting equations (6-58) through (6-65) into equation (6-57) and performing the integration to the final equation, one obtains the strain energy of the basic tri-axial structure as follows:

$$U_b = \frac{9.4713}{96} A_{11}^2 L(\frac{\pi}{L})^4 a^3 b E_L \tag{6-66}$$

Substituting equations (6-66) and (6-56) into equation (6-48) and solving for the thickness of the plate a_p, one obtains

$$a_p = a\left[\frac{b}{b_p}\frac{9.45713E_L}{Q_{p11}+\frac{8}{3}Q_{p12}+\frac{16}{9}Q_{p22}+\frac{16}{3}Q_{p66}}\right]^{\frac{1}{3}} \tag{6-67}$$

As mentioned at the beginning of the section, from equation (6-67) one can see that the equivalent thickness of the plate depends on the values of the equivalent material constants. Different values of the material constants will produce different value of the thickness of the plate.

Substituting the related geometric parameters and material constants of the basic tri-axial structure and the material constants of the equivalent plate listed in Table 1, one obtains the thickness of the equivalent plate as follows:

$$a_p = 0.23\ mm \tag{6-68}$$

The buckling load of the simply-supported rectangular anisotropic plate per unit length subjected to bi-directional loading is given by [67]

$$(P_{px_1}L^2 + P_{px_2}b_p^2)_{cr} = \frac{\pi^2 a_p^3}{12}\left[Q_{p11}(\frac{b_p}{L})^2 + 2(Q_{p12} + 2Q_{p66}) + Q_{p22}(\frac{L}{b_p})^2\right] \tag{6-69}$$

where the subscript *cr* denotes the critical load or buckling load.

Load equivalent conditions

As for the load equivalent condition, it can be obtained by equating the work done by the loads applied to the equivalent plate to the work done by the loads applied to the basic tri-axial structure as long as the two structures are equivalent each other, namely,

$$W_p = W_b \tag{6-70}$$

where the W_p is the work done by loads applied to the equivalent plate and W_b the work done by the loads applied to the basic tri-axial structure.

For the equivalent plate with reference to Fig. 6.10, if the edge displacements of the plate are assumed to be Δ_{x_1} for the right-hand side edge, Δ_{x_20} the lower edge and Δ_{x_2b} the upper edge, the work done onto the plate is given by

$$W_p = P_{px_1}b_p\Delta_{x_1} + P_{px_2}L\Delta_{x_20} + P_{px_2}L\Delta_{x_2b} \tag{6-71}$$

Since it has been assumed that the equivalent plate and the basic tri-axial structure have the same deformation, the edge displacements of the basic tri-axial structure should be equal to the corresponding edge displacements of the equivalent plate. The work done of the basic structure shown in Fig. 5.20 is given by

$$\begin{aligned} W_b = {} & (P_{F'1} + P_{B'1} + P_{A'1} + P_{D'1})\Delta_{x_1} + (P_{C2} + P_{D2} + P_{E'2} + P_{F'2})\Delta_{x_20} \\ & + (P_{E2} + P_{F2} + P_{C'2} + P_{D'2})\Delta_{x_2b} \end{aligned} \tag{6-72}$$

Substituting from equations (6-71) and (6-72) into (6-70) and rearranging, one obtains

$$(P_{F'1}+P_{B'1}+P_{A'1}+P_{D'1}-P_{px_1}b_p)\Delta_{x_1}+(P_{C2}+P_{D2}+P_{E'2}+P_{F'2}-P_{px_2}L)\Delta_{x_20}+$$
$$(P_{E2}+P_{F2}+P_{C'2}+P_{D'2}-P_{px_2}L)\Delta_{x_2b}=0 \tag{6-73}$$

This equation should hold for any edge displacements of the structures. Therefore, all the coefficients of the displacements have to vanish, that is,

$$\begin{cases} P_{F'1}+P_{B'1}+P_{A'1}+P_{D'1}-P_{px_1}b_p=0 \\ P_{C2}+P_{D2}+P_{E'2}+P_{F'2}-P_{px_2}L=0 \\ P_{E2}+P_{F2}+P_{C'2}+P_{D'2}-P_{px_2}L=0 \end{cases} \tag{6-74}$$

Equation (6-74) describes the relations between the loads applied to the equivalent plate and the basic tri-axial structure. Hence, it is also the said conditions for the load equivalent.

Considering that the forces $P_{F'1},P_{B'1},P_{A'1},P_{D'1}$ are equal in their values and forces P_{C2},P_{D2}, $P_{E'2},P_{F'2},P_{E2},P_{F2},P_{C'2}$ and $P_{D'2}$ are equal in their values in the present case, the second and the third equations of (6-74) are actually the same. Thus, only the second equation of (6-74) is to be retained for convenience. If $P_{F'1},P_{B'1},P_{A'1}$ and $P_{D'1}$ are denoted by P_{bx_1} and $P_{C2},P_{D2},P_{E'2}$, $P_{F'2}$, $P_{E2},P_{F2},P_{C'2}$ and $P_{D'2}$ by P_{bx_2}, the load equivalent conditions of equation (6-74) can be written as

$$\begin{cases} P_{px_1}b_p=4P_{bx_1} \\ P_{px_2}L=4P_{bx_2} \end{cases} \tag{6-75}$$

As in Section 5.7, two cases will be discussed in the following.

Case I: P_{px_2} is constant while P_{px_1} changes.

Solving for P_{px_1} from equation (6-69), one obtains the buckling load of the equivalent plate per unit width as follows:

$$(P_{px_1})_{cr} = \frac{\pi^2 a_p^3}{12L^2}\left[Q_{p11}(\frac{b_p}{L})^2 + 2(Q_{p12}+2Q_{p66}) + Q_{p22}(\frac{L}{b_p})^2\right] - P_{px_2}\frac{b_p^2}{L^2} \tag{6-76}$$

Substituting the load equivalent conditions given by equation (6-75) into equation (6-76), the approximate buckling load applied to the basic tri-axial structure can be written as

$$(P_{bx_1})_{cr} = \frac{\pi^2 b_p a_p^3}{48L^2}\left[Q_{p11}(\frac{b_p}{L})^2 + 2(Q_{p12}+2Q_{p66}) + Q_{p22}(\frac{L}{b_p})^2\right] - P_{bx_2}\frac{b_p^3}{L^3} \tag{6-77}$$

The Table 6.3 lists the values of the buckling load applied in x_1 direction calculated from equation (6-77) at different values of the loads applied in x_2 direction by substitution of the related geometric parameters and material constants of the plate. These results are also shown in Fig. 6.12.

Table 6. 3: Comparison of finite element solution and approximate solution

$P_{bx_2}/(\pi^2 E_L I/L^2)$	0.000	0.0759	0.1518	0.3036
$(P_{bx_1})_{cr}/(\pi^2 E_L I/L^2)^*$	1.5770	1.5755	1.5741	1.5711
$P_{cr}/(\pi^2 E_L I/L^2)^{**}$	1.4430	1.4415	1.4392	1.4336
$e_r(\%)^{***}$	8.50	8.51	8.57	8.75

* Present approximate solution.

** Non-linear finite element solution obtained in Section 5.7.

*** Relative error of non-linear finite element solution with respect to approximate analytical solution.

From this Table and the curve shown in Fig. 6.12, one can see that the error of the non-linear finite element solution with respect to the approximate equivalent plate solution becomes ever so slightly larger when loads applied in x_2 direction gets larger.

This may be because of the loading procedure. In finite element analysis, the loads in x_2 direction are applied in one step while the loads in x_1 direction are exerted gradually by an increment each time until the structure buckles. It is also worth to mention that the present approximate analytical solution does not consider the shear effect on the plate deformation. From these points of view, the accuracy of the solution of non-linear finite element analysis is confirmed.

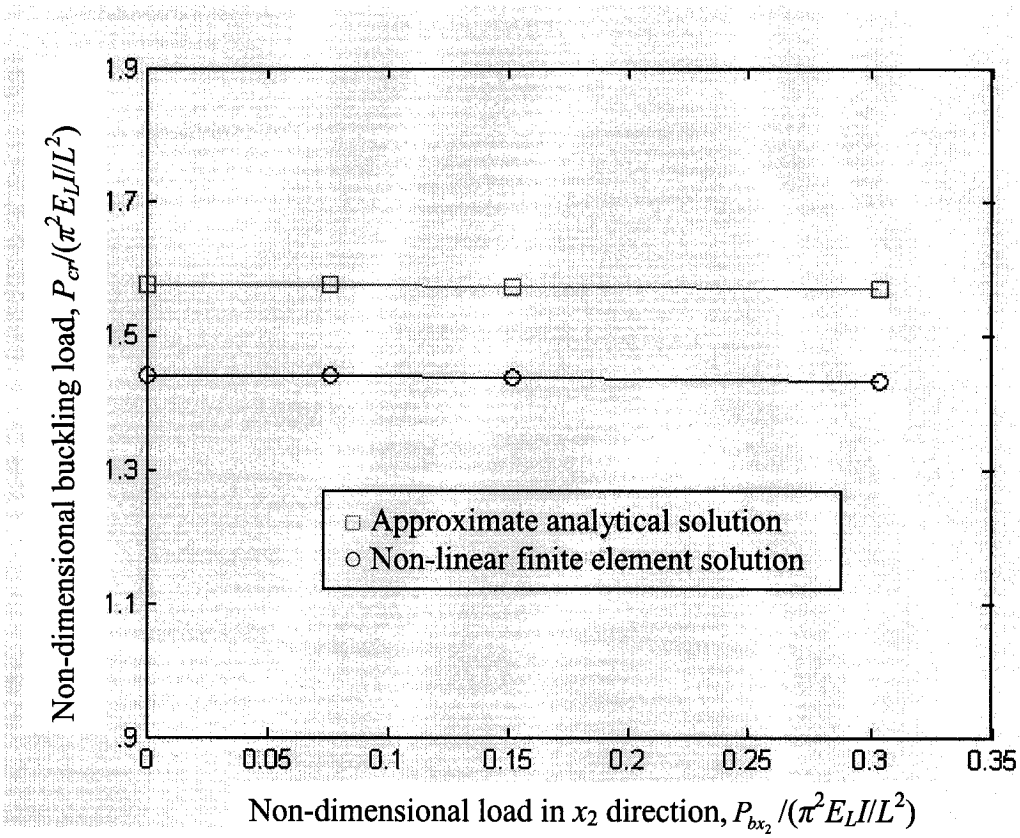

Fig. 6. 12: Comparison of the finite element solution and approximate solution

Case II: Varying both P_{px_1} and P_{px_2}

Because the uniform in-plane loading is applied to the basic tri-axial structure, the in-plane load exerted to the equivalent plate should be also of uniform form. Therefore, the following form of in-plane loading of the plate can be assumed.

$$P_{px_2} = RP_{px_1} \tag{6-78}$$

where R is the load ratio and its value can be obtained by dividing the first equation of (6-75) by the second one as follows:

$$R = \frac{P_{px_2}}{P_{px_1}} = \frac{4P_{bx_2}b_p}{4P_{bx_1}L} = \frac{\sqrt{3}}{2} \tag{6-79}$$

Substituting equations (6-79) and (6-78) into equation (6-69) and solving for P_{bx_1}, one obtains the approximate buckling load applied to the basic tri-axial structure as follows:

$$(P_{bx_1})_{cr} = \frac{\pi^2 b_p a_p^3}{48(L^2 + Rb_p^2)}\left[Q_{p11}(\frac{b_p}{L})^2 + 2(Q_{p12} + 2Q_{p66}) + Q_{p22}(\frac{L}{b_p})^2\right] \tag{6-80}$$

Substituting the required geometric parameters and material constants of the equivalent plate and related parameters into equation (6-80), one obtains the value of the buckling load of the basic tri-axial structure as follows

$$(P_{bx_1})_{cr} / (\pi^2 E_L I / L^2) = 0.9561 \tag{6-81}$$

Recalling that the value of the normalized buckling load for this case obtained in Section 5.7 by using non-linear finite element method is $P_{cr} / (\pi^2 E_L I / L^2) = 0.8729$, the error of this solution with respect to the approximate solution given in equation (6-81) is equal to 8.7%.

Again as in the last section and in case I of the present Section, the approximate analytical solution obtained here does not consider the shear effect of the equivalent

plate. Therefore, one can conclude that the non-linear finite element solution is comparable with the approximate analytical solution.

6.3 Conclusion

In order to provide confirmation to the numerical non-linear finite element solutions and to provide simpler ways to obtain the qualitative results, approximate analytical solution to the buckling load of the basic tri-axial structure subjected to uni-directional loading and bi-directional loading has been derived by using equivalent multi-layered plate theory and anisotropic plate theory, respectively. Comparing the numerical solution with the analytical solution, there is only 7-9% difference between them. Thus, a good agreement is obtained. Therefore, the equivalent plate method can be a simpler way to get the buckling load for the tri-axial woven fabric composite structure. The approximate analytical solution also provides the upper bound of the buckling load for the tri-axial woven fabric composite structure subjected to uni-directional loading.

Chapter 7

Conclusions

Based on the studies conducted in this dissertation, the following major conclusions can be drawn:

- A non-linear finite element formulation for the buckling analysis of tri-axial composite curved beam structures has been developed. Corresponding approximate analytical solutions to the structures are also presented. The accuracy of the numerical solutions has been confirmed by the approximate analytical solutions for corresponding structures.
- Buckling behavior of different forms of tri-axial woven fabric composite structure has been studied using non-linear finite element formulation. The structures include the basic tri-axial structure, modified basic tri-axial structures that are obtained by adding one or two X-crossovers horizontally to the basic tri-axial structure and enlarged basic tri-axial structure that is obtained by adding more X-crossover to the basic tri-axial structure both horizontally and vertically, two each in both directions. They are subjected to either uni-directional loading or bi-directional loading. The numerical results reveal that these tri-axial composite structures subjected to uni-directional loading have a little difference in the value of their buckling loads. As more tows are involved in tri-axial structure, the value of the buckling load of corresponding structure becomes higher. Buckling

analysis of the simply-supported basic tri-axial structure with imperfection in the form of initial deflection and basic tri-axial structure subjected to different boundary conditions is also performed.

- The investigation of the effect of the resin on the basic tri-axial structure shows that the Young's modulus of the resin has little effect on the buckling behavior of the basic tri-axial structure due to the interaction of the woven tows constituting the structure.
- Approximate analytical solutions to the buckling load of the basic tri-axial structure subjected to uni-directional loading and bi-directional loading obtained using multi-layered plate theory and anisotropic plate theory, respectively, are comparable to the corresponding non-linear finite element solution. Therefore, the approximate analytical methods used in the present thesis provide simpler ways to obtain the results.
- Extension to the buckling of real life large tri-axial structures is discussed. Buckling load of a real life large tri-axial structure can be obtained approximately by subtracting from the value of the approximate analytical solution by 8%. Thus determined value of buckling load for a real life larger sized tri-axial structure is on the safe side.

Chapter 8

Contributions of the research and recommendations for the future work

8.1 Contributions of the research

In this thesis, a detailed and efficient non-linear finite element model of tri-axial woven fabric composite tow structure is developed to investigate the buckling behavior and to determine the value of the buckling load. Analysis of buckling behavior and determination of the value of the buckling load for several tri-axial structures are performed. The results are compared with the approximate analytical solutions. Through this study, several contributions are made. They can be summarized as follows:

- Used curved beam formulation to model the tri-axial woven fabric composite tow structure.
- Developed the corresponding incremental non-linear finite element formulation for the tri-axial woven composite structure using updated Lagrangian approach in continuum mechanics theory.
- Investigated numerically the buckling behavior of several tri-axial structures, such as individual curved composite beam, composite tow structure with two intersected curved beams, tri-axial structure with three intersected curved beams,

basic tri-axial structure with six woven curved beams, modified basic tri-axial structures with eight and ten woven curved beams, respectively, and enlarged basic tri-axial structure with twelve curved beams. Corresponding buckling loads were also determined. These structures were subjected to different loading conditions such as uni-directional loading and bi-directional loading and change in boundary conditions from simply-supported ends to clamped ends. Conducted sensitivity of the buckling behavior of tri-axial structure to the imperfections in the form of initial deflections of the configuration. Analyzed the effect of Young's modulus of the resin on the tri-axial composite structure.

- Derived the corresponding approximate analytical solutions of the buckling loads to all the tri-axial composite structures investigated numerically using different techniques, such as energy method, equivalent multi-layered plate method and equivalent strain energy method. Approximate analytical solution serves as both the confirmation to the numerical results and simpler ways to obtain the results.
- Extension to the buckling of real life large tri-axial structures was discussed.

Portion of the research results have been either accepted as refereed journal articles or submitted for publication [69-71].

8.2 Recommendations for the future work

The thesis research presents a fundamental non-linear finite element analysis of buckling behavior for several forms of tri-axial woven fabric composite structure. It is

recommended that the following future studies should be undertaken to further explore the validation and the application potentials of the proposed methodologies to facilitate its realization and implementations.

- In practical application, tri-axial woven fabric composite structure is much larger in its size than those studied in the present thesis. Therefore, non-linear finite element analysis of buckling behavior for larger sized tri-axial structure needs to be investigated using more powerful computer.
- In order to confirm and validate the results of non-linear finite element solution for a large sized tri-axial structure subjected to different loading conditions and different boundary conditions, experiments need to be performed.
- For thorough understanding the buckling behavior of tri-axial woven fabric composite structure, post-buckling analysis of the structure needs to be conducted.
- The tri-axial structure may undergo instability or collapse during buckling. Therefore, progressive failure of the tri-axial structure under compressive loading needs to be carried out.

References

1. Akihiro Fujita, Hiroyuki Hamada and Zenichiro Maekawa, "Tensile properties of carbon fiber tri-axial woven fabric composites", J. of Composite Materials", vol. 27, No. 15, 1993, pp. 1428-1441
2. Zhao, Q. and Hoa S.V. "Tri-axial woven fabric (TWF) composite with open holes (Part I): Finite element models for composites", Journal of Composite Materials, vol. 37, No. 9, 2003, pp. 763-791.
3. Zhao, Q., Hoa, S.V. and Ouellette P. "Tri-axial woven fabric (TWF) composite with open holes (Part II): Verification of the finite element model", Journal of Composite Materials, vol. 37, No.10, 2003, pp. 849-875.
4. Zhao, Q. and Hoa, S.V. "Analysis of tri-axial woven fabric (TWF) composites for satellite applications", accepted for publication, Journal of Composite Materials, November 2002.
5. Zhao, Q. and Hoa, S.V. "Thermal deformation behavior of tri-axial woven fabric (TWF) composites with open holes", accepted for publication, Journal of Composite Materials, March 2003.
6. Zhao, Q. and Hoa, S.V. "Progressive Failure of Triaxial Woven Fabric (TWF) composites with open holes", accepted for publication, Journal of Composite structures, March 2003.
7. Schwartz, P., Fornes, R. E. and Mohamed, M. H., "Tensile Properties of Tri-axially Woven Fabrics Under Biaxial Loading", Journal of Engineering for Industry, vol. 102, Nov. 1980, pp. 327-331

8. Hewitt, J.A., Brown, D. and Clarke, R.B. 1995. "Computer Modeling of Woven Composite Materials", Composites, 26: 134-140
9. Dano, M.L., Gendron, H. and Picard, A., "Elastic Properties of a Carbon Fiber tri-axial Woven Composite," Proceeding of the Canadian Conference of Applied Mechanics, Toronto, May 1999.
10. Hoa, S.V. and Sheng, S.Z., "Three Dimensional Model for Elastic Properties of Textile Composites", Proc. 3rd Canadian International Conference on Composites, Montreal, Aug. 2001, published by Technomic.
11. Sheng, S.Z. and Hoa, S.V., "Modeling of Tri-axial Woven Fabric Composites", Proc. 2nd Taiwan Canada workshop on Aeronautics, Kaohsiung, Taiwan, May 2001.
12. Yong, Y. and Hoa, S.V., "Energy Approach for Prediction of Mechanical Behavior of 2-D Tri-axial Braided Composites, Part I: Model development", Journal of Composite Materials, vol. 36, No. 8, 2002, pp.963-982.
13. Yong, Y. and Hoa, S.V., "Energy Approach for Prediction of Mechanical Behavior of 2-D Tri-axial Braided Composites, Part II: Parameter analysis", Journal of Composite Materials, vol. 36, No. 10, 2002, pp. 1233-1254
14. Enrico D'Amato, "Finite Element Modeling of Textile Composites", Composite Structures, 54, 2001, pp. 467-475
15. Dow, N.F., Ramnath, V., "Analysis of Woven Fabric for Reinforced Composites", NASA-CR-178275, MSC-TFR-1715/0210, 1987.
16. Yang, J., Ma,C., Chow, Z., In: Proc. 29th SAMPE Symp., Reno, NV, 1984, pp. 292-294.

17. Hoa, S.V, Sheng, S.Z., Ouellette, P., "Determination of Elastic Properties of triax Composite Materials", Composite Science and Technology, 63, 2003, pp. 437-443

18. Sheng, S.Z., Hoa, S.V., "Three Dimensional Micro-mechanical Modeling of woven Fabric Composites", Journal of Composite materials, vol.35, No. 19, 2001, pp.1701-1729.

19. Naik, R.A., "Failure Analysis of Woven and Braided Fabric Reinforced Composites", Journal of Composite Materials, vol. 29, No. 17, 1995, pp.2334-2363.

20. Timoshenko, S.P. and Gere, J.M. *Theory of Elastic Stability*, McGraw-Hill, 1961.

21. Vlasov, V.Z., *Thin-Walled Elastic Beams*, 2nd edition, Israel Program for Science Translation, Jerusalem, Israel, 1961.

22. Argyris, J.H., Hilber, O., Malejannakis, G.A. and Scharpf, D.W., "On Large Displacement-Small Strain Analysis of Structures with Rotational Degrees of Freedom", Computer Methods in Applied Mechanics and Engineering, vol. 14, 1978, pp. 401-451.

23. Bathe, K.J., *Finite Element Procedures in Engineering Analysis*. Prentice-Hall, Englewood Cliffs, NJ, 1982.

24. Wunderlich, W., Obrecht, H. and Schrodter, V., "Non-linear analysis and elastic-plastic load-carrying behavior of thin-walled spatial beam structures with warping constraints", International Journal for Numerical Methods in Engineering, vol. 22, 1986, pp. 671-695.

25. Yang, Y.B. and McGuire, W., "Stiffness Matrix for Geometric non-linear analysis", Journal of Structural Engineering Division, ASCE, 112 (1986), pp. 853-877.

26. Argyris, J.H. and Dunne, P.C., "A simple theory of Geometrical Stiffness with Application to Beam and Shell Problems", 2nd Int. Symp. Computing Meth. Appl. Sci. & Engng., Versailles, France, 1975; ISD-Report No. 183, University of Stuggart.

27. Bazant, Z.P. and Nimeiri, M.E., "Large-deflection Spatial Buckling of Thin-walled Beams and Frames", Journal of Engineering Mechanics Division, ASCE, 1973, pp.10247-10281.

28. Oran, C. and Kassimaili, A., "Large Deflection of Framed Structures under Static and Dynamic Loads", Computers & Structures, vol. 6, 1976, pp.536-547.

29. Wu, R.W.H. and Witmer, E.A., "Non-linear Transit Responses of Structures by the Spatial Finite element Method", AIAA, J., vol.11, No.8, 1973, pp.1110-1117.

30. Yang, T.Y., "Matrix displacement solution to elastic Problems of Beams and Frames", International Journal of Solids and Structures, vol.9, 1973, pp.828-842.

31. Belytschko, T., Schwer, L. and Klein, M.J., "Large Displacement transient Analysis of Space Frame", International Journal for Numerical Methods in Engineering, vol. 11, 1977, pp.65-84.

32. Mallet, R.H. and Berke, L., "Automated method for the Large Deflection and Instability Analysis of Three-dimensional Truss and Frame Assemblies", AFFDL-TR-66-102, 1966.

33. Morris, D.L., "Curved Beam Stiffness Coefficients", Journal of Structural Engineering Division, ASCE, 94(ST5), 1968, pp.1165-1174

34. El-Amin, F.M. and Brotton, D.M., "Horizontally-curved beam finite element including warping", International Journal for Numerical Methods in Engineering, vol. 10, 1976, pp.1397-1428.

35. Chaudhuri, S.K. and Shore, S., "Thin-walled Curved Beam Finite Element", Journal of Engineering Mechanics Division, ASCE, 103(EM5), 1977, pp.921-937

36. Yoo, C.H., "Matrix Formulation of curved Girders", Journal of Engineering Mechanics Division, ASCE, 105(EM6), 1979, pp.971-987

37. El-Amin, F.M. and Kasem, M.A., "Higher-order Horizontally-curved Beam Finite Element Including Warping for Steel Bridges", International Journal for Numerical Methods in Engineering, vol. 12, 1978, pp.159-167.

38. Lebeck, A.O. and Knowlton, J.S., "A finite element for the three-dimensional deformation of a circular ring", International Journal for Numerical Methods in Engineering, vol. 21, 1985, pp. 421-435.

39. Yoo, C.H., "Flexural-torsional Stability of Curved Beam", Journal of Engineering Mechanics Division, ASCE, 108, 1982, pp.1351-1369.

40. Yoo, C.H. and Pfieffer, P.A., "Elastic Stability of Curved Members", Journal of Structural Engineering Division, ASCE, 109, 1983, pp.2922-2940.

41. Yang, Y.B. and Kuo, S.R., "Static Stability for Curved Thin Walled Beams", Journal of Structural Engineering Division, ASCE, 112, 1986, pp.821-841.

42. Rajasekaran, S. and Ramm, E., "Discussion of 'Flexural-torsional Stability of Curved Beam' by C.H. Yoo", Journal of Engineering Mechanics Division, ASCE, 110, 1984, pp. 114-148.

43. Yang, Y.B. and Kuo, S.R., "Effect of Curvature on Stability of curved beams", Journal of Structural Engineering Division, ASCE, 113, 1987, pp. 1185-1202.

44. Rajasekaran, S. and Sundararajan, T. and Rao, K.S., "Discussion of 'Static Stability for Curved Thin Walled Beams' Y.B. Yang and S.R. Kuo", Journal of Engineering Mechanics Division, ASCE, 114, 1988, pp. 915-918.

45. Papangelis, J.P. and Trahair, N.S., "Flexural-torsional of Buckling of Arches", Journal of Structural Engineering Division, ASCE, 113, 1989, pp. 880-906.

46. Yang, Y.B., Kuo, S.R. and Cherng, Y.D., "Curved Beam Elements for non-linear analysis", Journal of Engineering Mechanics Division, ASCE, 115, 1989, pp. 840-855.

47. Saleeb, A.F. and Gendy, A.S., "Shear Flexible Models for Spatial Buckling of Thin-Walled Curved Beams", International Journal for Numerical Methods in Engineering, vol. 31, 1991, pp.729-757.

48. Hu, N., Hu, B., Yan, B., Fukunaga, H. and Sekine, H., "Two Kinds of C^0-type Elements for Buckling Analysis of Thin-walled Curved Beams", Computer Methods in Applied Mechanics and Engineering, vol. 171, 1999, pp. 87-108.

49. Saleeb, A.F., Chang, T.Y.P. and Gendy, A.S., "Effective Modeling of Spatial Buckling of Beam Assemblages, Accounting for Warping Constraints and Rotation-dependency of Moments", International Journal for Numerical Methods in Engineering, vol. 33, 1992, pp. 469-502.

50. Saleeb, A.F. and Gendy, A.S., "Generalized Mixed Finite Element Model for Pre- and Post-quasistatic Buckling Response of Thin-walled Framed Structures", International Journal for Numerical Methods in Engineering, vol. 37, 1994, pp. 297-322.

51. Chen, H. and Blanford, G.E., "A C^0 Finite Element Formulation for Thin-walled Beams", International Journal for Numerical Methods in Engineering, vol.28, 1989, pp. 2239-2255.

52. Dvorkin, E.N., Celentano, D., Cuitino,A. and Gioai, G., "A Vlasov Beam Element", Computers & Structures, vol. 33, No. 1, 1989, pp. 187-196.

53. Babu, C.R. and Prathap, D., "A Linear Thick Curved Beam Element", International Journal for Numerical Methods in Engineering, vol. 23, 1986, pp. 1313-1328.

54. Prathap, D. and Babu, C.R., "An Iso-parametric Quadratic Thick Curved Beam Element", International Journal for Numerical Methods in Engineering, vol. 23, 1986, pp. 1583-1600.

55. Ashwell, D.G., Sabir, A.B. and Roberts, T.M., "Further Studies in the Application of Curved Finite Element to Circular Arches", International Journal of Mechanical Sciences, vol. 13, 1971, pp. 507-517.

56. Ashwell, D.G. and Gallagher, R.H., *Finite Elements for Thin Shells and Curved Members*, Wiley, London, 1976.

57. Choi, J.K. and Lim, J.K., "General Curved Beam Elements Based on the Assumed Strain Fields", Computers and Structures, vol. 55, No. 3, 1995, PP. 379-386.

58. Bathe, K.J., Ramm, E. and Wilson, E.L., "Finite Element Formulations for Large Deformation Dynamic Analysis", International Journal for Numerical Methods in Engineering, vol. 9, 1975, pp. 353-386.

59. Bathe, K.J., "An Assessment of Current Finite Element Analysis of Non-linear Problems in Solid Mechanics", Symposium for Numerical Solutions of Partial Differential Equations, University of Maryland, 1975.

60. Fergunson, G.H. and Clark, R.D., "A Variable Thickness, Curved Beam and Shell Stiffening Element with Shear Deformations", International Journal for Numerical Methods in Engineering, vol. 14, No. 4, 1979, pp. 581-592.

61. Frey, F. and Cescotto, S., "Some New Aspects of the Incremental Total Lagrangian Description", Proceeding of International Conference on Finite Element in Non-linear Solid and Structure Mechanics, Geilo, Norway, Aug. 1977, pp. 323-343.

62. Surana, K.S. and Sorem, R.M., "Geometrically Non-linear Formulation for Three Dimensional Curved Beam Elements with Large Rotations", International Journal for Numerical Methods in Engineering, vol. 28, No. 1, 1989, pp. 43-73.

63. K.J. Bathe, *Finite element procedures*, Englewood Cliffs, N.J.: Prentice Hall, 1996.

64. Bathe, K.J. and Bolourchi, S. "Large Displacement Analysis of Three-dimensional Beam Structure", International Journal for Numerical Methods in Engineering, vol.14 1979, pp. 961-986.

65. Cook, Robert D., Malkus, David S. and Plesha, Michael E., *Concepts and Applications of Finite Element Analysis*, Wiley, New York, 1989

66. Duouis, G.A., Hibbitt, H.D, McNamara, S.F. and Marcal, P.V., "Non-linear Material and Geometric Behavior of Shell Structures", Computers & Structures, vol. 1, No. 1, 1971, pp. 223-239.

67. Whitney, James M. and Ashton, J. E., *Structural Analysis of Laminated Anisotropic Plates*, Lancaster, Pa., U.S.A. 1987.

68. Daniel, Isaac M. and Ishai, Ori, *Engineering Mechanics of Composite Materials*, Oxford University Press, New York, 1994.

69. Xu, Duosheng, Ganesan, Rajamohan and Hoa, Suong V., "Buckling Analysis of Tri-axial Woven Fabric Composite Structures. Part I: Non-linear Finite Element Formulation", in press, Composite Structures, 2004

70. Xu, Duosheng, Hoa, Suong V. and Ganesan, Rajamohan, "Buckling Analysis of Tri-axial Woven Fabric Composite Structures. Part II: Parametric Study – Uni-directional Loading", submitted for publication, Composite Structures, 2004

71. Xu, Duosheng, Ganesan, Rajamohan and Hoa, Suong V., "Buckling Analysis of Tri-axial Woven Fabric Composite Structures. Part III: Parametric Study – bi-directional Loading", submitted for publication, Composite Structures, 2004